The fractionation of gum arabic using synthetic membranes

Manning, Harriet

Award date:
2015

Awarding institution:
University of Bath

THE FRACTIONATION OF GUM ARABIC USING SYNTHETIC MEMBRANES

Harriet Elizabeth Manning

A thesis submitted for the degree of Doctor of Philosophy

University of Bath

Centre for Sustainable Chemical Technologies

Department of Chemical Engineering

September 2015

I. Declaration of authorship

This is all my own work except where I have indicated via references or other forms of acknowledgement.

Signature: …….

Date:

II. Abstract

Gum arabic is a natural product used widely in the food industry as an emulsifier and stabilising agent. The gum contains 3 main fractions: an arabinogalactan (~80 wt%; AG) fraction, a glycoprotein (~ 2 wt%; GP) fraction and an arabinogalactan-protein complex (~18 wt%; AGP). This AGP fraction is largely responsible for the functional properties of gum arabic and, due to natural variation, the proportion of AGP within a gum arabic batch varies enormously. There is industrial interest, therefore, in fractionating the gum arabic to allow creation of a more homogenous product, as well as new products for the food industry.

The aim of this work was to investigate the feasibility of using membrane technology to fractionate gum arabic. Polymeric membranes were used initially and showed success at rejection of AGP by size exclusion. Polysulfone membranes of 0.1, 0.5 and 0.8 µm nominal pore size were employed and the rejection of AGP was seen to decrease with increasing pore size, but the overall transmission of solids was seen to increase. Beneficial fouling was observed with the larger two pore sizes, which allowed greater fractionation after a fouling layer had developed. It was hypothesised that the 0.1 µm PS membrane was fouled by mainly cake formation, whereas the 0.5 and 0.8 µm PS membranes were subject to more in pore fouling.

The critical flux of gum arabic was measured for these three pore sized membranes and was found to be highest (27 L m^{-2} h^{-1}) for the 0.1 µm PS membrane. This was attributed to the lack of in pore fouling, which the 0.5 and 0.8 µm membranes suffered and resulted in fouling occurring at lower fluxes for these membranes; the critical fluxes for these membranes was found to be 15 and 22 L m^{-2} h^{-1}, respectively Increasing the crossflow velocity (CFV) from 0.18 to 0.67 m s^{-1} was found to increase the critical flux. Filtration experiments above and below the critical flux for each pore size demonstrated the efficiency of operating below the critical flux, as operation could be sustained for much longer periods (up to 4h was tested) without the need for cleaning cycles. It also demonstrated the beneficial effect of the fouling layer with the 0.5

and 0.8 μm membranes, which showed little or no fractionation during operation below the critical flux.

Finally, filtration studies were carried out with 3 different membrane materials and detailed surface analysis was performed to explain the differences in performance observed. Both polysulfone and fluoropolymer membranes were fairly hydrophobic, with contact angles of between 70 and 90º, and showed very high overall rejection of solids. High transmission of solids is required together with good rejection of AGP for an effective fractionation process. Hydrophilic cellulose acetate, however, showed very high transmission of gum arabic (~ 75%), but no rejection of AGP.

Overall, the work has shown that fractionation of gum arabic with membranes is feasible using polysulfone membranes, but that further work is needed to optimise the separation. Higher transmission of the GP and AG are required whilst maintaining rejection of the AGP.

III. Acknowledgements

Firstly, I would like to thank my supervisor Dr. Mike Bird for his help and support throughout the project. I would also like to acknowledge the help given to me by my co-supervisors Dr. Darrell Patterson and Dr. Karen Edler. Thanks go to Asst. Prof. Tzyy Haur Chong (Ziggy) of NTU, Singapore for his help and supervision during my internship, David Carr of *Kerry Ingredients* for providing industrial relevance and guidance to the project and Dr. Arto Pihlajamäki for his help with zeta potential measurements at LUT, Finland.

I would like to thank Andy Rice and Bethan England of *Kerry Ingredients* for running many GPC samples for me and Frank Lipnizki of *Alfa Laval* for the generous donation of the membranes. I am very grateful to the EPSRC for funding through the Doctoral Training Centre in Sustainable Chemical Technologies, without which this project would not have been possible. Thanks also go to the extremely helpful technical staff in the Department of Chemical Engineering.

I am very grateful for the help and moral support provided by the members of the group, particularly Emily Hayward and Iain Argyle. Thanks go to my DTC cohort, especially Helen and Heather, for making the PhD immeasurably more enjoyable and finally to Ben for being unbelievably kind and supportive throughout.

IV. Table of contents

V. List of figures

VI. List of tables

bar TMP, 1.7 m s^{-1} CFV and 40 ºC

VII. Nomenclature

a	Channel width / m
A_m	Membrane area / m^2
b	Channel height / m
d	Channel diameter / m
C_b	Concentration in the bulk / wt%
C_F	Concentration in the feed / wt%
C_p	Concentration in permeate / wt%
C_w	Concentration at wall / wt%
D	Pore diameter / m
E_s	Streaming current / A
J	Flux / L m^{-2} h^{-1}
J_V	Volumetric flux / L m^{-2} h^{-1}
L	Channel length / m
K	Conductivity / S m^{-1}
M	Molar concentration / mol L^{-1}
N	Number of channels
P	Pressure / Pa
Q	Permeate flux / L m^{-2} h^{-1}
Q_0	Clean membrane flux / L m^{-2} h^{-1}
R_{CP}	Resistance due to concentration polarisation / m^{-1}
Re	Reynold's number
R_F	Resistance due to fouling / m^{-1}
$R_{F(clean)}$	Resistance removed by cleaning / m^{-1}
$R_{F(irr)}$	Resistance not removed by cleaning / m^{-1}
$R_{F(rinse)}$	Resistance removed by rinsing / m^{-1}
R_m	Membrane resistance / m^{-1}
R_T	Total resistance / m^{-1}
S_A	Roughness / nm
t	Time / s
T	Temperature / ºC
γ	Surface tension / N m^{-1}
ε	Dielectric constant / F m^{-1}
ε_0	Vacuum permittivity / F m^{-1}
ζ	Zeta potential / mV
θ	Contact angle / º
μ	Viscosity / Pa s
ρ	Density / kg m^{-3}

VIII. List of abbreviations

AFM	Atomic force microscopy
AG	Arabinogalactan
AGP	Arabinogalactan-protein complex
ATR-FTIR	Attenuated total reflection-Fourier transform Infra-red
CA	Cellulose acetate
CFV	Crossflow velocity
CIP	Cleaning-in-place
DOTM	Direct observation through membrane
FTIR	Fourier-transform Infra-red
FP	Fluoropolymer
GP	Glycoprotein
GPC	Gel permeation chromatography
HIC	Hydrophobic interaction chromatography
HPSEC	High-performance size exclusion chromatography
IEP	Isoelectric point
LMH	$L\ m^{-2}\ h^{-1}$
MF	Microfiltration
MW	Molecular weight
MWCO	Molecular weight cut off
PS	Polysulfone
PTFE	Polytetrafluoroethylene
PVDF	Polyvinylidene fluoride
PWF	Pure water flux
RI	Refractive index
RO	Reverse osmosis
SANS	Small angle neutron scattering
SEM	Scanning electron microscopy
TEM	Transmission electron microscopy
TMP	Transmembrane pressure
UF	Ultrafiltration
UV	Ultra violet
wt%	Weight percent

1. Introduction

1.1. Gum arabic as a food additive

Gum arabic is a natural exudate produced by *Acacia* trees all over the world. The properties of this natural product mean it has been used for centuries and today it finds uses in cosmetics, paints and in the food industry. Gum arabic is edible, with no taste or odour and often no colour making it ideal as a food additive. It is also water soluble, has a relatively low viscosity and is used as an emulsifying agent, stabiliser, thickener and as edible glue in a range of food products. Its remarkable emulsifying capability means that it is a vital ingredient particularly in soft drink syrups and there has been controversy over its supply as the highest grade gum arabic is exported from politically sensitive regions such as Sudan.

1.2. The potential value of gum arabic fractionation

One of the biggest issues with gum arabic is the huge natural variation in the gum quality depending on where the *Acacia* trees are located. The soil type, climate, rainfall and *Acacia* species all affect the quality of the gum and only the highest quality gum can be used as an emulsifying agent. Gum arabic with low viscosity, pale colour and high levels of arabinogalactan-protein complex commands the highest price. Being able to fractionate gum arabic into its component parts would allow recombination of the fractions to give a homogenous gum arabic. Opportunities for the development of new products such as an AGP enhanced emulsifying agent would also arise.

1.3. Membrane processing in the food industry

Membranes are widely used in the food industry for processes such as dewatering, clarification, bacterial spore removal and fractionation. The technology is well developed in some industries such as the dairy industry but issues associated with fouling and cleaning of the membranes are

still prevalent and prevent the technology being used more widely. Membranes provide a low energy and low cost method of separation, however, and can easily be used for large scale operations.

1.4. Research scope

This thesis aims to investigate the first use of membranes to fractionate gum arabic. Different pore sizes and membrane material as well as operating conditions will be investigated to try to achieve separation of the gum arabic species and achieve acceptable fluxes with this challenging feed. Whilst the aim is to fractionate the feed, a large part of the work is also focussed on understanding the fouling mechanisms and how these affect the filtration and fractionation performance of the membranes. The critical flux concept is investigated and the difference in performance when operating above and below the critical flux is demonstrated. The main objectives of this work are listed below.

- To investigate the feasibility of fractionating gum arabic into its component parts by size exclusion using commercially available polymeric membranes
- To optimise the filtration temperature, transmembrane pressure and crossflow velocity to achieve the best fluxes within the limits of the membrane module
- To understand the relationship between extent of fouling and filtration and fractionation performance
- To understand the fouling mechanisms and how they differ with different pore sized membranes for the filtration of gum arabic
- To measure the critical flux of gum arabic with three different pore sized membranes and demonstrate the effect of crossflow velocity on this critical flux
- To investigate whether operating below the critical flux, i.e. with little or no fouling, affects the filtration and fractionation performance of the membranes

- To investigate how membrane material affects the filtration and fractionation performance and carry out detailed surface analysis to explain the differences

1.5. Thesis structure

This thesis is divided into 7 chapters. Brief descriptions of the scope of each chapter are given below.

Chapter 1: Introduction

Chapter 2: This chapter discusses process considerations for membrane operation including fouling, cleaning and characterisation. A review of the literature in relevant areas of membrane processing and in previous work with gum arabic is given.

Chapter 3: Materials and experimental methods used in this thesis as well as all analytical techniques are described.

Chapter 4: Chapter 4 details the results obtained in the use of 3 different pore sized polysulfone membranes to fractionate gum arabic. Dead-end filtration is initially employed and then this is scaled up in a crossflow module. Flux and fractionation performance is analysed over multiple cycles and the membranes are characterised.

Chapter 5: The critical flux for gum arabic filtration is measured using a flux-stepping method. This is performed for the three PS membranes used in Chapter 4. The effect of crossflow velocity on critical flux is described and filtration and fractionation performance of the membranes when operating above and below the critical flux is studied.

Chapter 6: Chapter 6 describes the use of three different membrane materials with approximately the same nominal pore size in the filtration of gum arabic. The membrane surfaces are fully characterised in order to explain the difference in performance between the three membrane materials.

Chapter 7: Conclusions from the experimental work are drawn and recommendations made for future researchers in this area.

1.6. Dissemination of research

1.6.1. Journal articles

Manning, H. E. & Bird, M. R. 2015. Gum arabic fractionation using synthetic membranes: The importance of fouling. *Food and Bioproducts Processing*, 93**,** 298-303.

Manning, H. E., Carr, D., Chong, T. H. & Bird, M. R. Critical flux of gum arabic: Implications for fouling and fractionation performance of membranes. *Food and Bioproducts Processing*, Submitted February 2015, *Accepted with minor revisions*

1.6.2. Conference presentations

The work in this thesis was presented at the following conferences:

The 10th International Congress On Membranes And Membrane Processes (ICOM2014), Suzhou, China, July 2014, **Oral presentation**

The Centre for Sustainable Chemical Technologies Summer Showcase, The University of Bath, UK, July 2014, **Oral presentation**

Fouling and Cleaning in Food Processing: Green Cleaning, Cambridge, UK April 2014, **Oral presentation**

The 17th Gums and Stabilisers for the Food Industry Conference, Wrexham, UK, June 2013, **Poster presentation**

1.6.3. Awards

Royal Society of Chemistry overseas conference grant, Chemistry Biology Interface Division

IChemE Food and Drink Special Interest Group Conference Bursary

2. Literature review

2.1. Gum arabic

2.1.1. Introduction

Gum arabic is a predominantly carbohydrate-based gum exudate produced as a defence mechanism by *Acacia* trees native to the Sahel region of Africa. When the bark of the tree is damaged, a highly viscous, aqueous material is exuded, which dries to seal the trunk and prevent loss of water or infection. The International Numbering System for food additives (INS) number E-414 is given to gum arabic and its C.A.S number is 9000-01-5. The FAO/WHO Joint Expert Committee on Food Additives (JECFA) defines gum arabic as follows:

"Gum arabic is a dried exudate obtained from the stems and branches of *Acacia senegal* (L.) Willdenow or *Acacia seyal* (Fam. *Leguminosae*). Gum arabic consists of mainly high-molecular weight polysaccharides and their calcium, magnesium and potassium salts, which on hydrolysis yield arabinose, galactose, rhamnose and glucuronic acid. Items for commerce may contain extraneous material such as sand and pieces of bark, which must be removed before use in food".[2]

Gum arabic is one of the oldest natural plant gums and has been used since the ancient Egyptians discovered its utility as a pigment binder and adhesive in paints and in embalming procedures.[3] Today, the gum is collected, sorted, processed and is used primarily in the food industry as an emulsifying and stabilising agent but also in cosmetics, adhesives and in paint production. Sudan is the world's largest producer of gum arabic with Nigeria and Chad also being large exporters. Other countries with minor gum arabic industries include Ethiopia, Senegal, Burkina Faso, Mali, Niger, Mauritania, Kenya, Ghana and Zimbabwe.

Natural variation occurs between *Acacia* species and the composition of gum arabic is affected by the age of the tree as well as environmental factors such as temperature, rainfall levels and

soil type.[4] Colour of the gum is an important factor for the food industry so the palest gum is the most valuable. It also tends to be the least viscous, which is important for gum processing. Gum arabic from Sudan is of the highest quality and, therefore, commands a higher price than lower quality gum from other countries such as Nigeria and Chad.

2.1.2. Structure of gum arabic

Gum arabic is a complex, highly branched polysaccharide consisting of galactose, arabinose, rhamnose and glucuronic acid units[5-8] as well as small amounts of protein.[9-12]

The gum is obtained as a mixed potassium, calcium and magnesium salt and is usually slightly acidic. Chromatographic fractionation of gum arabic has shown the presence of three fractions of different structures and molecular weight (MW) distributions.[11, 12] Approximately 2 % of the gum is made up of a glycoprotein (GP) with an average MW of 250,000 g mol^{-1} and a relatively high protein content of ~50 %. The largest fraction (~88 % of the whole gum) is an arabinogalactan (AG) with an average MW of 280,000 g mol^{-1} and a much lower protein content (<1 %). The final fraction is the highest MW of average 1,500,000 g mol^{-1} and is an arabinogalactan-protein (AGP) complex, where arabinogalactans are covalently bound to a protein backbone consisting of ~250 amino acid residues via serine and hydroxyproline linkages.[7] It has been shown that the most abundant amino acids in the AGP and AG fractions are hydroxyproline, serine and proline, whereas aspartic acid is the most abundant in the GP fraction.[13, 14] The high molecular weight AGP complex has been shown to be vital to the emulsification properties of the gum.[11, 15] Yadav *et al.* showed that trace amounts of glycosylphosphatidylinositol lipids present in gum arabic also contribute to its emulsification properties, however further work is needed to confirm this.[16]

There has been much debate in the literature as to the structure of the different fractions within gum arabic. Anderson and Stoddard demonstrated the presence of main chain 1,3-linked β-D-galactopyranosyl units with side chains of 1,6-linked β-D-galactopyranosyl units and many α-

arabinosyl, glucuronic acid and rhamnose residues making up the main carbohydrate (or AG) portion of the gum.[10, 17] Sanchez *et al.* proposed a thin oblate ellipsoid structure for this AG portion of the gum with approximate dimensions of 20 nm by 2 nm[18] and this was confirmed by Nie and co-workers.[19, 20] The uronic acid (sugar acid) groups within the gum, as well as the protein, give gum arabic a negative charge above its isoelectric point, which is considered in the literature to be < pH 3, and will vary from sample to sample.[21] Agglomeration between gum molecules was shown to occur over time in solution and was more pronounced in gum arabic with the highest protein content.[22] This was concluded by Gashua *et al.* (2015) to be due to electrostatic interactions between the protein and glucuronic acid groups within gum arabic.[22]

Two different structures for the AGP fraction have been proposed and debated in the literature: a twisted hairy rope and a wattle-blossom structure. The twisted hairy rope model that was proposed by Qi *et al.* in 1991 consists of a rod-like protein backbone with a regular pattern of amino acid residues and many small, carbohydrate side chains.[23] The wattle-blossom structure for AGP consists of a polypeptide backbone made up of ~250 amino acid residues with side chains of large carbohydrate blocks of MW ~45,000 Da linked by serine and hydroxyproline moieties.[24, 25] The amino acid sequence of the peptide chain was elucidated by Goodrum *et al.* (2000).[7] Work carried out at Wrexham University[26-28] supports this to some extent and shows that the AGP is an aggregation of the AG and GP fractions that occurs with maturation of the gum and also subjection of the gum to processing such as spray drying and irradiation. The AG and GP units have the same carbohydrate and amino acid composition as the AGP fraction[28] and the proportion of high MW AGP increases with the age of the tree.[4] This, along with evidence from heat treatment studies of gum, which simulates the maturation of the gum over time and results in an increase in AGP, supports this theory.[26, 27]

Lopez-Torez *et al.* (2015) studied the whole structure of gum arabic species *Acacia Senegal* and found that in solution, the gum macromolecules adopted ellipsoid structure with an average radius of gyration of 30.8 nm.[29]

Particle size of gum arabic is difficult to estimate due to the large distribution of MWs and the wide variation within this. The AGP will also vary in terms of the degree of branching and, due to the polymeric nature of the particles within gum arabic their conformation is likely to change with environmental conditions. Renard *et al.* studied the structure of AGP, isolated by hydrophobic interaction chromatography (HIC), by high-performance size exclusion chromatography (HPSEC), small angle neutron scattering (SANS) and transmission electron microscopy (TEM).[30] They found that the AGP had an average molecular weight of 1,860,000 g mol^{-1} and an average radius of gyration of 30 nm. TEM observations indicated a wide range of particle sizes ranging from 10-20 nm for the smaller particles and up to 100 nm for the larger particles. 85% of the particles studied, however, showed diameters of between 20 nm and 80 nm. They noted the presence of higher MW, aggregated AGP particles, which displayed elongated structures (of minor and major axes of 20-30 nm and 80-100 nm, respectively) whereas the smaller particles were anisotropic spheroidal in shape (average diameter of 50-70 nm). The same conclusion was drawn from SANS data. HPSEC analysis revealed that the lower molecular weight particles had longer-chain branches and, therefore, had a more dense structure whereas the higher MW species had short-chain branches and were less dense.[30]

Gum arabic is generally agreed to display Newtonian behaviour at low concentrations (<40 wt%),[31] although some shear thinning properties are observed at low shear rates. Mothé and Rao (1999) found that gum arabic from concentrations 10 - 50 w/v % displayed shear thinning properties at shear rates lower than 100 s^{-1}; gum arabic of 4 w/v % displayed near-Newtonian behaviour.[32] Li *et al.* (2009) found that gum arabic of concentrations 1 wt% to 30 wt% also displayed shear thinning properties at shear rates lower than 10 s^{-1} and this was attributed to the shear-induced dissociation of aggregates in solution.[33]

2.1.3. Functionality of gum arabic

Gum arabic is widely used as an emulsifier and stabiliser for oil-in-water emulsions due to its amphiphilic properties, relatively low viscosity compared to other plant gums and its tasteless

and often colourless nature. In the beverage industry, the demands on gum arabic are high. The emulsion must be stable in both the original flavour syrup emulsion and in the diluted beverage itself, which can be up to a 500-fold dilution. These emulsions must also be stable for months.[34] Randall *et al.* (1988) showed that, although 12% w/w gum arabic was needed to stabilise a 20% w/w orange oil emulsion, only 1-2% of the gum was adsorbed at the interface. They demonstrated that it is predominantly the high molecular weight AGP fraction that is the functional emulsifying component.[11]

The amphiphilic nature of the AGP fraction allows it to sit at the oil-water interface with the hydrophobic protein interacting with the oil droplet and the hydrophilic carbohydrate forming an electrostatic and steric barrier preventing the droplets from agglomerating. Investigations into the zeta potential of gum arabic-coated droplets showed that a sufficient negative charge is present on the droplets at pH 4 to prevent aggregation. The presence of glucuronic acid groups on the surface is thought to be the cause of this.[35-37] Padala *et al.* estimated the amount of gum arabic adsorbed at the oil-water interface to be ~6.5 mg m^{-2} at pH 3.5 based on the intensity of gel permeation chromatography (GPC) peaks before and after emulsion preparation. This was higher than expected for monolayer coverage so it was proposed that multiple layers of gum arabic form at the interface.[37] This is suggested to be part of the reason why gum arabic is such an effective stabiliser of oil-in-water emulsions.

It has been shown that pH and salt concentration can affect gum arabic-stabilised emulsions. Nakauma *et al.* showed that 10% w/w gum arabic can effectively stabilise oil-in-water emulsions above pH 3.0 (up to pH 6.0, pHs higher than this were not studied), but a large increase in agglomeration is seen below this.[36] As the isoelectric point of gum arabic is < pH 3,[21] as this point is reached the electrostatic repulsion that aids stability of emulsions is lost, resulting in a higher rate of droplet aggregation.[36]

2.1.4. Industrial processing of gum arabic

Gum arabic is imported from the gum belt in Africa as small, dry lumps sorted by species and colour, which can range from light brown to dark orange. This is then milled and dissolved in water and subjected to a series of filtration steps to remove debris etc. The gum is pasteurised and spray or roller dried to produce a powder that is suitable for the food industry.

Researchers at Glyndwr University, Wrexham studied the effect of this processing on the structure of gum arabic.[38] It was found that temperature must be carefully controlled during the milling process to avoid aggregation of the proteinaceous components. This aggregation increases the viscosity and reduces the solubility of the AGP fraction, in turn reducing the gum quality. They also found that the heat involved in pasteurisation and spray drying results in an increase in MW and a reduction in the hydrophobic character of the gum as the protein starts to unfold. This is unfavourable as the gum loses some of its ability to bind to the oil phase of an oil-in-water emulsion.[38]

2.1.5. Modifications to gum arabic

As the AGP fraction of gum arabic is the main functional component in emulsification, it is of great interest to industry to be able to better control its content in gum. Natural variation due to age of tree, climate of harvest year, area of origin and storage conditions results in wide batch-to-batch variation in gum composition and molecular weight, which is undesirable.[4] Fractionation of the gum arabic would allow for blending to create new products containing consistent amounts of AGP. This would also allow the use of lower quality gums by blending with the high quality varieties. In addition to gum arabic blending to reduce natural variation, new products containing higher than natural levels of AGP have been investigated in order to create better emulsifying agents. The use of the remaining AG as a source of soluble dietary fibre or edible adhesive is also of interest.

TIC Gums Inc. (US) produce a gum called Ticamulsion® A-2010 that is a modified gum arabic with superior emulsifying properties. The modification process involves the esterification of gum arabic with dicarboxylic anhydrides and was patented in 2002.[39] Modification of gum arabic with n-octenyl succinic anhydride to increase its hydrophobicity has proved successful in increasing the efficacy of gum arabic in mint-oil micro-encapsulation.[40, 41] Wang *et al.* then took this further and investigated the effect of using different concentrations of dodecenyl succinic anhydride to see if the increased alkyl chain length further improved the gum arabic performance. They synthesised two gum arabic derivatives containing 5 wt% and 10 wt% dodecenyl succinic anhydride and found that both were more effective than unmodified gum arabic at stabilising emulsions.[42]

Reseachers at Glyndwr University used a series of heat treatments to artificially 'mature' gum arabic and increase its AGP content. No other modification was carried out other than subjecting the gum to conditions of controlled temperature and humidity, which caused complexation of the AG and GP fractions to form up to twice the original amount of AGP.[26, 43] Further studies showed that this AGP-enhanced gum demonstrated improved emulsification properties than standard gum arabic.[44] This process was patented in Europe in 2009[45] and the USA in 2013.[46]

PepsiCo Inc. were granted a US patent in 2013 for the modification of gum arabic by the addition of small amounts of pectin to improve the emulsification properties and lower production costs.[47] Heidebach *et al.* patented the process of modifying gum arabic by treatment with enzymes from glycosidases. The process improves the emulsifying properties of the gum and can be applied to raw as well as processed gum arabic.[48]

2.1.6. Fractionation of gum arabic

Gum arabic has been fractionated in the past by a variety of different chromatographic methods. This was done mainly on a small scale in order to elucidate the structure of the gum and better

understand its functionality. Gel permeation chromatography (GPC), hydrophobic interaction chromatography (HIC) and ion exchange chromatography have all been used to separate gum into its 3 fractions.

Anion exchange chromatography

Osman *et al.* fractionated gum arabic by anion-exchange chromatography on DEAE cellulose, which separates molecules according to the number of anionic groups present.[49] These groups interact with the positively charged groups on the ion exchange resin, resulting in highly charged molecules eluting last. They obtained 6 fractions by altering the ionic strength of the elution buffer from 1 mM phosphate buffer to 0.29 M NaCl in phosphate buffer in 6 steps. All fractions contained similar amino acid and carbohydrate compositions and GPC analysis of the 6 fractions showed them to each contain different proportions of the AGP, AG and GP fractions reported by other groups. Approximately 60% of the gum eluted with the phosphate buffer and did not bind with the cellulose. GPC analysis showed this fraction to contain most of the AGP fraction and some AG. The other fractions contained little AGP and varying amounts of AG and GP. It was predicted that the fractions would elute in order of their glucuronic acid content, which contains negatively charged carboxylate groups. This, however, was not the case and it was suggested that perhaps the carboxylate groups were sterically hindered and not accessible to bind with the column resin.[49]

Hydrophobic interaction chromatography (HIC)

Hydrophobic interaction chromatography (HIC) is used to separate proteins based on the interaction of their hydrophobic groups with a hydrophobic ligand on the chromatography matrix. Randall *et al.* first used HIC to separate gum arabic into 3 fractions and identified them as arabinogalactan, arabinogalactan-protein complex and a glycoprotein. Sugar, protein and amino acid analysis was performed on the fractions and GPC used to measure their molecular weights.[12] Osman *et al.* fractionated gum arabic into 4 fractions using HIC. The four fractions were all shown to be, or contain, AGP as they all precipitated with Yariv's reagent.[50] Ray *et al.*

also collected 4 fractions by HIC and showed that all except for the lowest molecular weight fraction (5 % of the total gum) were able to create good emulsions, although the highest protein, highest MW fraction performed best.[51]

Fauconnier *et al.* used hydrophobic interaction chromatography to separate the two gum arabic species of *Acacia Senegal* and *Acacia Seyal* into three fractions using 4.2 M NaCl, 2 M NaCl and deionised water.[52] Table 2.1 summarises the results.

Table 2.1: Results of fractionation of *Acacia Senegal* by hydrophobic interaction chromatography. Adapted from Fauconnier *et al.*[52]

Fraction	**Eluent solution**	**Proportion of total weight (%)**	**Protein content (%)**
Whole gum		100	2.8
Fraction 1	4.2 M NaCl	88	2.3
Fraction 2	2 M NaCl	10	11.0
Fraction 3	water	2	14.0

These results comply with previous literature and show the presence of AG, AGP and GP fractions within the gum. Their results also showed that all three fractions in the tested *Acacia Senegal* contained higher proportions of protein, compared to the *Acacia Seyal* tested, and that the *A. Senegal* contained a higher proportion of AGP.

High-performance size-exclusion chromatography (HPSEC)

Vandevelde and Fenyo described the fractionation of gum arabic by size exclusion chromatography. They recorded a molecular distribution of gum arabic by GPC and detection of the eluent by UV absorption at 214 nm. Three peaks were observed with the highest molecular peak containing the highest proportion of protein, which corresponds to later work showing the same 3 fractions.[53] Ray *et al.* undertook similar work but also studied the emulsifying properties of the different fractions. They concluded that, in general, higher MW,

higher protein content fractions produced more stable emulsions and that the lowest MW fractions (but with high protein content) produced a very poor emulsion.[51] This is in agreement with the literature that states that the AGP fraction is responsible for the good emulsifying properties of gum arabic.

Flow field flow fractionation (F4)

Flow field flow fractionation (F4) is a technique that is able to fractionate particles of a wide size range. It is able to separate soluble and colloidal particles and due to there being no stationary phase as in other chromatographic techniques, it is able to deal with 'sticky' samples. Particles are separated based on mass. Smaller, lighter particles are eluted first due to their faster diffusion rates. Picton *et al.* used this technique to separate gum arabic into AG and AGP fractions.[54] Andres-Brull *et al.* further studied the use of F4 as a characterisation technique for gum arabic and found the results to be in agreement with those obtained by gel permeation chromatography.[55]

Gel permeation chromatography (GPC)

Gel permeation chromatography (GPC) is widely used as a method for characterising gum arabic and is used as a quality control technique in its processing before supply to the food industry.[4, 27] The separation technique is based on size exclusion as the sample is passed through a column packed with porous beads. Small or low MW analytes can enter the pores, which slows down their passage through the column and increases their retention time. High MW analytes, therefore, elute first. This technique is typically used with a triple detection system. Dynamic light scattering provides information of the MW of the species, which is normally calibrated to dextrans of known MW. Intrinsic viscosity is measured to give an indication of molecular density, which allows the determination of size and conformation and concentration is measured by refractive index (RI) or ultra-violet (UV). In the case of gum arabic, both are used - RI measures direct concentration and UV absorbance indicates the

presence of protein. Flindt *et al.* carried out preparative GPC on samples of gum arabic species *Acacia Seyal* and analysed the fractions to determine MW, protein and amino acid content, sugar content and intrinsic viscosity.[6]

Ethanol precipitation

Fractionation of gum ghatti by gradual precipitation with ethanol was demonstrated by Kang *et al.*[56] This technique separates components based on their solubility in both water and ethanol. Ibrahim *et al.* briefly investigated the use of ethanol precipitation to separate *Acacia Senegal* into 4 fractions of differing protein content and intrinsic viscosity.[57]

2.1.7. Filtration of gum arabic

Previous work in the Bird group at the University of Bath by Peter Bechervaise has studied the microfiltration of gum arabic with the aim of developing a cold pasteurisation technique.[58] He used tubular ceramic membranes to filter 15 wt% gum arabic with crossflow velocities of up to 8.5 m s^{-1}. He found that polymeric membranes were not suitable for high solids contents as they suffered a severe flux decline. High crossflow velocities are required to create turbulent flow and minimise fouling. He also found that harsh cleaning agents (such as hypochlorite) were required to restore permeate flux and polymeric membranes are unable to withstand such conditions. The effect of pH on filtration of gum arabic was briefly investigated and it was found that at pH 12.1, feed viscosity reduced from 9.66 cP to 5.1 cP, which, along with evidence of a loss of emulsifying functionality at this elevated pH, was attributed to destruction of the AGP fraction.[58] This is due to base hydrolysis of the proteinaceous components in the gum arabic.

Decloux *et al.* (1996) studied microfiltration with gum arabic for clarification and cold-pasteurisation using tubular ceramic membranes.[59] They used a co-current permeate flow system, where a permeate circulation loop is added to the filtration set-up to create a permeate pressure profile similar to that in the retentate stream. This removes the, often high, pressure

drop along the length of the membrane associated with viscous feeds and provides more even filtration. They observed the best fluxes, clarification and solids transmission with 18 wt% gum arabic solutions at high CFVs (7.5 m s^{-1}) and low TMP (0.3 bar) using 1.4 µm tubular ceramic membrane at 70 ºC.[59]

2.2. Membrane processes

A membrane can be defined as a 'phase that acts as a barrier preventing mass movement but allowing restricted or regulated passage of one or more species through it'.[60] This could refer to solid, liquid or gas mixtures. A driving force is required to facilitate transport of species through the membrane, which in the case of synthetic membranes used for industrial applications is typically a pressure difference across the membrane. The initial feed solution is separated into the components that pass through the membrane (known as the permeate) and those that are retained by the membrane, known as the retentate.

2.2.1. Membrane classification

Membranes are typically classified by pore size as shown in Figure 2.1.

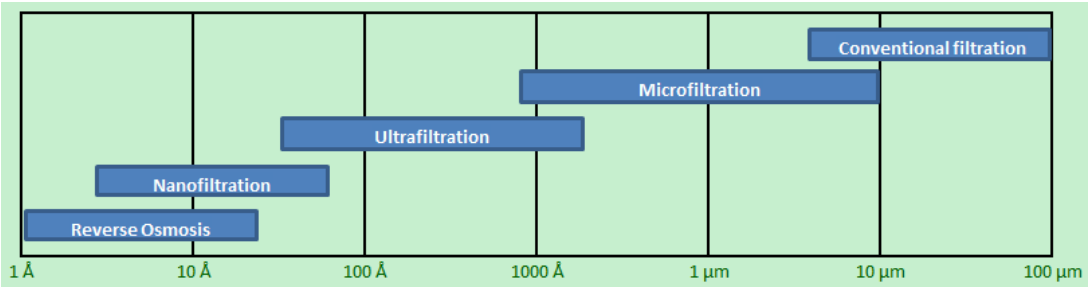

Figure 2.1: The classification of membrane filtrations based on pore size

Microfiltration (MF) describes membranes of pore sizes ranging from about 0.1 µm to 10 µm. The pore sizes for ultrafiltration (UF) membranes are usually given as molecular weight cut offs (MWCO) based on the membrane's ability to reject molecules of a certain molecular weight. As most synthetic membranes display a pore size distribution, the MWCO is defined as the

molecular weight where 90% of the solute is retained by the membrane. There is an overlap between ultrafiltration and microfiltration membranes and, due to the different methods of classifying the pore sizes, it is not always easy to directly compare the two, but manufacturers are starting to use pore dimensions for UF membranes also.

2.2.2. Filtration modes

Membrane filtrations can be classified into two main modes of operation: dead-end and crossflow filtration (Figure 2.2).

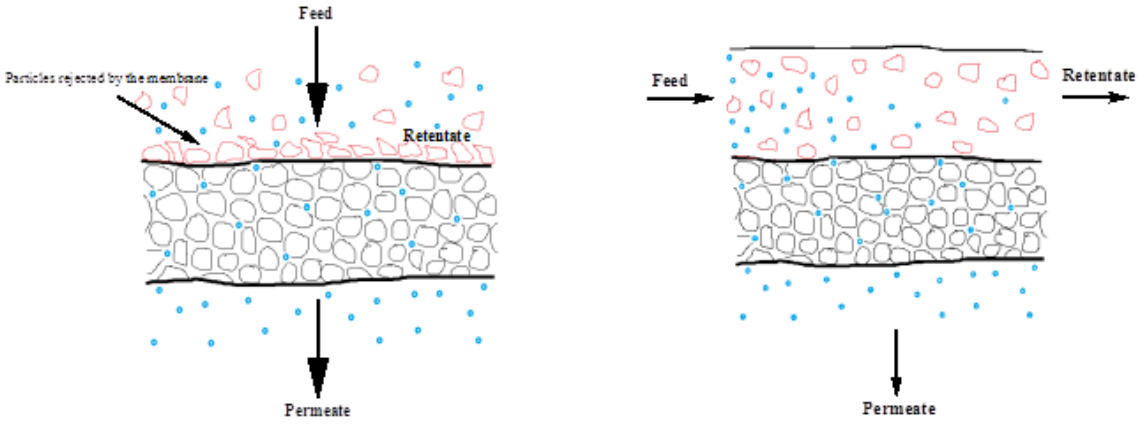

Figure 2.2: The difference between dead end filtration (left) and crossflow filtration (right)

Operation in dead-end filtration mode involves the feed flowing perpendicular to the membrane and rejected components accumulate at the membrane surface forming a cake layer. This mode of operation results in large and rapid flux decline as the cake layer builds up and the feed is concentrated. Due to this intense fouling, dead-end filtration is little used at a large, industrial scale but can be of use for small-scale membrane testing. The flux decline seen with dead-end filtration can be reduced by introducing stirring to the module. A rapid stirring of the feed side of the membrane module reduces the build-up of a cake layer at the surface and provides a pseudo-crossflow filtration environment.

During crossflow filtration, the feed is run parallel to the membrane so that, as components pass through the membrane, the composition of the feed changes along its length. This mode of operation is more widely employed as a lower flux decline is seen. The flow of feed across the surface (known as crossflow velocity) disrupts concentration boundary layer, but flux decline still occurs to some extent due concentration polarisation and other membrane fouling mechanisms.[61]

Crossflow filtration can be operated in several different modes. The simplest is single pass operation, where the feed is passed once across the membrane and split into retentate and permeate steams, which are collected. This mode is suitable for sensitive feeds that are damaged in high shear environments but separation of species is low due to the small contact time with the membrane. A recycle loop can be added so that the retentate goes back to the feed tank and undergoes a number of passes. This results in better separation of species but the feed will concentrate over time as permeate is being removed so that flux decline will be observed over time. To prevent this feed concentration, water can be added to the feed tank to maintain a constant volume (diafiltration) or more feed can be added (fed-batch).

2.3. Membrane properties and characterisation

2.3.1. Membrane materials

Membranes are a class of screen filter, which retain particles on the surface of the membrane like a sieve. Depth filters such as glass fibre or diatomaceous earth trap species within the body of the filter, making the trapped particles hard to recover. Membranes can be further categorised into either symmetric or asymmetric membranes based on their structure; both have defined pore sizes. Symmetric membranes have equal structure throughout the cross section of the membrane whereas asymmetric membranes have a dense skin layer that performs the separation with a more open support layer to provide mechanical strength.

Membranes commonly used in industrial applications are either polymeric or ceramic. Polymeric membranes include polysulfone (PS), polyethersulfone, fluoropolymer (FP), poly(vinylidene) fluoride, regenerated cellulose and cellulose acetate (CA). Ceramic membrane materials include alumina, titania and zirconia.

Polysulfone, fluoropolymer and cellulose acetate will be used in this thesis. Polysulfone is a widely used material in microfiltration. The polymer repeating unit is shown in Figure 2.3.

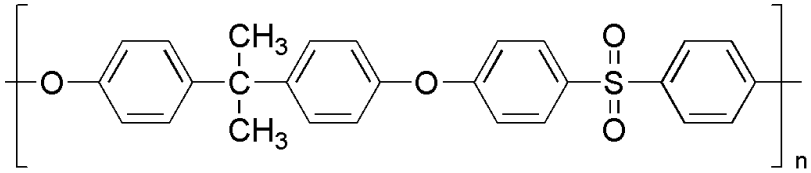

Figure 2.3: Polysulfone repeating unit

The SO_2 group is particularly stable within this structure due to conjugation of its lone pairs of electrons to the adjacent aromatic rings. The oxygen groups can also hydrogen bond to solvent molecules and the phenolic groups are unable to rotate, providing rigidity to the structure. PS is typically stable up to temperatures of 75 ºC, can withstand pHs from 1 – 13, which is useful for cleaning regimes and it is easy to form into membranes of a wide range of pore sizes. PS is hydrophobic, however, making it prone to fouling by a range of different species.[62]

The manufacturers do not detail the structure of the fluoropolymer used in this thesis, but typical fluoropolymers include polytetrafluoroethane (PTFE) and polyvinylidene fluoride (PVDF). Fluoropolymers are characterised by good structural rigidity, high resistance to chemical cleaning agents and stability at high temperatures. FPs are also hydrophobic so prone to fouling.

Cellulose acetate is a membrane prepared by partial acetylation of cellulose by reaction with acetic anhydride, acetic acid and sulphuric acid. The resulting material is highly hydrophilic, making it less prone to fouling than PS or FP, and is easy to form into membranes of a wide

range of pore sizes. Although hydrophilic materials are often less prone to fouling, the adhesion strength can be greater due to the potential for forming strong hydrogen bonds. Cellulose acetate membranes are less robust than PS or FP, however, and are both unstable at high pHs and biodegradable over time.[62] The repeating unit for cellulose diacetate is shown in Figure 2.4.

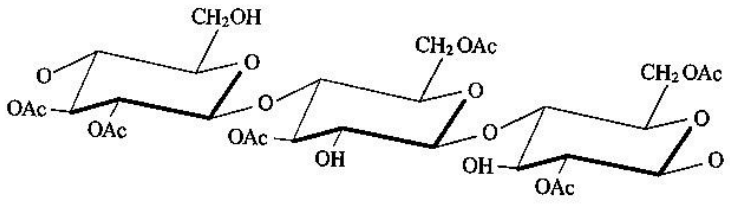

Figure 2.4: Repeating unit for cellulose diacetate

2.3.2. Membrane modules

There are several common crossflow membrane module designs commonly used in industry. The modules are tubular, hollow fibre, plate-and-frame and spiral wound and are chosen for a specific application based on cost, size, hydrodynamic properties and throughput volume.

In tubular modules, the feed is passed through channels within the membrane material (typically ceramic) and permeate passes through the membrane pores into the void space between the membrane and the module. The permeate is collected and the retentate passes through the end of the tubular membrane to be recycled. The channel size can be designed such that large flow rates can be achieved and high solids content feeds can be processed. Ceramics are very resistant to harsh chemical cleaning processes, making these membranes suitable for processes that require sterile environments. Tubular ceramics are expensive and, due to their low surface area to volume ratio, have high special requirements but they have a long life time compared to polymeric membranes.

Hollow fibre modules consist of bundles of individual tubular membranes that are self-supporting and require no separate casing. The feed can be passed either down the centre of the

tubes (and permeate passes to the outside of the tubes) or down the outside (and permeate passes into the centre). The hollow fibres are typically made of polymers such as polysulfone, regenerated cellulose or polyaniline and can be fabricated to different lengths, channel widths and membrane thickness depending on the application. Bundles of fibres are bound together within a cartridge and the high surface area to volume ratio means these modules are less bulky than tubular ceramics. The fibres cannot withstand such high pressures as the tubular ceramics, but the narrow channel size means that high shear rates are obtained. The modules are expensive and the hollow fibres can be prone to plugging.[62]

Plate and frame modules consist of plates upon which the flat sheet membranes are placed, sealed with another plate on top and a spacer allows room for permeate flow. Several plates can be stacked on top of each other and the membranes connected in series to provide a higher membrane surface area. The thickness of the spacer dictates the channel height, which in turn dictates the hydrodynamic conditions. The plate and frame modules are robust and the flat sheet polymeric membranes can be easily replaced. Low hold-up volumes within the module mean that a high percentage product recovery can be obtained.[63]

Finally, spiral wound modules are similar to plate and frame modules in that they hold pairs of flat sheet membranes but they are connected to and wound round a central tube. The membranes are sealed such that they form two compartments. The feed is flowed through the feed compartment, passes through the membranes into the permeate compartment and the permeate from each of the membranes passes towards the central tube and is collected together. This module has the advantage that large throughputs can be processed and the modules are relatively inexpensive.

2.3.3. Membrane fabrication

Flat sheet polymeric membranes are employed in this thesis, which are typically fabricated via a phase inversion technique. Here, the desired polymer is dissolved in a solvent and cast (usually

onto a support material) into a sheet of appropriate thickness. Precipitation of the membrane is brought about by either immersing the membrane in a non-solvent, allowing the solvent to evaporate, lowering the temperature to induce precipitation or using a non-solvent vapour to induce demixing and precipitation. The polymer precipitates and pores are left as the solvent escapes the polymer matrix. Each of these methods will give different properties to the membrane such as pore size, porosity and active layer thickness. The ratio of polymer : solvent, solubility of the membrane in the solvent and non-solvent, the temperature and the rate of precipitation will also affect the final membrane properties.

2.3.4. Membrane characterisation

The membrane performance can be measured by flux and rejection, as discussed in Section 2.4, but it is important to understand the surface properties of the membranes in order to successfully choose an appropriate membrane for a particular application. Monitoring of the effect of filtration and cleaning on the membrane properties is also important to maintain continued filtration efficiency throughout its lifespan.

Membrane porosity

Accurately measuring the pore size of a membrane is a crucial characterisation technique for membrane processes. Manufacturers typically quote a nominal pore size of a membrane but this gives no information about the distribution of pore sizes or the membrane porosity. There are many different techniques for measuring pore size, which can be divided into visual methods, gas/liquid permeation methods and solute permeate methods. Visual techniques involve the use of microscopy, such as Scanning Electron Microscopy (SEM) or Atomic Force Microscopy (AFM) to image the membrane and physically measure the pore sizes from the images using image analysis. This technique allows direct observation but the samples can be prone to artefacts. The drying process must be done carefully so that the pores do not collapse and cross-

sectioning can be difficult without damaging the membrane structure.[64] SEM and AFM are discussed in more detail below.

The solute permeation method is used to classify UF membranes based on a MWCO. The membrane is defined by the maximum MW of solute particle (often polyethylene glycols or dextrans) for which 90% of that particle is rejected by the membrane. This method can also be used to give pore sizes based on a particle's Stokes radius.[65] This method assumes no interactions between the membrane and solute particles.

Permeation of gas or liquid through a membrane is a common method that can measure the pore size and pore size distribution of a wetted membrane. One such technique is Capillary Flow Porometry which relies on forcing gas through a membrane wetted with a fluid of known surface tension. The pressure applied to the gas is increased incrementally until the pressure is enough to break the surface tension. This is known as the bubble point pressure and increasing the pressure further removes the fluid from smaller pores until all pores are empty. Curves of pressure vs gas flow rate are obtained and curves of gas flow through the dry membrane are compared to that of the wetted membrane. These two should meet once all the pores are free of liquid and a 'half dry' curve is calculated as the average of the two. Figure 2.5 shows an example curve with the key pressures labelled.

The pore size can be calculated from the pressure using Equation 2.1.

$$D = \frac{4\gamma cos\theta}{P} \qquad \text{Equation 2.1}$$

where D is the pore diameter, γ is the surface tension of the wetting fluid, θ is the contact angle of the fluid with the sample and P is the pressure.

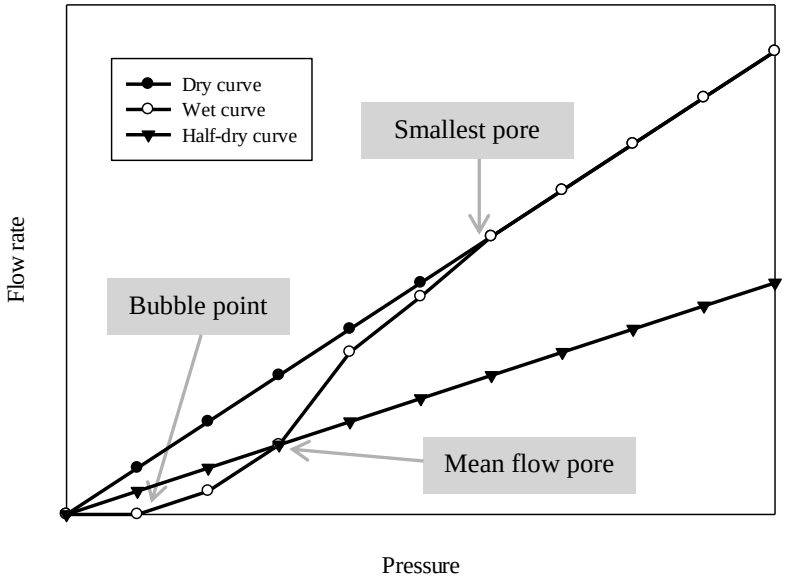

Figure 2.5: Dry and wet flow rate vs pressure curves for capillary flow porometry showing the key parameter points

Membrane hydrophobicity

The degree of wettability of a membrane can be determined by measuring the contact angle that forms between the membrane and a drop of water, called the sessile drop method. The material is typically classed as hydrophobic if the contact angle is greater than 90º and hydrophilic if the angle is closer to zero (Figure 2.6). This method gives a good indication of the membrane wettability but can be affected by surface roughness and requires the membrane to be dried before analysis. Hydrophobic membranes tend to be more susceptible to fouling than hydrophilic membranes as feed streams often contain hydrophobic organic matter that will favourably bind to the hydrophobic membrane surface.[62] The effect of hydrophobicity on fouling propensity is discussed in more detail in Section 2.5.3.

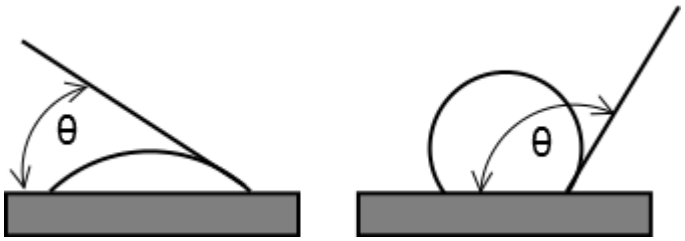

Figure 2.6: Contact angles indicating a hydrophilic membrane (left) and a hydrophobic membrane (right)

Surface roughness

Topographical information about the surface of a membrane can be obtained by Atomic Force Microscopy (AFM). 3D images of an area of the membrane surface are produced and average roughness values for that area can be calculated. This is done by taking the average 'height' between the peaks and troughs as the normal x-y plane and averaging the deviation from that plane over the area measured to give a roughness value (S_A) in nm. The roughness of a surface can be an important factor in the fouling tendency of a membrane and this will be discussed further in Section 2.5.3.

AFM involves the use of a cantilever with a very sharp, nano-sized tip that is scanned across the surface of the membrane. A laser aligned so that it reflects off the cantilever onto an photodiode detector allows detection of the deflection of the cantilever as it is moved across the surface and these signals are converted into a 3D topographical image of the surface.[66] A diagram of an AFM is shown in Figure 2.7.

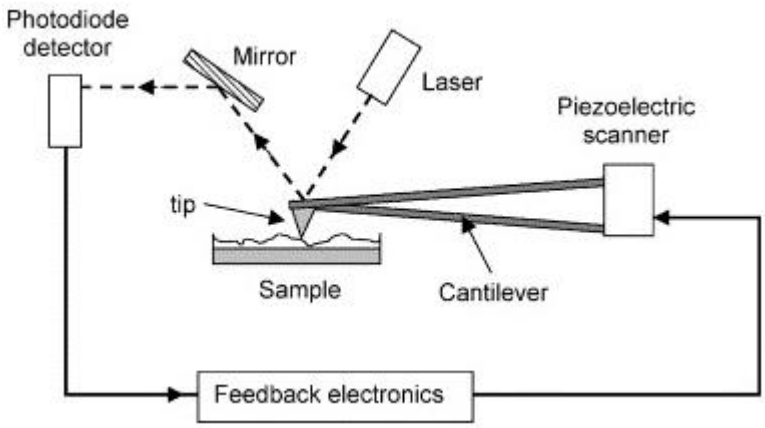

Figure 2.7: Schematic of an AFM after Chan and Chen (2004)[66]

AFM can be operated in different modes depending on the movement of the cantilever. In contact mode, the cantilever is in constant contact with the surface, in tapping mode there is intermittent contact with the surface and in non-contact mode, the tip does not touch the surface but is deflected by forces between the surface and the AFM tip.

Fourier-Transform Infra-Red Spectroscopy (FTIR)

Attenuated total reflection-Fourier transform infrared spectroscopy (ATR-FTIR) can be used to determine chemical functional groups present on the surface of membranes, therefore being an indicator of species adsorption and the effectiveness of cleaning regimes.[67, 68] In this technique, the membrane sample is pressed against a diamond total reflection element. An infrared beam is passed down the element so that it reflects multiple times off the membrane surface. The infrared beam is absorbed by the vibration of chemical bonds, with different functional groups absorbing different wavelengths. A detector collects the infrared signals and these are then converted to wavenumbers by Fourier transform. FTIR can give valuable information about the presence or absence of chemical species but there can be overlap of absorption from functional groups of similar species, making distinction difficult.

Zeta potential

The charge on a membrane surface during a filtration process can affect the amount and type of species adsorption. The charges (or zeta potential) arise from the dissociation of certain species on the surface, leaving behind a charged functional group. The same is true of particles within the feed solution, leading to potentially attractive or repulsive forces between the feed and membrane. The effect of membrane charge on fouling propensity is discussed in Section 2.5.3.

Electrokinetic analysis by measurement of a streaming potential can be used to derive the zeta potential of a membrane surface (or inside the pores), and therefore indicate changes in zeta potential due to fouling and cleaning.[69, 70] Where a solution containing ions meets a charged surface, an electric double layer will form, consisting of ions of opposite charge to the membrane, brought there by attractive forces. The ions closest to the membrane form a static layer (the Stern layer) and those further away form a more mobile, or diffuse, layer. The thickness of this double layer is known as the Debye length and its length depends on the magnitude of the surface charge and the size of the ions in solution.

To measure the zeta potential of a membrane surface an electrolyte solution is flowed across a stationary membrane surface (or through a gap between 2 identical facing membrane surfaces), causing an electric double layer to form. The flow of electrolyte causes movement in the diffuse layer in the direction of flow, which in turn creates a flow of potential in the opposite direction. A steady state is reached and the resulting stable potential is the streaming potential, which is measured using electrodes at either end of the flow cell, as shown in Figure 2.8. This can be converted to a zeta potential using the Helmholz-Smoluchowski equation given below and the zeta potential corresponds to the potential difference between that at the outer edge of the Stern layer and that in the bulk solution.[71]

$$\zeta = \frac{\Delta E_S}{\Delta P}\frac{\mu \mathrm{K}}{\varepsilon_0 \varepsilon}$$

Equation 2.2: Helmholz-Smoluchowski equation

where $\Delta E_s/\Delta P$ is the change in streaming potential with respect to pressure, μ is the electrolyte viscosity, K is the electrolyte conductivity, ε_0 is the vacuum permittivity and ε is the dielectric constant of the electrolyte solution.

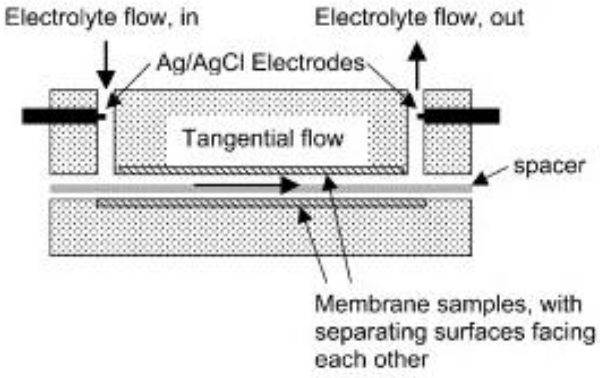

Figure 2.8: Schematic showing the apparatus for measurement of streaming potential across a membrane surface after Chan and Chen (2004)[66]

Direct observation (SEM)

Scanning electron microscopy is a common technique used to image the surface or cross section of membranes. These images can be analysed to measure the membrane pore size, porosity, extent of fouling and the effectiveness of cleaning regimes. Sample surfaces are scanned by a focussed beam of electrons under high vacuum. The species in the sample are excited by the beam and emit secondary electrons, which are detected by a secondary electron detector and converted into an image.

2.4. Membrane performance characteristics

2.4.1. Flux

Flux is a measure of the transport of solvent through a membrane per unit area per unit time and is given by the equation:

$$J_V = \frac{\Delta V}{\Delta t \times A_m} \qquad \text{Equation 2.3}$$

where J_v is the volumetric flux, ΔV is the change in volume, Δt is the change in time and A_m is the area of the membrane. Units of L m^{-2} h^{-1} (LMH) are often used for volumetric flux, but mass fluxes can also be measured. Flux measurements are taken for deionised water (pure water flux, PWF), which will have no fouling effects, through the membrane prior to process filtration so that resistances due to fouling can be separated from resistances due to the membrane (Section 2.4.4.). Flux can be described as shown below:

$$\text{Flux} = \frac{\text{Driving force}}{\text{Viscosity x Total resistances}} \qquad \text{Equation 2.4}$$

With high flux MF membranes, it is important to ensure back transport of rejected particles (shear induced diffusion in the case of large particles) is greater than the forces drawing particles towards the membrane to prevent fouling. Therefore, operating at low TMP and high CFV will minimise the membrane fouling, which leads to flux decline and change in selectivity.[62]

2.4.2. Membrane selectivity

Rejection is a measure of how well species are prevented from passing through the membrane. It can be defined as:

$$\text{Rejection} = 1 - \frac{C_p}{C_F} \qquad \text{Equation 2.5}$$

where C_p is the concentration of the component in the permeate and C_F is the concentration of the component in the feed. For total solids rejection, the dry mass of feed and permeate samples are measured and C_p and C_F are replaced by the concentration of solids in either stream as a weight percentage (wt%). Quoted rejection figures are typically 'apparent' rejection values as true rejection figures should use the boundary layer concentration as the feed concentration, rather than that in the bulk, but this is very difficult to measure or predict. Membrane selectivity is of great importance, especially in fractionation processes, and can be greatly altered by fouling mechanisms. In-pore fouling can alter the pore size and cake formation can act as a secondary membrane to reject smaller species than the membrane itself, making choosing the right membrane for a particular process very challenging.[72]

2.4.3. Flux decline

Filtration of a solute-containing feed stream generally demonstrates a lower flux than that of pure water under the same conditions due to the different properties of the feed. From a purely hydrodynamic point of view, the flux will be lower if the feed viscosity, density and diffusivity differ from pure water.[62] Membranes also typically undergo a severe flux decline during operation due to a number of combined resistances, which are summarised in Figure 2.9. The initial pure water flux gives an indication of the membrane resistance. The fouling resistance can be divided into reversible fouling, which includes concentration polarisation (Section 2.4.6) and rinsible fouling. Rinsible fouling is typically loose cake formation or pore constriction and can be removed by flushing the membrane with water. Non-rinsible fouling is fouling that can be removed by cleaning agents and irreversible fouling is not removed at all during the process and affects the overall life time of the membrane. Irreversible fouling tends to be strongly adsorbed species either on the membrane surface or within the pores.[72] The mechanisms and causes of fouling are discussed in more detail in Section 2.5.

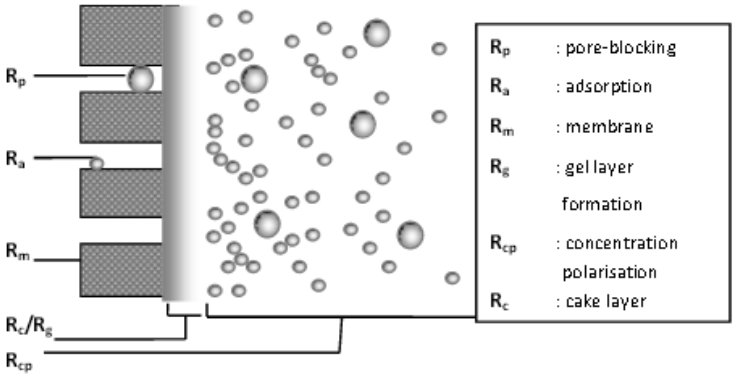

Figure 2.9: Summary of the types of resistance to mass transfer through a membrane during filtration adapted from Mulder (2000)[73] by Jones (2012)[74]

2.4.4. Resistance-in-series model

A common model for describing the pressure-flux relationship in ultrafiltration and microfiltration is the resistance-in-series model. The flux of pure water through a membrane can be written as:

$$J = \frac{TMP}{\mu \times R_m} \qquad \text{Equation 2.6}$$

where TMP is the transmembrane pressure, μ is the permeate viscosity and R_m is the membrane resistance. The membrane resistance can be measured experimentally by carrying out pure water flux measurements at constant temperature, pressure and crossflow velocity. For the filtration of a solute in solution, the resistances due to concentration polarisation (R_{CP}) and resistance due to fouling (R_F) must also be taken into account (Equation 2.7). The fouling resistance can be further divided into resistances due to cake formation, adsorption, pore blocking and gel layer formation, but for experimental purposes is often divided into resistances due to fouling that is rinsible (removed by water rinsing), non-rinsible (removed by cleaning agents) and irreversible.

$$J = \frac{TMP}{\mu(R_M + R_F + R_{CP})} \qquad \text{Equation 2.7}$$

2.4.5. Limiting flux

Limiting flux is the maximum flux that can be achieved by increasing the TMP with a given feed under a certain set of hydrodynamic conditions. Up to the limiting flux, an increased driving force (TMP) results in greater permeate flux but above this, flux no longer increases. At this limiting flux, the 'fouling saturates the filtration capacity of the membrane'.[75] This maximum flux is attributed to the formation of a gel layer, where rejected solute at the membrane surface becomes concentrated enough that under the exerted pressure it reconfigures to form a solid-like gel layer. The high concentration of solute at the surface creates a concentration gradient such that material diffuses away from the surface. This is balanced by the convective movement of material towards the membrane such that a steady state is achieved. Increasing the TMP has no effect on the flux in this state and the only way to increase the flux is to increase the rate of mass transfer away from the membrane, such as by increasing the shear induced diffusion.[62]

2.4.6. Concentration polarisation

Concentration polarisation is the flux-reducing phenomenon that occurs due to convective movement of solute particles towards the membrane. Particles that are small enough will pass through the membrane, but those rejected will build up in a layer on the retentate side of the membrane, thus creating a barrier to membrane passage and reducing permeate flux.[62] This is known as the concentration boundary layer as shown in Figure 2.10, where C_w is the wall concentration and C_B is the bulk concentration of solute. Due to this concentration of solute at the boundary layer, diffusion of material away from the surface also occurs, having a reducing effect on the flux. Concentration polarisation is a reversible mechanism as, if the transmembrane pressure (TMP) is reduced, the accumulated solute particles at the membrane will diffuse away. The effect can be reduced by using lower TMPs, increasing turbulence at the membrane surface and reducing the solute concentration in the feed.

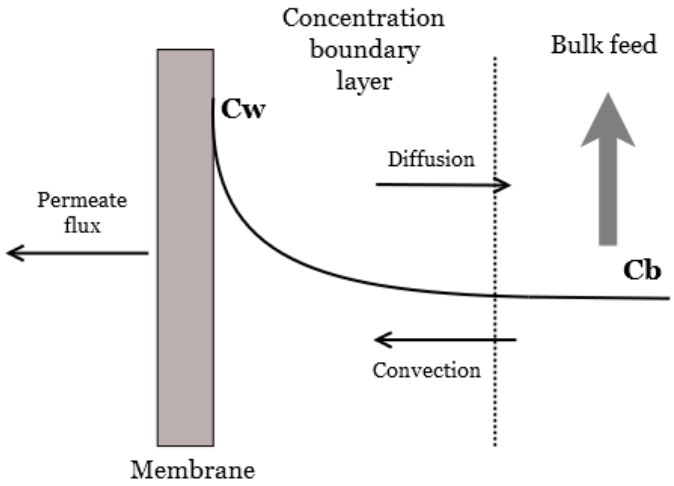

Figure 2.10: Schematic showing the mass transport mechanisms within the concentration boundary layer, adapted from Cheryan (1998)[62]

Concentration polarisation is not to be confused with membrane fouling, which arises due to membrane-solute interactions whereas concentration polarisation is simply a result of accumulation of rejected species near the membrane surface. This high concentration on the feed side of the membrane also creates an osmotic pressure which leads to transport of water back through the membrane in the opposite direction to permeate flux. In nanofiltration and reverse osmosis processes this can be a significant factor in reducing the driving force, but is negligible in comparison to the transmembrane pressure for microfiltration.

2.5. Membrane fouling

Membrane fouling is a major limiting factor in the use of membranes in food processing. Fane and Fell (1987) stated that anything causing a reduction in flux that could not be reversed by a change in operating conditions could be described as fouling.[76] This section reviews the types of potential foulant, the mechanisms of fouling and factors that affect its severity.

2.5.1. Types of foulant

Inorganic fouling

The presence of minerals within a feed can exacerbate the membrane fouling. Ions within the feed can bind to the membrane surface due to charge interaction or poor solubility. The presence of calcium in dairy streams is a major cause of fouling due to its ability to bind to the membrane and proteins within the feed. This allows a salt bridge to form increasing the deposition of proteins on the membrane surface.[62] This was also found to be true in a study of humic acid fouling. AFM was used to measure the interaction forces between a humic acid-coated (or carboxylate equivalent) AFM tip and a clean and fouled membrane surface. They found that a much greater attractive force was present between the fouled membrane surface and the AFM tip representing foulant in the bulk when Ca^{2+} ions were present. This was attributed to the ability of Ca^{2+} ions to complex between carboxylate groups of different humic acid particles. This results in a denser fouling layer with a greater hydraulic resistance than one where no Ca^{2+} was present. The effect of different metal cations was also studied and it was found that Ca^{2+} resulted in a greater flux decline than both Mg^{2+} and Na^{+}.[77] The Ca^{2+} ions also have a neutralising effect on the negatively charged foulant, removing the repulsive electrostatic forces between foulant and membrane, which increases the rate of deposition. The concentration of Ca^{2+} was found to be important as, although the above mentioned factors create a greater flux decline at low Ca^{2+} concentrations, at higher Ca^{2+} concentrations, foulant flocs can form, resulting in lower cake resistance.[78]

Organic fouling

Proteins are a major cause of membrane fouling in food processing applications. The presence of many amino acids each containing different functional groups of varying charge and hydrophobicity as well as the ability of proteins to change conformation depending on the environment means proteins can easily bind to many surfaces. Protein properties are also easily affected by pH, ionic strength, temperature and hydrodynamic conditions. Accumulation of

proteins on the surface can affect the filtration performance of the membrane but can also lead to bacterial growth if not properly cleaned.

Polysaccharide fouling is less well understood but can also cause major issues due to the often broad range of MWs present in polysaccharides and their ability to form sticky deposits and hydrogels on a membrane surface.[79] Saha *et al.* (2007) investigated the ultrafiltration of sugarcane juice and found a high MW polysaccharide-rich arabinogalactan protein to be mainly responsible for the large flux decline observed using PS and PES membranes. The polysaccharide initially caused pore blocking followed by formation of a cake layer.[80] Nataraj *et al.* (2007) studied the fouling effects of model polysaccharides (xanthan gum, actigum CS 11 and glucan) and found that the fouling behaviour differed for the different polysaccharides. They also found that deposition of small quantities of polysaccharides on regenerated cellulose membranes resulted in severe flux decline and that microaggregates were found in the cake layer.[81]

Susanto *et al.* (2008) analysed the effects of multiple component feeds on the fouling severity. They studied polysaccharide-protein mixtures and found that having both components resulted in a greater flux decline than with feeds of the same concentration, but containing only one component. They attributed this to crosslinking between the polysaccharide and protein, which together formed a cake layer of a higher hydraulic resistance than those of the individual components.[82]

2.5.2. Fouling mechanisms

Fouling can take the form of initial adsorption of species to the surface of the membrane, which is a flux-independent process; pore blocking, the different mechanisms of which are discussed in detail below; gel formation, which occurs with certain macromolecules as a result of concentration polarisation; and cake formation, which is the deposition of layers of particles on the membrane. Tracey and Davis (1994) categorised fouling mechanisms into internal fouling

and external fouling, as shown in Figure 2.11. External fouling was described as foulant adhering to the membrane surface,causing pore blocking, pore constriction and cake formation. This type of fouling was shown to give a resistance – time curve of decreasing gradient, whereas internal fouling gave an increasing gradient. Internal fouling was described as foulant adhering within the membrane pores, causing reduction in the effective pore size and pore plugging.[83]

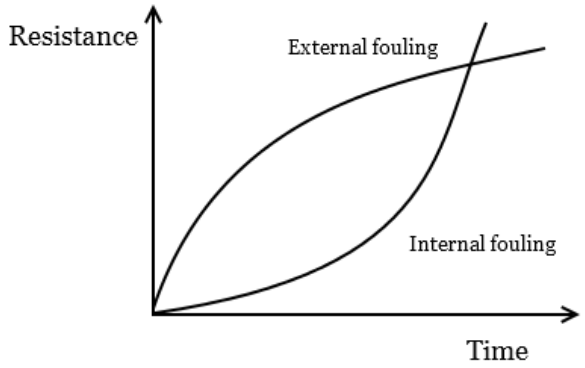

Figure 2.11: Resistance vs time graphs for external and internal membrane fouling after Tracey and Davis (1994)[83]

Bowen *et al.* (1995) described the onset of fouling during microfiltration by four mechanisms as described below and illustrated in Figure 2.12.[84]

i) *Complete pore blocking*, during which large particles completely cover the entrance to the pore preventing anything passing through

ii) *Standard pore blocking* occurs when smaller particles adhere to the inner surface of the pore, reducing the pore size

iii) *Intermediate pore blocking*: particles are deposited on already existing particles at the pore opening or block the pores themselves

iv) *Cake formation*: particles cover the surface of the membrane, blocking the pores and building up into a layer of fouling

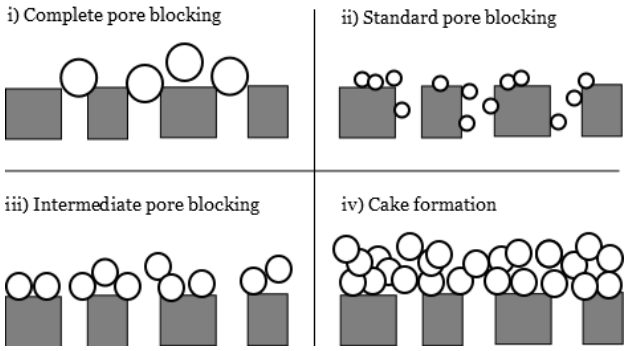

Figure 2.12: Pore blocking mechanisms adapted from Bowen *et al*. (1995)[84]

Hermia (1982) developed characteristic equations for these blocking laws by making a few assumptions. The models assumed that complete pore blocking results in a reduction in the number of available pores but the pore diameters and lengths remain the same, standard pore blocking results in a reduction in the pore diameter but the number of pores remains the same and cake formation does not affect the internal pores but only increases the cake resistance.[85]

Linearisation of these models has been performed by a number of authors[81, 83, 86] and by plotting the relevant parameters, the dominant fouling mechanisms for fouling can be determined by the closeness of the line fit. Equations 2.8, 2.9 and 2.10 describe the linear relationships for complete pore blocking, standard blocking and cake formation, respectively.

$$Q = Q_0 - K_{CPB}\,V \qquad \text{Equation 2.8}$$

$$\frac{t}{V} = K_{SPB}t + \frac{1}{Q_0} \qquad \text{Equation 2.9}$$

$$\frac{t}{V} = K_{CF}V + \frac{1}{Q_0} \qquad \text{Equation 2.10}$$

where Q is the permeate flux, Q_0 is the PWF, V is the cumulative permeate volume, t is the filtration time and $K_{CPB,}$ K_{SPB} and K_{CF} are all constants relating to the complete pore blocking, standard pore blocking and cake filtration models, respectively.[83]

2.5.3. Factors affecting membrane fouling

Temperature

Many factors contribute to, and therefore can be exploited to minimise, fouling. Operating temperature will affect the viscosity of the feed solution as well as the solubility of the components and the rate of mass transfer. The increase in diffusion rate will aid the back transport of accumulated species at the surface, reducing the boundary layer thickness. The limits to temperature are usually set by the filtration components rather than the membranes being used, especially in the case of protein filtration. Decloux *et al.* investigated the microfiltration of gum arabic and found that there was a permanent reduction in viscosity of the gum seen when operating at 80 ºC, indicating a breakdown of the gum structure.[59]

Crossflow velocity

Operating at high crossflow velocities, or in turbulent flow, can reduce the accumulation of particles on the surface of the membrane, which leads to fouling. The higher crossflow velocity increases the shear rate at the surface, which acts to 'sweep away' species rejected by the membrane. For small particles, the dominant back transport mechanism is Brownian motion, which is unaffected by shear rates, but in the case of most food processing applications, the particles are too large for Brownian diffusion to be important.[62] Sim *et al.* (2014) studied colloidal silica fouling during filtration using Ultrasonic Time Domain Reflectrometry, a technique that allows the measurement of the thickness and density of a fouling layer. They found that the silica underwent a transition from a fluid-like concentration polarisation layer to a dense, solid-like gel layer at a certain flux, which greatly increased the fouling resistance. Increasing the CFV of the system delayed the onset of this phase transition, as did lowering the flux and feed concentration.[87]

Transmembrane pressure

Transmembrane pressure is the main driving force for most filtration processes. Increasing the TMP will result in an increase in flux up to the limiting flux, as discussed in Section 2.4.5. Here, the concentration of foulant particles at the surface is such that they form a gel layer and any further increase in TMP can lead to further compaction of this gel and a subsequent reduction in flux.[88, 89] Giri *et al.* (2014) showed that increasing the TMP increased the flux of soymilk during its concentration with hollow fibre membranes, indicating that operation was within the pressure-driven region.[90] de Barros *et al.* (2003) studied the filtration of depectinized pineapple juice and found a decrease in flux with high operating TMP and determined that the limiting flux had been reached.[91] Another factor to consider when operating at high pressures with polymeric membranes is compaction of the membrane. This will reduce the effective pore size and can lead to severe flux decline as well as increased rejection of species.[92]

Feed properties

Permeate flux typically decreases exponentially with increasing feed concentration, due to increased viscosity of the feed and the greater likelihood of particles adhering to the surface.[62] The pH of a feed can also affect the solubility, conformation (and therefore the size) of particles and their charge. Lim *et al*. (2012) studied the ultrafiltration of gelatin using polyethersulfone membranes and found that fouling was greatest near the isoelectric point (IEP) of the gelatin, as above this pH, the protein was negatively charged and therefore repelled by the negatively charged membrane.[93] At the isoelectric point, the protein carried no net charge so was able to assemble more densely in the concentration boundary layer, creating a greater resistance to flux. Prefiltration of a feed can significantly reduce the fouling if large, unwanted particles can be removed using a large pore sized membrane initially. The particle size of components within a feed is another important factor. It has been shown that particles of a similar size to the membrane pore size have the greatest fouling propensity due to pore plugging or adsorption

within the pores. This results in a rapid flux decline, often within the first few minutes of operation.[94]

Membrane hydrophobicity

Hydrophobicity of the membrane is significant as highly hydrophobic membranes attract hydrophobic solute particles that will adsorb readily to the surface, increasing fouling. Lockley *et al.* (1988) showed this in a study that compared protein adsorption to hydrophobic polyvinylidene fluoride and polysulfone to hydrophilic cellulose acetate. Fouling was much more evident in the case of the hydrophobic membranes.[95] The adsorption effect can be quite significant as shown by Chang *et al.* (2002), who saw high levels of adsorption of steroid estrogens to hydrophobic hollow fibre membranes, despite the large pore size. Transmission increased once the adsorption capacity of the membrane was saturated.[96] Ideally membranes will be highly hydrophilic as water molecules can hydrogen bond to the surface, reducing direct adsorption of solute particles to the membrane.[97, 98] The majority of commercial membranes are, however, hydrophobic due to their superior stability and robustness.

Surface roughness

Surface roughness can be measured by AFM and can be a significant factor in affecting the fouling tendency of a membrane. It is generally acknowledged that rougher membrane surfaces have a greater tendency to foul than smooth membranes.[62, 99] For example, Evans *et al.* (2008) studied the ultrafiltration of black tea using 10 kDa, 30 kDa and 100 kDa fluoropolymer membranes and found that the order of permeate flux value correlated with the surface roughness such that 30 kDa (roughness = 59 nm) had a lower flux than 10 kDa (roughness 27 nm) and 100 kDa (roughness = 11 nm).[67] Weis *et al.* (2005) found that for polysulfone and polyethersulfone membranes of the same hydrophobicity, the rougher polysulfone membrane showed greater flux decline during the filtration of spent sulphite liquor.[100] They also found, however, that the rougher but more hydrophilic regenerated cellulose membrane showed a

greater resistance to adhesion, demonstrating the importance to consider all surface properties together. Riedl *et al.* (1998) found that during the filtration of apple juice, smoother nylon and PS membranes formed a dense fouling layer with a high fouling resistance whereas the rougher PES and PVDF membranes formed a more open fouling layer and demonstrated higher permeate fluxes.[101]

Surface charge

Most commercial membranes carry a net negative charge, which can create electrostatic interaction when filtering charged particles. This can be exploited to prevent adhesion of species to the membrane surface, for example by altering the pH of the feed such that species carry a net negative charge and will be repelled by the membrane (as discussed above). Nyström *et al.* (1994) combined the measurement of membrane surface charge by the streaming potential method with flux data for the filtration of BSA using PS membranes. They found that adsorption of BSA onto the surface resulted in a change in the surface zeta potential to that of the protein. At very high or very low pH, where the membrane and the protein exhibited the same (positive or negative) charge, adsorption of the protein decreased and the zeta potential of the membrane did not change to that of the protein.[102] The presence of salts within the feed can also affect the fouling of membranes as charge interactions are shielded by the high concentration of ions in solution. Charged particles and residual charges on the membrane are masked by the ions, reducing the attractive or repulsive interactions between membrane and solute.

2.6. Critical flux concept

The critical flux concept was first introduced by Field *et al.* (1995).[103] This phenomenon describes filtration upon start up that, below a threshold flux, demonstrates little or no fouling. In operations at constant flux, this results in a constant TMP. If the flux is increased above this

critical value however, fouling occurs that cannot be removed when the flux is lowered once again.

Two forms of this theory exist and were described by Field *et al.* (1995). The first is the strong form of the critical flux where the flux is equal to that of pure water during operation, under the same conditions. The second is the weak form of the critical flux where upon start up a constant flux is quickly established and continues with no rise in TMP, although the TMP is higher than that with water only. The weak form of the critical flux is often observed due to adsorption of species on the membrane surface. If attractive interactions exist, adsorption will occur until the adsorption layer is complete and this is not dependent on the flux.[75] Figure 2.13 shows the strong and weak forms of the critical flux.

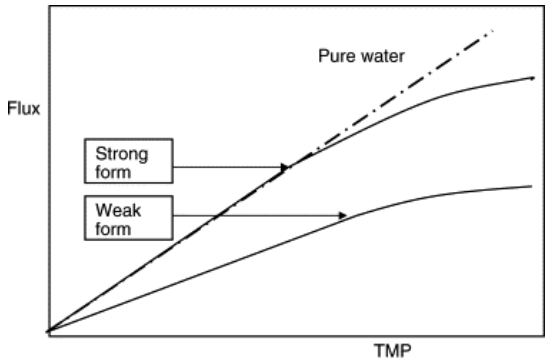

Figure 2.13: Flux-TMP curve demonstrating the deviation from linearity that marks the critical flux after Bacchin *et al*. (2006)[75]

The physical mechanism behind the critical flux can be described as the flux required to overcome both back transport mechanisms and particle repulsion from the surface and lead to coagulation or accumulation on the surface[104] Operating below the critical flux not only allows a more sustained operation, as the need for membrane cleaning is removed or reduced, but it also provides a more constant membrane system. Fouling of the membrane can significantly alter the surface properties or the membrane, making it hard to study the performance of the membrane alone. This is expected to affect the membrane selectivity as well as the flux due to

the absence of a fouling layer that is often responsible for rejection of species more so than the membrane itself.

2.6.1. Factors affecting critical flux

The stability of the suspension within a feed can have a dramatic effect on the critical flux. Altering the pH or the ionic strength of the solution can increase or decrease the strength of the particle-membrane interactions. As the absence of fouling relies on a balance between the repulsion of particles from the surface, stronger or weaker particle interactions will affect the critical flux. For example, increasing the pH above the isoelectric point of the solute results in an increased negative charge and therefore increased repulsion from a negatively charged membrane. An increase in the critical flux is therefore seen.[105, 106]

The effect of particle size on critical flux is hard to predict as diffusion will be greater for smaller particles but surface repulsive forces will be higher for larger particles.[75] Li *et al.* (2000) saw an increase in critical flux with particle size during the filtration of latex particles.[107]

The effect of CFV on critical flux has been described as a power law relationship.[62] The increase in the strength of the hydrodynamics results in an increase in the critical flux as the back transport mechanisms such as lateral migration and shear induced diffusion are higher at higher CFVs. This is limited, however, by differences in TMP across the membrane surface. If the pressure drop across the membrane is large, this may mean that the inlet TMP is such that the localised permeate flux exceeds the critical flux, leading to localised fouling.[108]

Membrane properties are also important in influencing the critical flux. Membranes of a higher porosity have a more even distribution of the permeate flux across the membrane surface, minimising localised differences that could lead to exceeding the critical flux and allowing deposition of particles on the surface.[75] Huisman *et al.* (1999) studied the effect of membrane material and zeta potential on the critical flux of a silica particle suspension. They found that the three ceramic membrane materials they tested showed no difference in critical flux, even at

different pHs that changed the membrane zeta potential from positive to negative. They found the hydrodynamic conditions to be more important than the particle-membrane interactions.[109]

2.6.2. Measuring critical flux

A number of methods have been used to determine critical flux, the most common being from flux/TMP measurements obtained by pressure or flux-stepping. Other methods include particle mass balance and direct observation through the membrane (DOTM).

Direct observation through the membrane (DOTM)

DOTM is used to measure the first point at which particles deposit on a transparent membrane. Microscope images taken during the constant flux filtration of 3, 6.4 and 12 μm latex particles showed little or no deposition below the critical flux and significant deposition at or above it. The critical flux increased with particle size and CFV.[110] More recently, Zamani *et al.* (2014) suggested the use of a critical Peclet number, rather than a flux to indicate the point of particle deposition on the surface during DOTM studies with latex particles. This value gives a ratio between convective and diffusive transport but is not valid where Brownian motion or particle interactions are important.[111] The DOTM method is advantageous in that the flux resulting in deposition can be directly observed, as it is often lower than flux that results in performance decline.[112, 113] Once deposition occurs however, this often leads to further accumulation[110] so direct observation may result in a more sustainable operation of the membrane. This technique is limited to particulate feeds and transparent membranes.

Particle mass balance

Several authors have reported critical flux values measured by particle mass balance. By recording particle concentration in the outlet, or retentate, stream, the amount of deposition can be determined after initial adsorption has been accounted for. Deposition rate at several fluxes is measured then the graph extrapolated to find the flux where zero deposition occurs.[114-116]

This method has proven to give quite different results when compared to pressure/flux methods and cannot be relied upon solely.

Pressure/flux relationship

The most common method for determining critical flux is by measuring the relationship between pressure and flux by imposing either a constant flux or pressure. This is then increased step-wise and the effect on the dependent variable is recorded. The point at which this relationship deviates from linearity is the critical flux. The TMP/flux should remain constant over the time step and the point at which an increase in TMP (or decrease in flux) is observed over that step period indicates the onset of fouling and that the critical flux has been exceeded. It is important, however, to consider the timescale and sensitivity of this experiment as membrane fouling may appear to be non-existent in the time period measured, but may in reality be significant over a longer operation time.

Le Clech *et al.* (2003) proposed 3 TMP based parameters to measure the critical flux. Their experiments with real and synthetic sewage found that at no point above 2 LMH was dTMP/dt = 0. They did find a significant difference between low and high fouling rates, however, and defined a pseudo-critical flux where dTMP/dt < 0.1 mbar min^{-1}. This could now be defined as a threshold flux (Section 2.6.3). They also used the average TMP vs flux curve and found a critical value as the point of deviation from linearity and they used a third parameter, ΔP_o. This was defined as the difference between the final TMP of one flux step and the initial TMP of the next flux step. This also showed the difference between low and high fouling. All three parameters were compared and gave similar values for the 'threshold flux'.[1]

The constant flux method has the advantage over the constant pressure method in that TMP is very hard to control at very low values, meaning that accuracy in the critical flux value is hard to achieve. When operating at constant flux, the permeate can be pumped accurately at low fluxes using a mass flow controller.

2.6.3. Sustainable and threshold fluxes

The concept of a sustainable flux was first introduced to describe a flux that balances capital outputs with operating costs. It is often not economically viable for a process to be operated below the critical flux as the outputs are not sufficient. Instead, a sustainable flux allows some fouling but not so much that cleaning and membrane replacement costs outweigh the output capital.[75, 117]

A threshold flux is described as a flux below which a low and near constant rate of fouling is observed and above which a rapid increase in fouling is seen.[117] This is often described as a point in the pressure-flux curve where fouling is suddenly rapid and severe. If prior to this the fouling is minimal, but not zero such that a critical flux cannot be described, this is then termed the threshold flux.

2.7. Membrane cleaning

Cleaning and disinfection of membranes is an important stage in food processing applications, which is generally performed at least once a day. A membrane can be physically clean (where all visible deposits are removed), chemically clean (where all deposits are removed) or biologically clean (where all living organisms are removed) but generally, the process should remove all unwanted deposits on the membrane without affecting the membrane properties.[118]

2.7.1. Hydraulic cleaning

Hydraulic cleaning employs the use of high shear at the membrane surface to remove deposits. The CFV should be high (ideally providing turbulent flow) during cleaning cycles and the TMP should be kept low to prevent refouling of the membrane.[62] Back flushing is a technique where a pressure is applied on the permeate side, forcing permeate back through the membrane to dislodge deposits in the pores and on the membrane surface. Back pulsing or back shocking involves short back washing bursts during filtration that can be more effective, although this

technique is often ineffective for sticky or flexible deposits. Borujeni *et al.* (2015) utilized a periodic back pulsing technique in the ultrafiltration of plasmid DNA, which resulted in greater flux and better recovery of the plasmid DNA.[119] Back flushing methods are often used with tubular ceramics or hollow fibre membranes; it is harder to achieve with flat sheet membrane modules.

2.7.2. Chemical cleaning

The use of chemical cleaning agents is common in food industry applications and the mechanism for cleaning can be divided into physical and chemical processes. Physical processes include swelling, solvation, wetting, emulsification, deflocculation and desorption; chemical processes include hydrolysis, peptization and chelation.[118] The cleaning usually takes places within the membrane module (Cleaning in place; CIP). A number of different cleaning agents can be employed to achieve these cleaning processes, and the chosen agent will depend on the nature of the deposits to be cleaned, although for food applications the cleaning agents must be compatible for use with food.

Common cleaning agents include acids, alkalis, surfactants and disinfectants. Citric acid is commonly used in the food industry and has the effect of dissolving inorganic salt deposits. Sodium hydroxide is also commonly used with a range of different feeds due to its ability to saponificate lipids and solubilize proteins, enabling easier removal. For example, sodium hydroxide has been used to clean membranes during filtration processes with milk protein isolate,[120] apple juice,[88] black tea liquor [121] and spent sulphite liquor.[100] Surfactants improve the wettability and rinsability of the membrane surface, allowing better contact with the cleaning agents.[118]

Li *et al.* (2004) demonstrated the effectiveness of using the chelating agent ethylenediaminetetraacetic acid (EDTA) in cleaning organic deposits stabilised by Ca^{2+}. The EDTA forms more stable complexes with Ca^{2+} than with the humic acid carboxylate groups, so

that ligand exchange occurs, breaking the dense, cross-linked gel layer and allowing the organic deposits to be more easily removed by hydraulic action.[77]

2.8. Membranes in the food industry

Membranes have found a wide range of uses in the food industry and have been a major tool in food processing for the last 40 years.[122] Between 20 and 30% of the membranes produced worldwide are used in the food industry in applications that include dairy processing, sugar refining and clarification and concentration of fruit juices and alcoholic beverages. Membrane processes have advantages over other separation technologies in that they have low capital costs, are low energy to run, have low environmental impact and can optimise the use of raw materials.[123] Dealing with food products has particular requirements that are not present in other industries. The safety and quality of the final product must be ensured when applying a membrane process such that the product meets the requirements with regards to microbial levels and taste, texture and functionality. This can be achieved by careful study of the rheological, physico-chemical and structural properties of the feed and how these change during the filtration process.[122]

2.9. Membrane fractionation processes

Fractionation of species can be easily and accurately achieved by chromatographic techniques but the volumes of feeds that can be separated are limited. Membrane fractionation offers a much higher throughput method, as well as being cheaper to run. Fractionation of different species within in a feed stream is a challenging process that can be achieved by different mechanisms. Size exclusion is the simplest method where, if the species to be separated have significant differences in size, the membrane pore size can be chosen such that the smaller species is transmitted whereas the larger species is rejected. Electrostatic interactions can also be employed so that one species is electrostatically repelled by the membrane whereas the other is not. Modification of pH can be used to fractionate different proteins in a feed stream. If the

pH is altered such that one protein is at its isoelectric point and the other has the same charge as the membrane, then the latter protein will be better retained by the membrane than the former.[62] Addition of salt to a feed stream masks the charges so that highly charged proteins see greater transmission. The opposite effect is often seen for proteins at their IEP, however, as they take on charge and rejection is increased.

Due to the challenging nature of fractionation using membranes, it is important to maintain constant conditions as much as possible throughout the process. Uniformity of pore size is important if size exclusion is the main fractionation method. Many commercial membranes have a broad pore size distribution that would make separation of similarly sized species difficult. The process conditions should also be kept as constant as possible across the whole membrane surface; large pressure drops along the membrane will result in different separation characteristics. Membrane fouling can significantly affect the selectivity of a membrane. Internal fouling can narrow the pore size and cake formation creates a secondary membrane with different selectivity to the membrane itself. Operation below the critical flux will minimise the effects of fouling on selectivity but if this is not possible, the effects of membrane fouling must be taken into account.[72]

Cheryan (1998) described a theoretical two stage filtration to separate three proteins X, Y and Z of MW 3000, 40 000 and 500 000 kg mol^{-1}, respectively and a concentration each of 1% w/v. The first stage would be filtration of the feed containing all three proteins through a 20 kDa membrane to a volume concentration ratio of 10. The 3 kDa protein would pass into the permeate. The retentate from this filtration would then be diluted with water back to the original volume and passed through a 100 kDa membrane until a 10-fold reduction in volume was achieved. This would separate proteins Y and Z, with Y passing into the permeate stream and Z being retained by the membrane.[62] In reality however, this method would be unlikely to provide good separation. Membranes typically have a wide pore size distribution and the difference in protein molar mass is unlikely to be large enough to get good separation by size

exclusion. The proteins would also be likely to associate with each other through charge interactions and fouling of the membrane over time would alter its separation characteristics, making the separation more challenging than predicted in this example.

Nyström *et al.* (1998) demonstrated the possibilities of protein fractionation by altering the process conditions such as pH, charge and membrane hydrophilicity. They showed that proteins at their IEP were able to pass through the membrane whereas those that were not were retained by the membrane. The proteins had the smallest hydrodynamic radius at their IEP and this, combined with the charge interactions allowed very good separation of similar sized proteins.[124]

Brans *et al.* (2004) gave a review on fractionation of milk using membrane technology, which can lead to better use of the milk components. Milk is composed of an emulsion of fat globules suspended in an aqueous phase consisting of casein micelles, serum proteins, lactose and salts, all with broad particle size distributions. This makes fractionation of whole milk a challenging task and work in this field has typically focussed on single stages of fractionation. These stages include separation of the milk and milk fat, concentration of casein micelles from skim milk, recovery of serum proteins from cheese whey and removal of bacterial spores by cold pasteurisation. Whilst these processes are possible, the authors highlight the need for more work on improving selectivity so that membranes can fully retain large molecules and fully transmit smaller ones. They also focus on the importance of fouling control, as selectivity is hard to maintain under high levels of fouling.[72] Improved selectivity can be achieved by applying a charge to the membrane surface.[125]

Wallberg *et al.* (2003) attempted the fractionation of kraft black liquor which is a by-product of paper milling, to extract the lignin for use as a biofuel. Polymeric membranes of 4, 8 and 20 kDa MWCO were tested with 15 wt% kraft black liquor, which gave lignin rejections of 80%, 67% and 45%, respectively. Although the tighter membranes gave the highest recovery of lignin, the larger MWCO membranes produced purer lignin, as the larger pore size allowed the removal of some organic impurities such as acids and sugars.[126]

Membrane fractionation is a very promising process that would find applications in a range of industries, including the food industry. The challenges lie in controlling the effects of fouling and being able to predict the separation characteristics of membranes towards a range of complex feed components.

3. Materials and methods

The work presented in Chapter 5, together with the Capillary Flow Porometry described in Chapter 4 was carried out by the author during an internship at Nanyang Technological University, Singapore. The zeta potential measurements were taken by the author at Lappeenranta University of Technology. Gel Permeation Chromatography (GPC) was done by the technicians at *Kerry Ingredients and Flavours* (Cam, Gloucestershire) and elemental analysis was done by Stephen Boyer at London Metropolitan University.

3.1. Materials

3.1.1. Gum arabic

Gum arabic used in this project was supplied by *Kerry Ingredients and Flavours* (Cam, Gloucestershire) as a milled, raw material from *Acacia Senegal* trees in Sudan. All the gum used in the project was from the same batch in order to try and minimise variation. The gum was supplied in 25 kg bags and the work in Chapter 4 used gum from one bag and the work in Chapters 5 and 6 used another bag, which had a slightly different AGP content. The feed contained approximately 5% insoluble matter (bark, sand, other plant matter), which was removed by prefiltration whereby the feed was dissolved in RO water and passed through a 50 µm wound stainless steel cartridge filter.

3.1.2. Water

All water used in Chapters 4 and 6 for dissolving the gum arabic, conditioning and cleaning the membranes and general laboratory use was filtered by a Sirion midiRO reverse osmosis system (Veolia Water, Paris, France). The water had a conductivity of 10 – 20 µS cm^{-1}. Milli-Q water (Millipore) was used for feed preparation and filtrations in Chapter 5.

3.1.3. Cleaning agents

Sodium hydroxide used for cleaning the membranes was purchased from Fisher Scientific (Loughborough, UK).

3.1.4. Membranes

The flat sheet, polysulfone and fluoropolymer membranes used were all commercially available and kindly donated by *Alfa Laval* (Nakskov, Denmark). The membranes consisted of an active layer of polysulfone cast onto a polypropylene backing layer. These membranes were coated in glycerol to protect the membrane and this was removed prior to use.

The cellulose acetate membranes were obtained from Sterlitech Corporation (Kent, USA) and were symmetric in structure and made from pure cellulose diacetate. Table 3.1 details all membranes used in this work.

Table 3.1: The manufacturer's codes, active layer material and nominal pore sizes of all the membranes used in this work

Manufacturer product code	**Active layer material**	**Nominal pore size / µm**
MFG1	PS	0.1
GRM-RT5	PS	0.5
GRM-RT8	PS	0.8
MFP5	FP	0.5
-	CA	0.45
-	CA	0.2

Table 3.2 details the operation limits for the membranes used in this work as specified by the manufacturer.

Table 3.2: The operation limits of all the membranes used in this work

Material	**Process**	**pH**	**Temperature / ºC**	**Pressure / bar**
PS	Production	1.5-12	5 - 75	1 - 3
PS	Cleaning	1-13	5 - 75	1 - 3
FP	Production	1 – 11	5 - 60	1 - 3
FP	Cleaning	1 – 11.5	5 - 65	1 - 3
CA	All	4 - 8	Up to 135	1 - 5

3.2. Apparatus

3.2.1. Dead-end filtration

A 200 mL Amicon (Merck Millipore, Billerica, USA) stirred dead-end filtration cell was used for all dead-end experiments. The cell and the cell housing was placed in a water bath set on a stirrer hot plate to maintain the feed temperature and pressure was applied to the feed side of the membrane from an N_2 cylinder. The permeate was collected in a beaker set on a balance. Mass readings were taken every 5 s for PWF and every 20 s during fouling and were recorded using a LabView programme.

3.2.2. Crossflow filtration

M10 filtration system

A DSS Labstak M10 module (now *Alfa Laval*, Nakskov, Denmark) was used for crossflow filtration experiments in Chapters 4 and 6. The plate and frame module consists of 4 plates

connected in series and holds 4 membrane sheets giving a total membrane area 336 cm^2. The plates are stacked together in pairs with a permeate line per pair of plates.

The M10 module was connected to a DSS LabUnit filtration system with a 10 L feed tank and a gear pump as shown in Figure 3.1. The dead volume of the system was 700 mL calculated by dilution of gum arabic solutions. The retentate line could either be returned to the tank or sent to the drain.

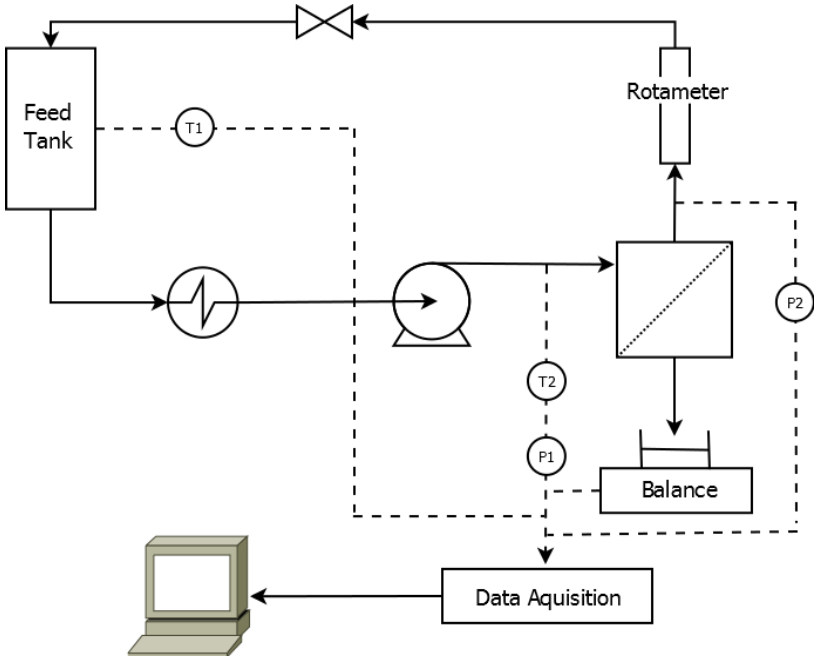

Figure 3.1: P & ID of the M10 filtration system

Stainless steel 316 piping and high durability flexible hosing were used to connect system parts and the module was connected to the piping with ½ inch (12.7 mm) dairy clamps. Nylon clamps were used on the flexible hose permeate lines and drainage lines. The back pressure valve was an EPM diaphragm valve (GEMU Valves GMBH, Ingelfingen-Criesbach, Germany). Together with the variable speed pump, this allowed control of the flow rate / system pressure.

The pump used was an ECO Gearchem variable speed positive displacement pump (Pulsafeeder, NY, USA). A shell and tube heat exchanger (*Alfa Laval*, Nakskov) was used for temperature control fed by hot water from a water bath containing an immersion circulator.

Flow rate was measured with a Rotameter on the retentate side of the module as seen in Figure 3.1. Calibration together with example crossflow velocity calculations are shown in Appendix A and B.

The feed tank was custom built of borosilicate glass (Soham Scientific, Soham, UK) and set approximately 0.5 m above the pump to ensure adequate pump priming. Temperature of the feed was recorded prior to entry into the module with a thermocouple. Pressure was recorded at the feed and retentate sides of the module using pressure transducers of 0 - 7 bar and 0 – 4 bar, respectively, allowing the calculation of TMP and pressure drop across the module.

Permeate flow rate was measured by recording the permeate mass readings every 20 s using a balance (College B3001-S, Mettler Toledo AG, Greifensee, Switzerland). Data from the balance, thermocouple and pressure transducers were collected via a 4-channel remote data acquisition module (model ADAM-4012, Advantech, Milpitas, USA). LabView software was then used to monitor the temperature, control the TMP and record the permeate flux.

Critical flux filtration system

The work in Chapter 5 used a crossflow filtration cell (Ying Kwang Trading, custom made) for measuring critical flux. The cell has parallel plate geometry with an active membrane area of 0.0054 m^2 (0.18 m x 0.03 m) and a channel height of 1.5 mm. A photograph of the filtration cell is shown in Figure 3.2. The set-up consisted of a 10 L feed tank fitted with an overhead stirrer (Panasonic, model MX8G5B) connected to a gear pump (Cole-Palmer, model 74013-45). Feed temperature was maintained at 40 ºC by a heating/cooling system (Polyscience, model 9112) and permeate flux was controlled by a mass flow controller (Brooks Instrument, model 5882). Pressure transducers in the feed, permeate and retentate streams recorded the pressure and from these the TMP and pressure drop across the module could be calculated. All data from the pressure transducers and mass flow controller were recorded using LabView software.

Figure 3.2: Photograph of the filtration cell used in the critical flux chapter of this work

Prefiltration system

The gum arabic dry feed contained approximately 5 wt% insoluble plant matter that needed to be removed prior to filtration. A prefiltration unit was designed and constructed using an Amicon 5 L pressurised feed vessel (Merck Millipore, Billerica, USA) connected to a N_2 cylinder and a PCI- Memtech (Swansea, UK) stainless steel 50 µm cartridge filter and module. The feed tank and filter were connected with stainless steel piping and Swagelok fittings. A system diagram and is shown in Figure 3.3.

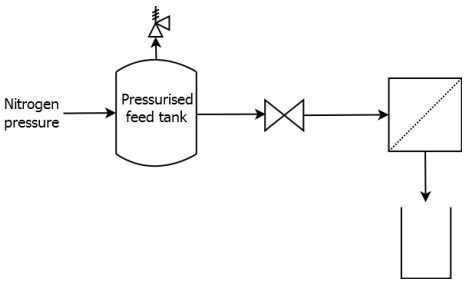

Figure 3.3: P & ID of the prefiltration system

3.3. Experimental procedure

Experimental procedures are given at the start of each results chapter.

3.4. Analytical techniques

3.4.1. Elemental analysis

Samples were sent to London Metropolitan University where they were analysed for their C, H and N content using a Carlo Erba Flash 2000 Elemental Analyser configured for mass fraction of C, H and N. The mass fraction of protein can then be estimated from the fraction of N by multiplying by a conversion factor of 6.6, calculated from the amino acid content of gum arabic.[13]

3.4.2. Viscosity

The viscosity of gum arabic feeds of varying concentrations was measured using a Cannon Fenske Routine 150 viscometry tube (Cannon Instrument Co., State College, Pa, USA) suspended in a water bath set to 40 ºC. The kinematic viscosity determined by this method was then converted to dynamic viscosity by multiplying by the fluid density.

3.4.3. Fourier transform infra-red (FTIR)

Gum arabic samples and virgin, fouled and cleaned membranes were analysed by FTIR using a PerkinElmer 100 FTIR spectrophotometer with a Universal ATR accessory for sampling (PerkinElmer, Waltham Massachusetts, USA).

3.4.4. Scanning electron microscopy (SEM)

Top surface and cross sectional images of membranes were taken using a JEOL SEM6480LV instrument (JEOL, Sollentuna, Sweden) after sputter-coating with gold for 4 minutes using an Edwards S150B sputter coater. Cross sections were obtained using a very sharp blade on the back of the membrane to reduce damage to the active layer caused by pressure from the blade.

3.4.5. Gel permeation chromatography (GPC)

In Chapter 4 dried samples were dissolved to a concentration of 5 mg mL^{-1} in 20 mM Na_2HPO_4 and sent to *Kerry Ingredients and Flavours* (Cam, Gloucestershire) where gel permeation chromatography (GPC) analysis was performed. For the work in Chapters 5 and 6, the samples were sent dry and made up to the correct concentration by the technicians at *Kerry*.

The sample solutions were filtered through 0.2 µm syringe filters before injection into a Malvern GPC-Max instrument fitted with a GE Superose-6 10/300 GL gel column and a triple detection system (right angle light scattering (RALS) / low angle light scattering (LALS), refractive index and UV). The sample run rate was 0.5 mL min^{-1}.

3.4.6. Atomic force microscopy

AFM was carried out using a NanoSurf Easyscan 2 Flux AFM system in dynamic (tapping) mode. The tips used were Budget Sensors Tap 190Al-G with a resonant frequency of 190 Hz and a force constant of 48 N m^{-1}. Areas of 100 μm^2 were scanned with a total of 256 lines each taking 0.7 s. Three different areas were scanned for each sample and the average roughness over the area of each was calculated. The average of these three values was plotted with errors representing ± 1 standard deviation for the 3 areas.

3.4.7. Zeta potential

An Anton Paar SurPass Version 2.20 electrokinetic analyser was used to calculate the zeta potential of membranes' surface from pH 3 – pH 8 by measurement of the streaming potential across the surface. The software used was Attract 2.1.

3.4.8. Contact angle measurements

Contact angle measurements were recorded using a Dataphysics Contact Angle System OCA goniometer (Dataphysics, Germany). The sessile drop method was employed using a Hamilton 1750 TLL 500 µL syringe. Due to the porous nature of the membranes, dynamic tracking mode

was used where 10 images per second were recorded and the first image where the 5 µL Milli-Q water droplet had settled on the surface was used to record the contact angle.

3.4.9. Capillary flow porometry

The bubble point and mean flow pore size of freeze dried virgin, fouled and cleaned 0.1, 0.5 and 0.8 µm PS membranes was measured using a PMI CFP-1500A capillary flow porometer. The data was analysed using Capwin software. Silwick was used as the operating fluid which has a surface tension of 20.1 dynes cm^{-1} and a 'wet up, dry up' program was used up to 150 psi (10.3 bar).

3.4.10. Mastersizer

A Mastersizer 2000 (Malvern, UK) was used to measure the size of insoluble particles in the gum arabic feed to determine the nature of prefiltration that would be required.

4. Fractionation of gum arabic using polysulfone membranes

4.1. Introduction

This work details the performance of 0.1, 0.5 and 0.8 µm PS membranes in the filtration and fractionation of gum arabic. Dead end filtration was employed initially to test if filtration would be possible. This was then scaled up to a larger module operating in crossflow. Operating conditions were modified to obtain the best flux and the solids transmission and gum arabic fractionation was measured for each pore size over a number of foul-clean cycles.

The fouling mechanism was assessed for each pore size and the efficacy of the cleaning protocol was also evaluated. Finally, filtrations were carried out with more concentrated gum arabic (up to 8 wt%) to see if this higher concentration affects the fractionation performance.

4.2. Experimental Methods

4.2.1. Feed preparation

Gum arabic feed was prepared by dissolving the appropriate amount of dry gum arabic in RO water at 40 ºC. The feed was stirred with an overhead stirrer for at least 1 h to ensure complete dissolution. The feed was then prefiltered with a 50 µm wound stainless steel cartridge filter using the prefiltration rig described above.

4.2.2. Dead end filtration

New 0.1 µm PS membranes were used for each experiment and they were conditioned by first soaking in 60 ºC water for 30 min then passing at least 3 cell volumes of 60 ºC water through the membrane in the dead end cell at 1 bar TMP.

PWF measurements were recorded for 1 cell volume at 40 ºC and 1 bar TMP. Fouling tests was then performed using prefiltered 2 wt% gum arabic at 2 bar TMP, 40 ºC and both with and without stirring of the feed in the cell.

Solids content of the feed and permeate were recorded by drying the sample by rotary evaporation at 50 ºC to remove the water and then in an oven overnight at 50 ºC to ensure complete drying. The feed and permeate samples were then analysed by elemental analysis and GPC as detailed in Sections 3.4.1. and 3.4.5.

4.2.3. Crossflow filtration

Membrane conditioning

All PS and FP membranes were coated in glycerol by the manufacturer and this was removed prior to filtration experiments. The membranes were washed with RO at 60 ºC, 1 bar TMP for 0.1 µm membranes and 0.25 bar for 0.5 and 0.8 µm membranes and a CFV of 1 m s^{-1} for 90 minutes. This protocol was determined by Weis *et al.* (2005) to be effective in removing the glycerol coating and this was therefore adopted in this work.[100] Severe flux decline was observed during the conditioning treatment when this was conducted at 0.5 or 1 bar TMP with the 0.5 and 0.8 µm PS membranes, which is suspected to be due to membrane compaction. This is discussed further in Section 4.3.1.

Membrane permeability

The membrane permeability can be described as the gradient of flux vs TMP for the virgin membrane. This was recorded for each of the membranes at the standard operating temperature of 40 ºC, after the membranes were conditioned. The membrane resistance could then also be calculated.

Pure water flux

The PWF of a membrane was recorded before each experiment, after rinsing and after cleaning of the membrane. Details of the full foul – clean cycle conditions are given in 3.3.1.4. The standard conditions of 40 ºC, 0.5 bar TMP and 1.7 m s^{-1} CFV was adopted but optimising of these conditions was carried out and is detailed below.

Diafiltration experiments

All filtrations were performed in diafiltration mode where the permeate was collected and not returned to the feed tank. Instead, RO water was added to the feed tank at the same rate as the permeate flux to prevent feed concentration.

Diafiltrations were carried out using 0.1, 0.5 and 0.8 µm polysulfone (PS) membranes using a M10 module. A relatively low concentration of 2 wt% was chosen initially in order to test the feasibility of the separation of species without additional complications of a much more concentrated feed. Permeate flux was measured using a balance with mass readings taken every 20 s. Permeate samples were taken throughout the experiment and retentate was returned to the tank.

Effect of CFV

The effect of CFV was investigated by carrying out filtrations of 2 wt% gum arabic using 0.1 µm PS membranes at 1.0, 1.45 and 1.7 m s^{-1}. The TMP was 1 bar and the temperature was 40 ºC.

Effect of TMP

The effect of operating at different TMPs was investigated by ramping up the TMP in 10 min, 0.25 bar increments from 0.5 bar to 1.5 bar during filtration of 2 wt% gum arabic with 0.1 µm PS membranes at 40 ºC and 1.7 m s^{-1}. This was repeated 3 times with new, conditioned

membranes each time and averages were taken with error bars representing ± one standard deviation.

Effect of temperature

Filtration of 2 wt% gum arabic using 0.1 µm PS membranes was performed at 25 ºC and 40 ºC. This was repeated 3 times at each temperature and averages were taken. Error bars represent ± one standard deviation. The filtration was carried out with 0.5 bar TMP and a CFV of 1.7 m s^{-1}.

Effect of feed concentration

The effectiveness of gum arabic filtration and fractionation with feed concentrations of 2, 4, 6 and 8 wt% was tested with 0.8 µm PS membranes. Three repeats of each feed concentration were done using new, conditioned membranes each time. The feed was prepared in the same way as the 2 wt% feed and filtration conditions were identical to those described above.

Three consecutive foul-clean cycles with the same membrane were performed with 0.5 µm PS and 0.8 µm PS using 6 wt% feed to see the effect of the build-up of fouling on filtration and fractionation performance.

Resistance calculations

All flux measurements were converted to membrane resistances using the equation:

$$\text{Total Resistance} = \frac{\Delta P}{\mu \text{ x J}} \qquad \text{Equation 4.1}$$

where ΔP is the TMP, μ is the permeate viscosity and J is the flux. Average permeate viscosities were measured as 1.01 mPa s for the 0.8 µm membranes, 0.89 mPa s for the 0.5 µm membranes and 0.83 mPa s for the 0.1 µm membranes. The feed viscosity was 2.15 mPa s.

Hermia modelling

Linearised Hermia modelling was performed on flux decline curves for 0.1, 0.5 and 0.8 µm PS membranes for the filtration of 2 wt% gum arabic under the standard conditions of 40 ºC, 0.5 bar TMP and 1.7 m s^{-1} CFV. The method used was based on the work by Nataraj *et al.* (2008). Using this method, the extent of complete pore blocking was determined by the linearity of a plot of permeate flux vs cumulative permeate volume. Pore constriction was determined by the linearity of a plot of cumulative filtration time / permeate volume vs filtration time and cake formation by a plot of filtration time / permeate volume vs permeate volume. For the mechanism to be considered dominant, the R^2 value for the plot must be greater than 0.99; if no mechanism satisfied this requirement, a combination of mechanisms were assumed to be occurring.[81]

4.2.4. Membrane cleaning

Cleaning of the membrane was carried out by first rinsing the membrane with water at 40 ºC, recording the PWF, cleaning with 0.5 wt% NaOH at 40 ºC, 1 bar TMP (0.1 µm) or 0.5 bar TMP (0.5 and 0.8 µm membranes) and a constant CFV throughout, rinsing with water and recording a final PWF. The conditions for these 7 process steps are detailed in Table 4.1.

Table 4.1: Summary of the conditions for fouling/cleaning cycles

	PWF	**Separation**	**Rinse**	**PWF 2**	**Clean**	**Rinse 2**	**PWF 3**
Feed solution	water	2 wt% gum arabic	water	water	0.5 wt% NaOH	water	water
Time / min	20	various	15	20	20	15	20

4.2.5. Gum arabic analysis

Samples were dried by rotary evaporation using a Buchi Rotavapor R-3 (Büchi Labortechnik AG, Flawil, Switzerland) at 55 ºC then placed in an oven overnight at 50 ºC to ensure complete removal of water. Dried feed, permeate and retentate samples were weighed and concentrations were calculated in wt%. Solids rejection coefficients were calculated using the equation:

$$R = 1 - \frac{C_p}{C_B} \qquad \text{Equation 4.2}$$

where C_p is the gum solids concentration in the permeate and C_B is the gum solids concentration in the bulk feed. Feed and permeate samples were analysed by elemental analysis and GPC to determine the protein and AGP content, respectively.

4.2.6. Membrane characterisation

In order to analyse the surface of the membrane under different conditions, all membranes were freeze dried at different stages of the foul/clean cycle. 'Virgin' membranes were conditioned to remove the glycerol and the PWF was recorded before drying. 'Fouled and soaked' membranes were used to filter gum arabic solutions as detailed above, and then removed from the filtration rig before rinsing. They were placed for 10 minutes in a bucket of RO water to allow gum to diffuse away from the surface and then freeze dried. 'Fouled and cleaned' membranes were freeze dried after the full cycle was completed.

All membranes were then analysed by FTIR, SEM and the membrane porosity was measured. The virgin membranes were also analysed by AFM to determine the surface roughness.

4.3. Characterisation

4.3.1. Virgin membrane characterisation

Conditioning

All membranes in this section underwent hot water conditioning prior to use to remove the protective glycerol coating applied by the manufacturer. The protocol developed by Weis *et al.* (2005) showed that a 90 min washing of the membranes in the filtration rig using 60 ºC water at 1 bar TMP and a CFV of 1 m s^{-1} was sufficient to remove the coating.[100] This protocol was initially adopted for this work but severe flux decline was observed for the 0.5 and 0.8 µm PS membranes at 1 bar TMP. 0.25 bar TMP was therefore adopted.

Some flux decline is expected due to the removal of the glycerol coating transforming the surface from hydrophilic to more hydrophobic. Membrane hydrophobicity is discussed further in Section 4.5.5.. Some flux decline due to membrane compaction was also observed for all membranes during the conditioning treatment. The average flux decline values during conditioning treatment at 0.25 bar are shown in Table 4.2. Conditioning at 1 bar TMP with the 0.5 µm PS membranes resulted in severe flux decline, which is proposed to be due to the more open active layer structure compressing under the higher TMP (Figure 4.2). Argyle (2014) observed similar large flux declines with MF membranes during conditioning treatment.[127] It is also likely that the polymer is more flexible at 60 ºC than at 40 ºC and is therefore more susceptible to compaction. The 0.8 µm membranes also showed flux decline with conditioning at 1 bar TMP, but this is masked by the error bars due to the large membrane to membrane variation.

Table 4.2: Flux decline during the hot water conditioning treatment of 0.1, 0.5 and 0.8 µm PS membranes at 60 ºC, 0.25 bar TMP and 1 m s^{-1} CFV

Membrane pore size / µm	**Flux decline during hot water conditioning (0.25 bar TMP) / LMH**
0.1	16
0.5	650
0.8	639

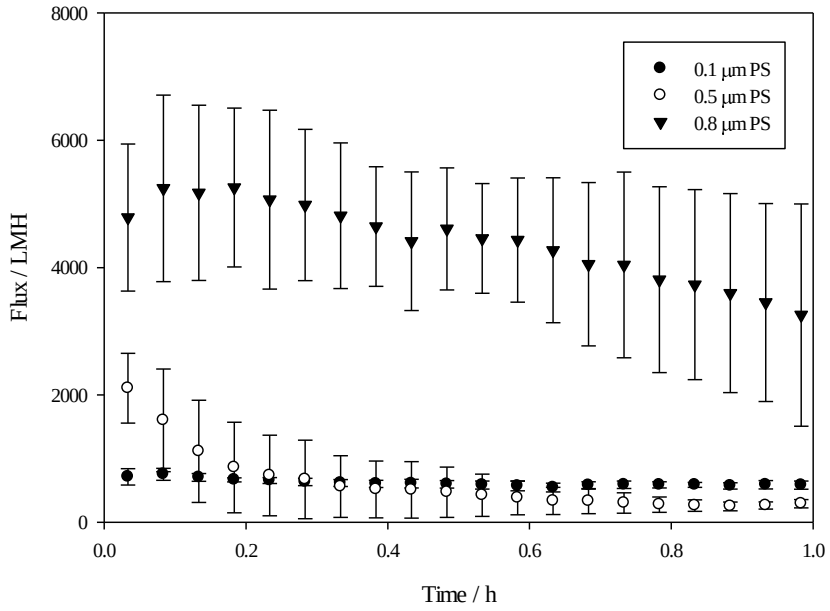

Figure 4.1: Flux decline during the hot water conditioning of PS membranes at 1 bar TMP

Permeability

The membrane permeability for 0.1, 0.5 and 0.8 µm PS membranes was measured by carrying out TMP stepping with RO water for each membrane after conditioning (Figure 4.2). The permeability is equal to the gradient for this curve and these values are displayed in Table 4.3 together with the membrane resistances.

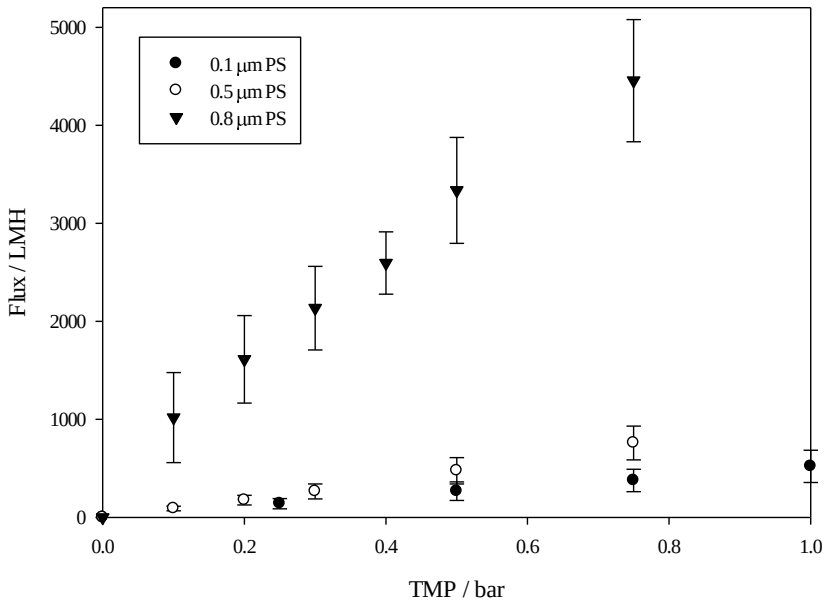

Figure 4.2: Flux vs TMP curves for 0.1, 0.5 and 0.8 µm PS membranes measured at 40 ºC and 1 m s^{-1} CFV

Table 4.3: Permeability and membrane resistances for 0.1, 0.5 and 0.8 µm PS membranes after conditioning treatment.

Membrane	**Membrane resistance / x 10^{12} m^{-1}**	**Permeability / L m^{-2} h^{-1} bar^{-1}**
0.1 µm PS	1.1 ± 0.33	502 ± 151
0.5 µm PS	0.55 ± 0.15	997 ± 269
0.8 µm PS	0.09 ± 0.02	6394 ± 1439

Membrane porosity

From capillary pore experiments, the bubble point and mean flow pore size of the 0.1, 0.5 and 0.8 µm PS membranes were measured. This was repeated 5 times on different sections for each membrane. Table 4.4 shows the mean values and standard deviations.

Table 4.4: Capillary pore data for virgin 0.1, 0.5 and 0.8 µm PS membranes

Membrane	Bubble point pore diameter / µm	Mean flow pore diameter / µm
0.1 µm PS	0.19 ± 0.03	0.15 ± 0.03
0.5 µm PS	0.68 ± 0.14	0.44 ± 0.19
0.8 µm PS	1.62 ± 0.15	0.92 ± 0.07

The bubble point is the pressure at which gas first flows through the membrane and the corresponding pore diameter represents the largest pore size within the membrane. Table 4.4 shows the largest pore size to be 190 %, 136 % and 203 % larger than the nominal pore size for the 0.1, 0.5 and 0.8 µm membranes, respectively.

The mean flow pore diameter is the diameter of the pores where the gas flow through the membranes is at 50 %. It is therefore a measure of the average pore size. Both the 0.1 and 0.8 µm membranes have average pore sizes larger than that quoted by the manufacturer, but the 0.5 µm membrane has a mean flow pore diameter of only 0.44 µm. This may result in a lower than expected flux through the 0.5 µm PS membrane, although the pore size does not give information about the membrane porosity or tortuosity, which will also affect the flux.

Membrane structure

All three pore sized membranes studied in this chapter are manufactured by *Alfa Laval* and consist of a polysulfone active layer with a polypropylene backing layer. Figure 4.3 shows cross sectional SEM images of the three membranes after conditioning and freeze drying.

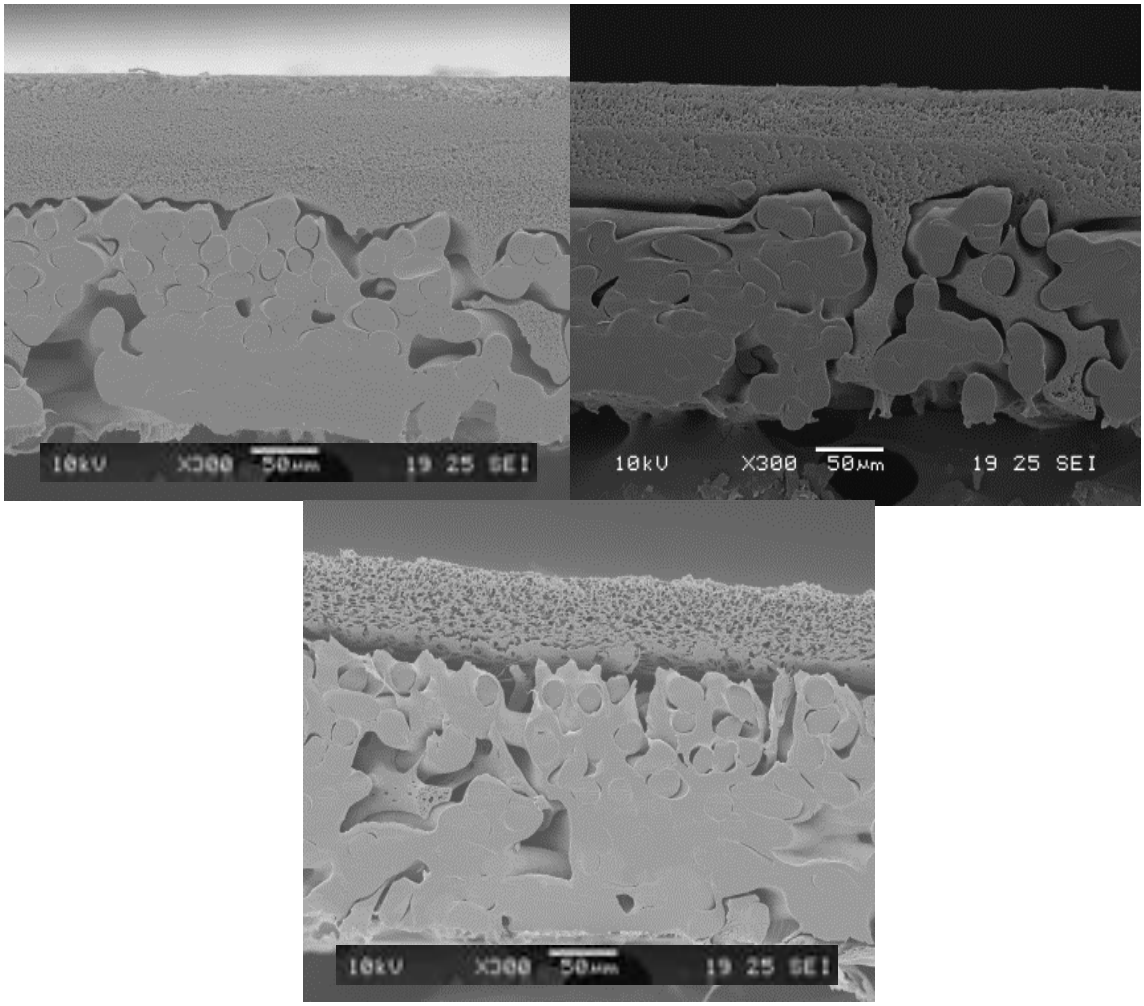

Figure 4.3: Cross sectional images of 0.1 (top, left), 0.5 (top, right) and 0.8 (bottom) µm PS membranes

The active layer can clearly be seen in the SEM images in Figure 4.3. The difference in pore size is also clear with the 0.8 µm structure being much more open than the 0.5 µm and the 0.1 µm membranes. The support layer has been slightly compressed due to the cross-sectioning process but the difference between the two layers is clear.

Surface roughness

Atomic force microscopy was used to measure the roughness of the surface of each of the three conditioned membranes. Three 100 μm^2 areas of each membrane were measured and averages were taken. The results are shown in Table 4.5.

Table 4.5: Average surface roughness of virgin 0.1, 0.5 and 0.8 µm PS membranes measured by AFM

Membrane	**Surface roughness / nm**
0.1 µm PS	204.2 ± 102.9
0.5 µm PS	120.6 ± 17.1
0.8 µm PS	138.6 ± 5.4

The 0.1 µm PS membrane is much more variable in the surface roughness than the 0.5 and 0.8 µm PS. Although this will average out over the 336 cm^2 total filtration area, studies have shown that membranes with a rougher surface structure can be prone to fouling as discussed in Section 2.5.3.

4.3.2. Feed characterisation

Insoluble solids content

The gum arabic used in this work was supplied by *Kerry Ingredients and Flavours* (Cam, Gloucestershire, UK) as a milled, raw product from *Acacia Senegal* trees in Sudan. This material contained insoluble plant matter which was removed by prefiltration. Particle size analysis of the dissolved raw feed showed that the majority of the insoluble matter is > 50 µm (Figure 4.4), so prefiltration of this size is sufficient. A smaller filter could have been used, but 50 µm is the prefilter size used in the process plant at *Kerry Ingredients*, so this was chosen to provide an industrially relevant feed.

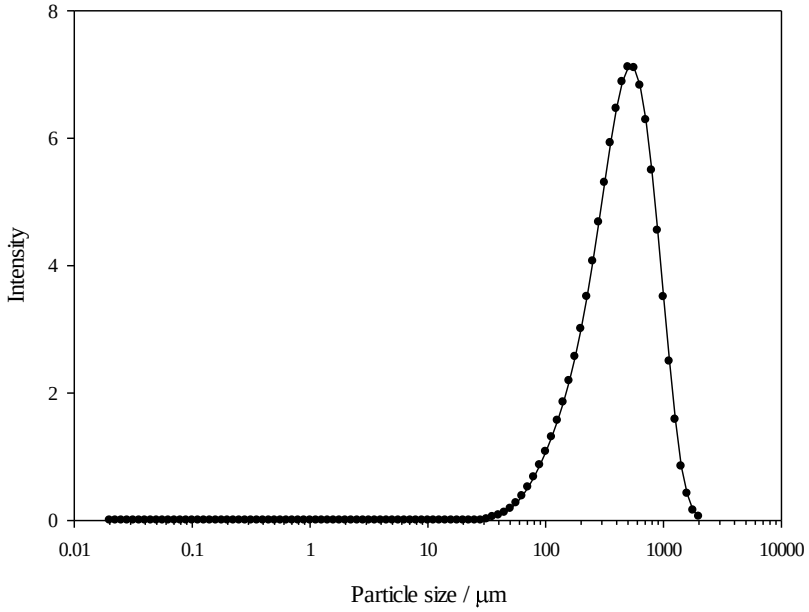

Figure 4.4: Particle size analysis of raw gum arabic feed showing the insoluble matter content

The raw gum arabic contains an average of 5 wt% insoluble matter of particle size greater than 50 μm. This was measured by dry weight of a 2 wt% gum arabic solution before and after prefiltration with a 50 μm stainless steel filter. Future feed was prepared to take into account this 5 wt% insoluble matter.

pH

The pH of gum arabic solution was measured at different feed concentrations and the data are displayed in Figure 4.5.

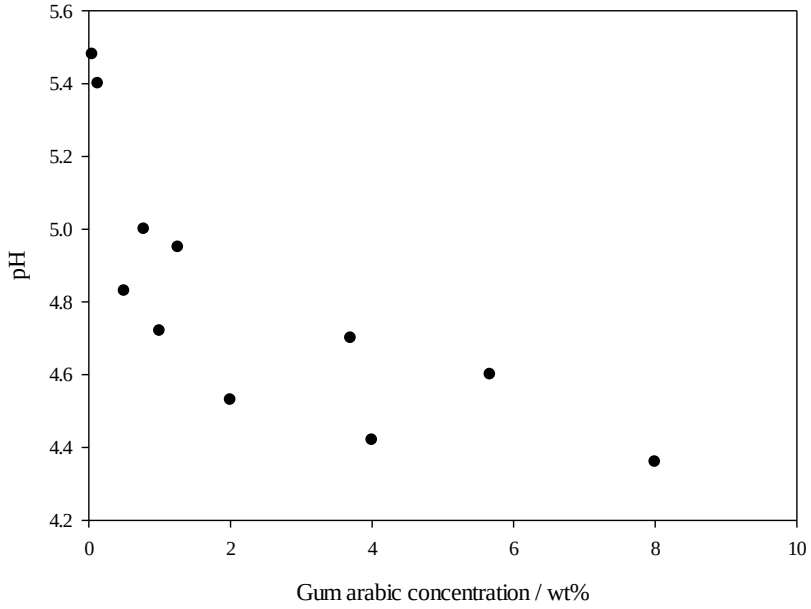

Figure 4.5: pH of gum arabic solutions of different concentrations

Figure 4.5 shows that gum arabic is a slightly acidic substance in solution due to the presence of glucuronic acid groups. The pH decreases as the gum arabic concentration increases but even at very low gum arabic concentrations the pH is approximately pH 5.5.

Elemental analysis (C, H and N)

The C, H and N content of the prefiltered was measured and the results are show in Table 4.6.

Table 4.6: Elemental analysis of the prefiltered gum arabic feed

C Mass fraction	**H Mass fraction**	**N Mass fraction**	**Protein Mass fraction**
0.389 ± 0.007	0.067 ± 0.005	0.007 ± 0.002	0.049 ± 0.015

The protein mass fraction is calculated from the %N using a conversion factor of 6.6 [13]. The batch of gum arabic used in this work has a protein content of about 5 %.

Gel permeation chromatography

The AGP mass fraction of gum arabic feed (prefiltered and dried) was measured to be 0.177 ± 0.0113 by gel permeation chromatography for the majority of the work in this chapter. A different 25 kg sack was used for the work in Section 4.6 on differing the feed concentration and the AGP mass fraction of that batch was 0.146 ± 0.009. The exact AGP content of the feed was measured for each experiment.

Viscosity

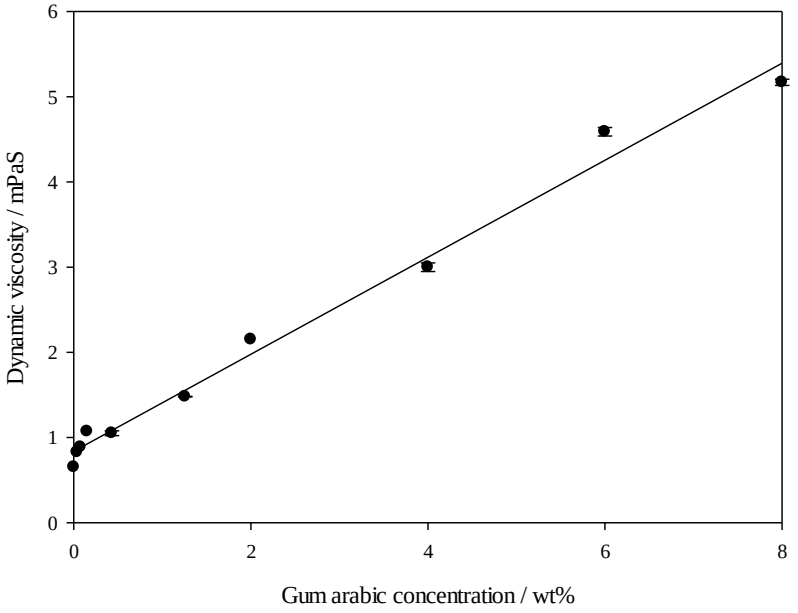

Figure 4.6: The viscosity of gum arabic feed at different concentrations carried out at 40 ºC

Figure 4.6 shows the increase in feed viscosity with concentration is linear within the range utilised in this work. The viscosity of 2 wt% gum arabic after prefiltration was measured to be 2.15 mPa s at 40 ºC.

4.4. Dead end filtration

Dead-end filtration was used initially to test the feasibility of gum arabic filtration and whether or not fractionation would be possible. 0.1 µm PS membranes were employed and 2 wt%

prefiltered gum arabic was used as the feed. Figure 4.7 shows the membrane resistance and the fouling resistance with the gum arabic feed over 30 min filtration both with stirring of the feed and without.

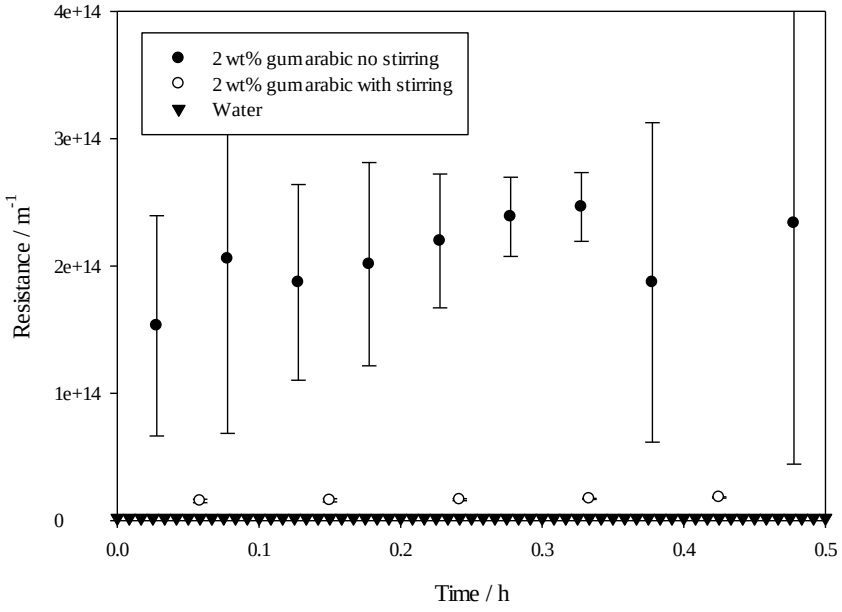

Figure 4.7: Membrane and total fouling resistance changes over 30 min dead end filtration

The filtration of gum arabic was repeated with 3 different 0.1 µm PS membranes and the error bars represent ± 1 standard deviation. Figure 4.7 clearly shows the importance of disruption of the boundary layer to aid filtration. The lack of stirring of the feed leads to rapid build-up of rejected species at the surface of the membrane, inhibiting mass transfer and causing the resistance values to be an order of magnitude higher than in the case with stirring. Stirring of the feed close to the membrane surface creates a pseudo-crossflow velocity, disrupting the formation of a dense boundary layer. Figure 4.8 displays the same data but without the data for the no stirring experiment.

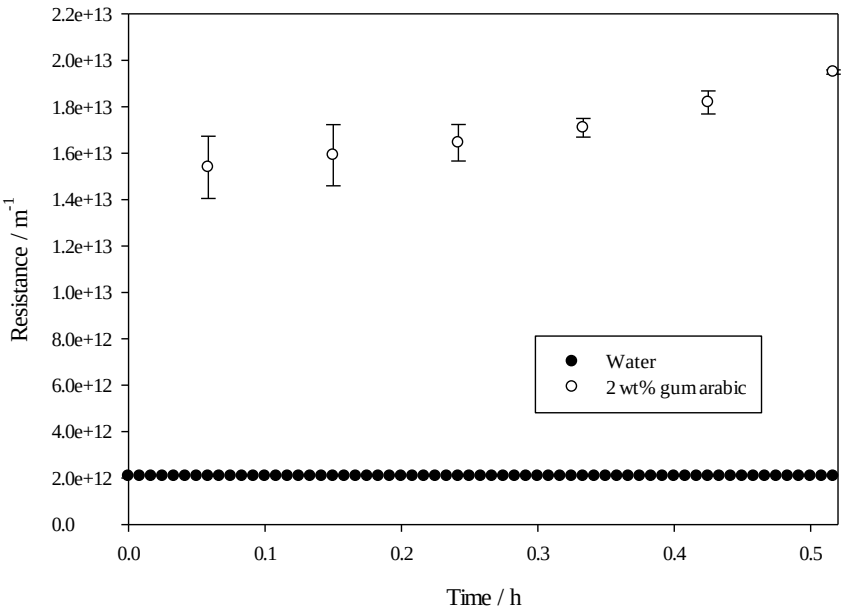

Figure 4.8: Membrane and total fouling resistance changes over 30 min dead end filtration

The fouling resistance is nearly an order of magnitude greater than the membrane resistance measured from the PWF. This is due to concentration polarisation and membrane fouling, which increase over time as the feed concentrates. The stirring of the feed at the membrane surface has a great effect on reducing the accumulation of rejected species at the surface (as seen above) but the nature of dead-end filtration is such that fouling is hard to avoid.

Feed and permeate samples from the stirred filtration experiments were dried and the solids, AGP and protein content of each was measured and are displayed in Table 4.7.

Table 4.7: Solids content, AGP and protein mass fraction of dried feed and permeate samples from the dead end filtration of 2 wt% gum arabic using 0.1 µm PS membranes

	Feed	**Permeate**
Solids content / wt%	2	0.058 ± 0.034
AGP mass fraction (dehydrated)	0.176 ± 0.017	0.064 ± 0.002
Protein mass fraction (dehydrated)	0.042 ± 0.002	0.129 ± 0.006

The results from the dead end filtration show that gum arabic fractionation occurs with 0.1 µm PS membranes. The dried permeate had a lower AGP content than the dried feed indicating that the high molecular weight AGP complex is being rejected by the membrane. The protein content of the dried permeate is also higher than in the feed, meaning that protein is passing through the membrane more easily than the other species. As the only protein-containing species in gum arabic are AGP and GP, and AGP is being rejected by the membrane, the glycoprotein must be passing easily into the permeate stream. This is the lowest MW species so it appears that fractionation by size exclusion is occurring in this instance.

Overall solids transmission though the membrane, however, was very low at less than 3 wt%. This value needs to be greater in order to viably fractionate large quantities of gum arabic.

4.5. Crossflow filtration

4.5.1. Filtration performance

The aim of this work was to determine the feasibility of using polymeric membranes to separate the different fractions in gum arabic. After the initial positive results from the dead-end experiments, filtrations were performed in crossflow to determine if the addition of a CFV would allow greater solids transmission. 0.1, 0.5 and 0.8 µm PS membranes in diafiltration

mode were tested to try and remove the low molecular AG and GP fractions whilst retaining the AGP fraction in the retentate steam. Assessment of the effects of fouling on the separation of species was also carried out.

Gum arabic solutions of 2 wt% in water were filtered through 0.1, 0.5 and 0.8 µm polysulfone membranes. The raw gum contained about 5 wt% insoluble matter of size > 50 µm, which was removed during the prefiltration. The feed was prepared to be 2 wt% after this prefiltration.

The effect of crossflow velocity on flux

Figure 4.9 demonstrates the effect of crossflow velocity on resistance over time during the diafiltration of 2 wt% gum arabic through a 0.1 µm PS membrane at 40 ºC and 1 bar TMP. Five repeats of the filtration at 1.45 m s^{-1} were performed and the error bars represent ± 1 standard deviation.

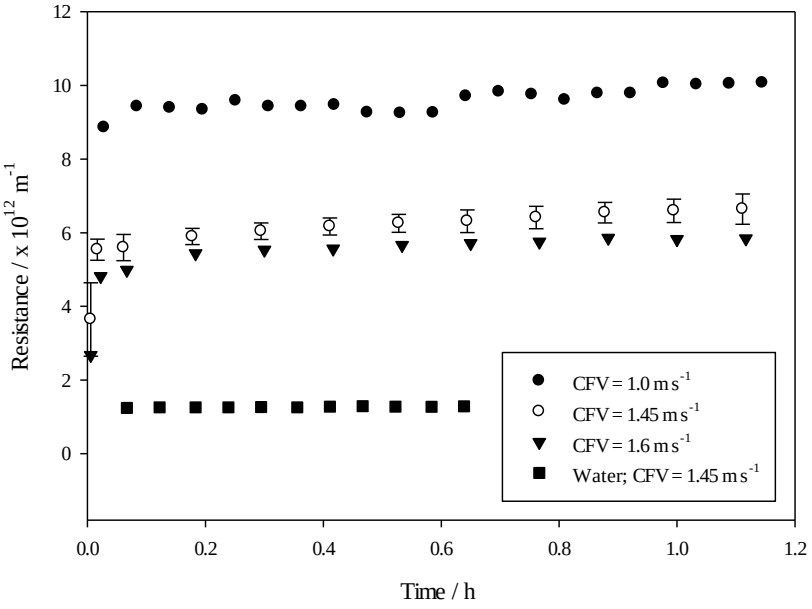

Figure 4.9: Resistance curves for 2 wt% gum arabic solution at 40 ºC and 1 bar TMP. Polysulfone flat sheet membrane: 336 cm^2 area and 0.1 µm pore size. Resistances correspond to average fluxes of 45, 70 and 77 LMH for CFV of 1.0, 1.45 and 1.7 m s^{-1}, respectively. Also shown is the pure water hydraulic resistance. At 1 bar TMP and 40 ºC, this corresponds to an average flux of 434 LMH

The crossflow velocities 1.0 m s^{-1}, 1.45 m s^{-1} and 1.7 m s^{-1} correspond to Reynolds numbers through the module channels of 2000, 2900 and 3400 for water and 600, 900 and 1000 for 2 wt% gum arabic. The membrane resistance was found to be 1.32 x 10^{12} m^{-1} and the resistance of the fouled membrane after rinsing with water is 2.90 x 10^{12} m^{-1}. This gives a value of 1.58 x 10^{12} m^{-1} for the gum fouling not removed by water rinsing (for the 1.45 m s^{-1} CFV data). Figure 4.9 shows a considerable increase in flux when operating at higher CFVs. This is possibly due to the increased shear in the flow channel at the membrane surface, reducing the build-up of surface fouling and allowing a greater flux.

The effect of TMP on flux

Previous work by Decloux *et al.* (1996) and Bechervaise (2013) has shown that operating at lower TMP is more effective at maintaining flux for longer periods of time during the filtration of gum arabic with ceramic membranes.[58, 59] Experiments were carried out to determine if the same is true for polymeric membranes also. Figure 4.10 shows how flux changes as the TMP is increased incrementally during the filtration of 2 wt% gum arabic with 0.1 µm PS membranes at 40 ºC and a CFV of 1.7 m s^{-1}. The filtration was measured for 10 min at each pressure as this was considered long enough for a steady state to be reached, based on previous filtration experiments. This was repeated three times and averages were taken. Error bars represent ± 1 standard deviation.

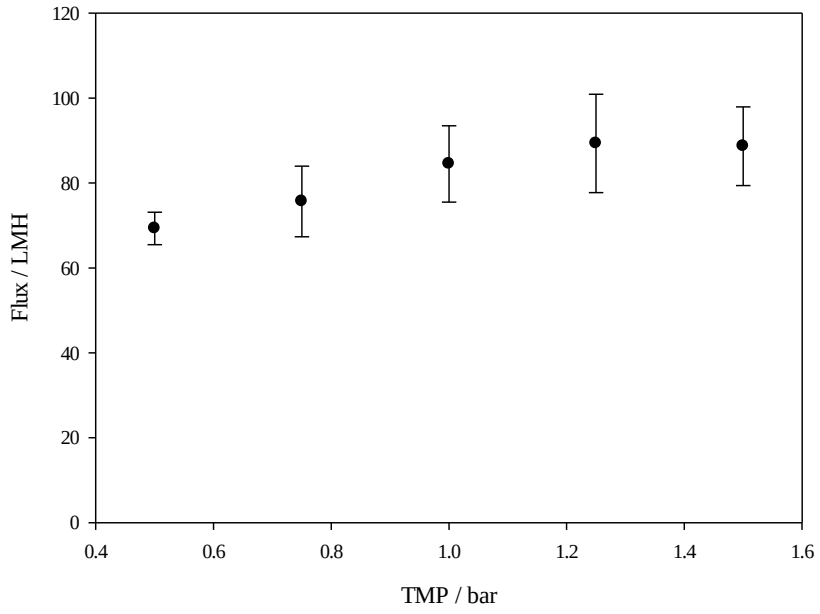

Figure 4.10: The effect of TMP on flux during the filtration of 2 wt% gum arabic using 0.1 µm PS membranes at 40 ºC and a CFV of 1.7 m s^{-1}

There is a slight increase in flux from 0.5 – 1.5 bar but a limiting flux is reached at about 1.25 bar. Future experiments are conducted at 0.5 bar TMP in order to remain within the pressure-limited region.

The effect of temperature on flux

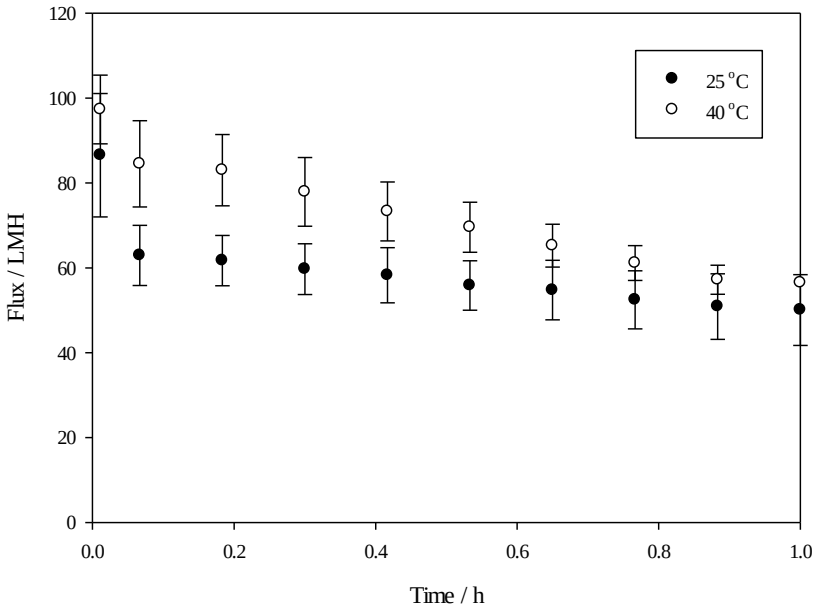

Figure 4.11: Flux curves for the filtration of 2 wt% gum arabic at 25 ºC and 40 ºC using 0.1 µm PS membranes. The CFV was 1.7 m s^{-1} and the TMP was 0.5 bar

Figure 4.11 demonstrates that operating at 40 ºC rather than 25 ºC gives a slight increase in flux, although the drop in flux over time appears to be steeper at 40 ºC. The higher flux can be attributed to the reduction in viscosity associated with the higher temperature, and as gum arabic processing is carried out at temperatures greater than 25 ºC, 40 ºC was chosen for future experiments. Higher temperature would decrease the viscosity further but keeping gum solutions at greater than 50 ºC for long periods of time can cause polymerisation and aggregation of the gum species.[26, 43]

The effect of pore size on flux

As the crossflow velocity of 1.7 m s^{-1} showed the highest flux during filtration, this was adopted for further experiments. Experiments with 0.1 µm membranes were performed at 1 bar TMP but 0.5 bar was used for 0.5 and 0.8 µm filtrations. A temperature of 40 ºC was used.

Using these conditions, filtration of 2 wt% gum arabic was carried out using 0.1, 0.5 and 0.8 µm PS membranes.

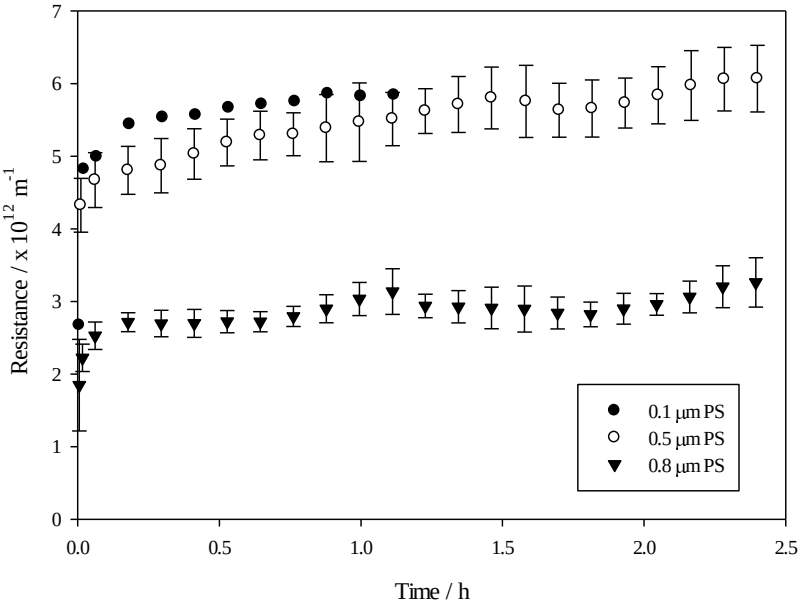

Figure 4.12: Resistance curves for the diafiltration of 2 wt% gum arabic through 0.1, 0.5 and 0.8 µm PS membranes at 40 ºC and 1.7 m s^{-1} CFV. These correspond to average fluxes of 77 LMH for 0.1 µm (1 bar TMP), 36 LMH for 0.5 µm (0.5 bar TMP) and 58 LMH for 0.8 µm (0.5 bar TMP)

As can be seen from Figure 4.12, the fouled resistance of the 0.5 µm membranes is higher than the 0.8 µm membranes as expected due to the smaller pore diameter. However, the 0.1 and 0.5 µm membranes demonstrate similar resistances during filtration. This is suspected to be due to gum aggregates of similar size to the 0.5 µm membrane pore size causing pore blocking and increasing the resistance compared to the 0.1 µm membranes. Renard *et al.* (2012) studied the structure of gum arabic AGP and found that some larger particles were up to 100 nm in length.[30] Aggregations of several particles of this size could block the pores in 0.5 µm membranes. The 0.5 µm PS membranes also had a mean flow pore diameter of only 0.44 µm PS whereas the 0.1 and 0.8 µm membranes both had mean flow pore diameters higher than that quoted by the

manufacturer. This may be part of the reason for the higher than expected resistance observed with the 0.5 µm membranes. Analysis of the fouling mechanisms is given in Section 4.5.3..

4.5.2. Gum arabic fractionation

Solids rejection

Permeate samples were taken at intervals throughout the crossflow diafiltrations of 2 wt% gum using 0.1, 0.5 and 0.8 µm PS membranes. These samples were dried and weighed to determine the solids content. Feed solids content was also verified by this method.

Figure 4.13 shows how the rejection of solids by 0.1, 0.5 and 0.8 µm PS membranes increases over time during the experiment as a fouling layer builds up and adds another layer of filtration. Both the 0.1 and 0.5 µm membranes show rejection of over 95% from the beginning of the filtration, suggesting that the pore size is sufficiently small to reject a high proportion of the gum particles. The 0.8 µm membrane allows a greater transmission of solids over the first hour of filtration. As the aim is to separate the low MW AG and GP from the AGP, a high transmission of the AG and GP into the permeate is desired.

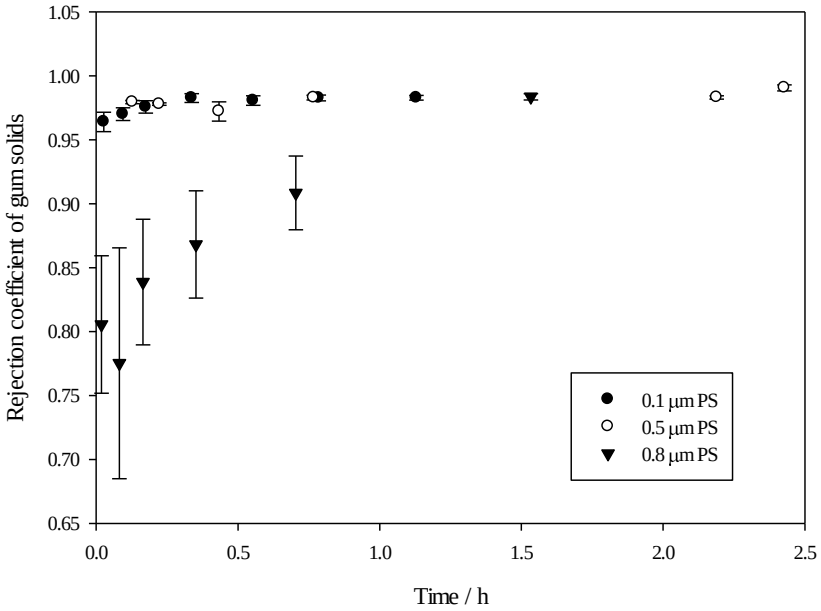

Figure 4.13: Solids rejection coefficients over time during filtration of 2 wt% gum arabic through 0.1, 0.5 and 0.8 µm PS membranes

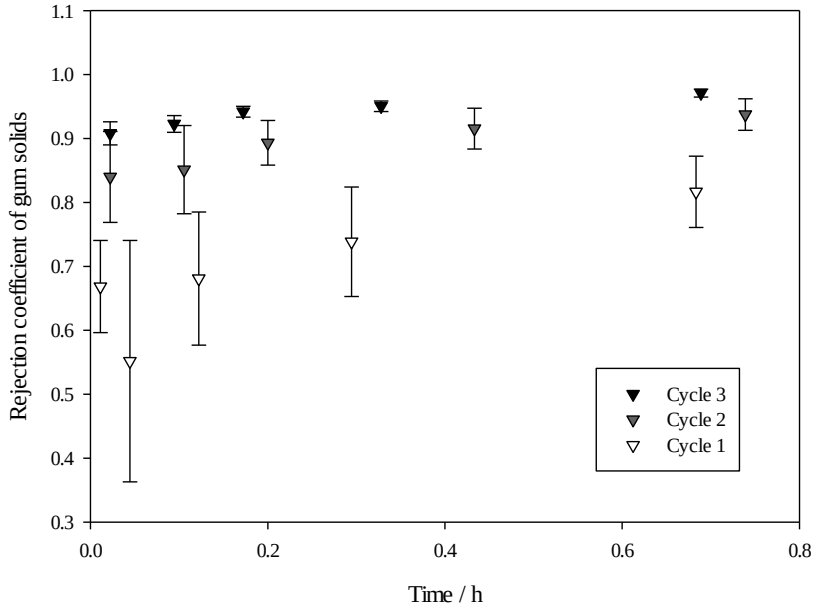

Figure 4.14: Solids rejection by 0.8 µm membrane during foul-clean cycles 1 (virgin membrane), 2 and 3

Figure 4.14 shows how the overall gum solids rejection by 0.8 µm membranes increases over time throughout the fouling experiment and also after each foul-clean cycle. The initial solids rejection seen with a virgin membrane is less than 70 %, but this increases to more than 90 % after the third cycle. This suggests that a considerable amount of in-pore or surface fouling is building up and is not being removed by the NaOH clean, causing a greater rejection of solids with each cycle.

Elemental analysis

Permeate and feed samples were taken from each of the experiments, dried and the protein mass fraction was measured by elemental analysis and the AGP content by triple detection GPC.

Table 4.8: The protein content of dried feed and permeate samples from diafiltrations of 2 wt% gum arabic through 0.1, 0.5 and 0.8 µm PS membranes

Membrane pore size / µm	**Feed protein mass fraction**	**Permeate protein mass fraction**
0.1	0.054 ± 0.010	0.127 ± 0.020
0.5	0.051 ± 0.003	0.110 ± 0.005
0.8	0.051 ± 0.017	0.083 ± 0.029

Table 4.8 shows the protein content of the dried, prefiltered feed and permeate samples based on the mass fraction of N from elemental analysis. The error bars represent ± one standard deviation. Transmission of protein is seen through all three membranes and this is proposed to be due to the low MW glycoprotein (GP) passing through the membrane in preference to the larger arabinogalactan (AG) and arabinogalactan-protein complex (AGP). The percentage protein seen in the permeate reduces as the membrane pore size increases. This is because larger overall solids transmission is seen with the larger pore sizes, and so more of the protein-

free arabinogalactan fraction is passing through the membrane, effectively reducing the protein concentration.

Gel permeation chromatography

Table 4.9: The AGP content of dried feed and permeate streams for diafiltration experiments carried out using 0.1, 0.5 and 0.8 µm PS membranes at 40 ºC

Membrane pore size / µm	**Feed AGP mass fraction**	**Permeate AGP mass fraction**
0.1	0.19 ± 0.025	0.0105 ± 0.01101
0.5	0.195 ± 0.021	0.064 ± 0
0.8	0.197 ± 0.005	0.145 ± 0.052

Table 4.10: The AGP content of dried permeate streams from consecutive diafiltration experiments carried out using a 0.8 µm PS membrane at 40 ºC

Cycle Number	**1**	**2**	**3**
Permeate AGP mass fraction	0.22 ± 0.014	0.14 ± 0.012	0.07 ± 0.012

Table 4.9 shows the AGP content of feed and permeate samples taken from 0.1, 0.5 and 0.8 µm PS diafiltration experiments. It can be seen that the 0.1 µm pore size is suitable to reject almost all the AGP within the gum. This is promising; however the low overall solids transmission seen in Figure 4.13 is such that diafiltration experiments would need to be run for a very long time, using large quantities of water in order to sufficiently remove enough of the low MW components and concentrate the AGP. The 0.5 and 0.8 µm PS membranes demonstrate lower rejection of AGP although some AGP is rejected in both cases.

Table 4.10 demonstrates the effect of the build-up of fouling on the 0.8 µm PS membranes, which increases the rejection of AGP after 3 foul – clean cycles. A virgin 0.8 µm membrane (cycle 1) does not selectively reject the AGP but after three cycles a marked increase in AGP rejection is seen. The challenge is to balance high overall solids transmission with selective rejection of AGP, but these data show that gum arabic fractionation by microfiltration is possible.

4.5.3. Multiple foul-clean cycles

The diafiltration of 2 wt% gum arabic was repeated over 5 cycles to assess the membrane performance over time and the effectiveness of the cleaning operations.

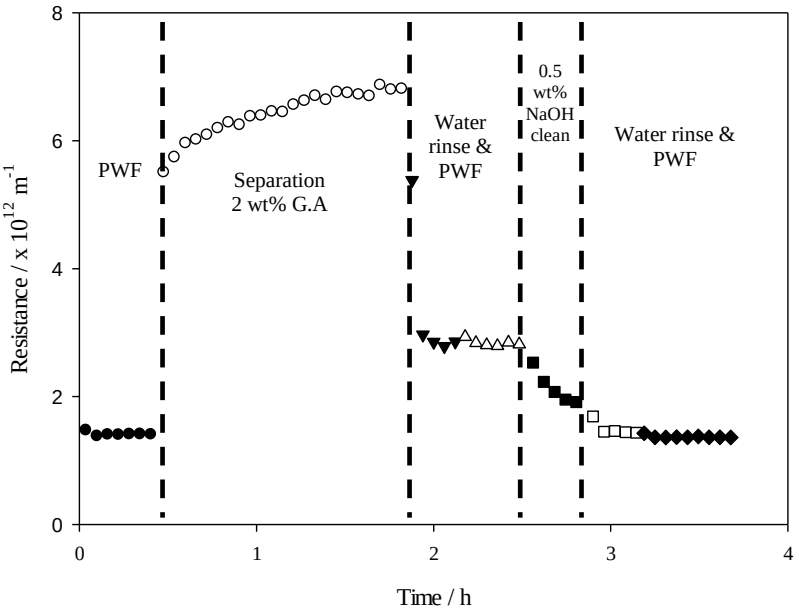

Figure 4.15: A foul-clean cycle profile for 2 wt% gum arabic using a 0.1 µm PS membrane

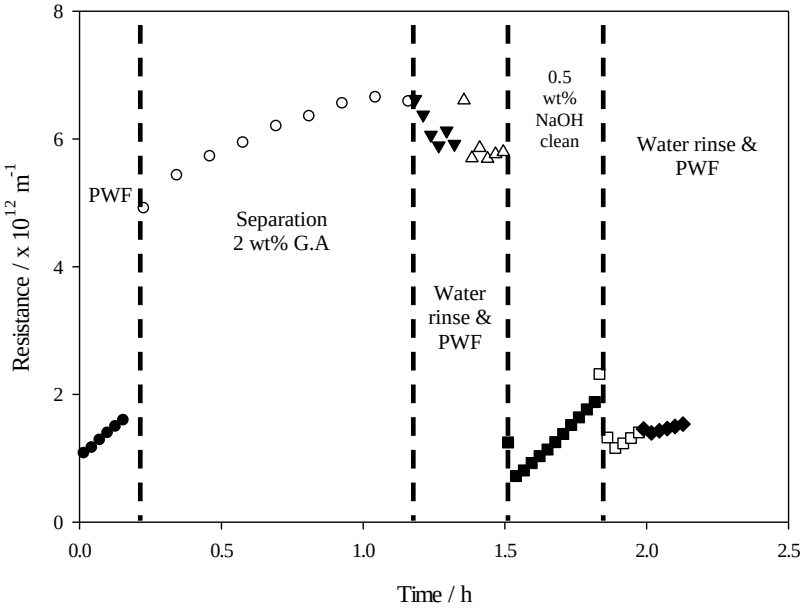

Figure 4.16: A foul-clean cycle profile for 2 wt% gum arabic using a 0.5 µm PS membrane

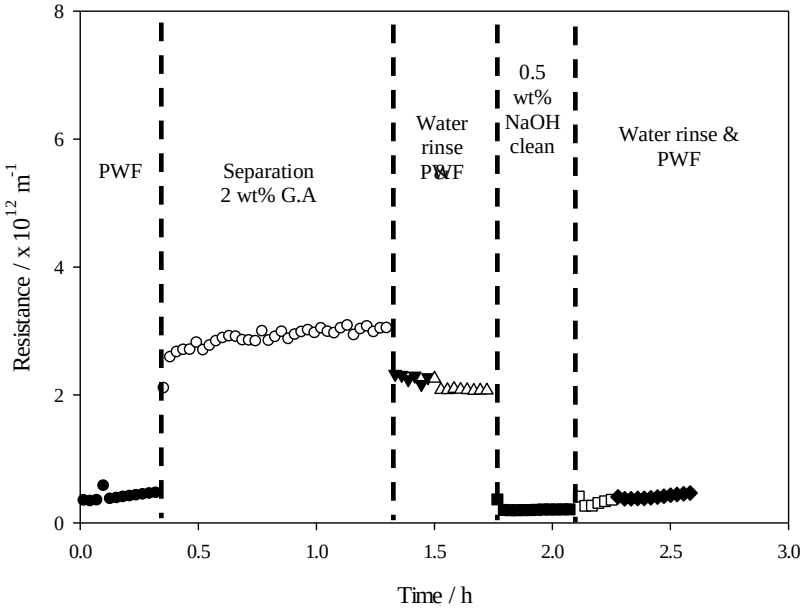

Figure 4.17: A foul-clean cycle profile for 2 wt% gum arabic using a 0.8 µm PS membrane

Figure 4.15 shows an example foul-clean profile for 0.1 µm PS membranes, demonstrating good recovery of flux after cleaning as the resistance drops back to the initial value. A similar profile is seen with the 0.5 µm PS membranes in Figure 4.16, although the water rinse does not recover the flux as well as with the 0.1 µm PS membranes. This suggests that the fouling is not as easy

to remove by hydraulic action only. An increase in resistance is also seen during the NaOH clean with the 0.5 µm PS membrane, which could be due to swelling of gum species approximately the same size as the pores. Proteinaceous deposits are known to swell in alkali solutions[128] and this would further constrict the pore causing an increase in resistance. The TMP during cleaning may also force the swollen gum further into the pores. The effect of cleaning is further discussed in Section 4.5.4.. Figure 4.18 shows how the a layer of concentrated gum arabic (50 wt%) swells in 0.5 wt% NaOH solution over time. The solution was left for 1 h so that the swelling was evident in the photograph but swelling will occur more quickly than this on the membrane surface. A photo of the swelling / species breakdown after 24 h is also shown. The swelling is likely to be due to breakdown of the intermolecular forces within the gum proteins, which may be followed by hydrolysis of the peptide chains.[25, 128-130]

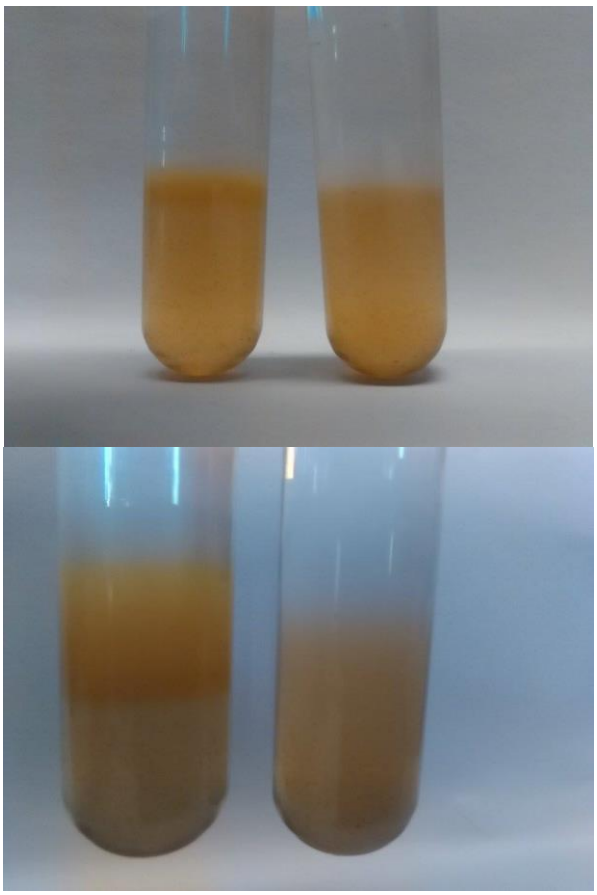

Figure 4.18: Swelling of 50 wt% gum arabic in 0.5 wt% NaOH (left) and water (right) after 1 h (top) and 24 h (bottom)

The profile for the 0.8 µm membrane shows lower resistances than the 0.1 and 0.5 µm PS membranes. The water rinsing removes some of the fouling but the NaOH is very effective at reducing the flux. It is suspected that the 0.8 µm PS membrane will demonstrate in pore fouling due to the larger pore diameter, the pores are larger, however than the 0.5 µm membrane so swelling appears not to cause constriction. The swelling of the gum arabic deposits would decrease fouling density and allow easier removal.

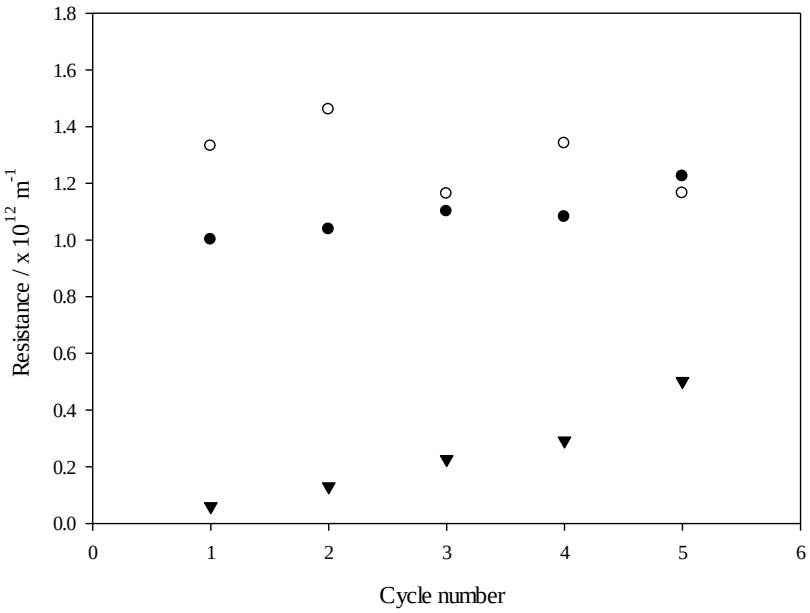

Figure 4.19: Average membrane resistances for 0.1, 0.5 and 0.8 µm PS membranes before each fouling cycle

Figure 4.19 shows how the membrane resistance changes after multiple foul-clean cycles for 0.1, 0.5 and 0.8 µm PS membranes, indicating the amount of irreversible fouling after each cycle. Cycle 1 represents the clean membrane resistance calculated from the PWF. Cycle 2 is the PWF after the first foul-clean cycle etc. The 0.5 µm membrane shows a greater resistance than the 0.1 µm membrane and this is likely to be due to a susceptibility of the membrane to compress over time, as discussed in Section 4.3.1, combined with greater in pore fouling. During the conditioning process (using water), all membranes demonstrate a slight reduction in flux, due to the removal of the hydrophilic glycerol coating as observed previously in the group

by Weis *et al.* (2005).[100] This was observed less for the less open 0.1 µm PS structure and had a more dramatic effect on flux with the 0.8 µm PS membranes, which suggests there is some membrane compaction in addition to the increase in hydrophobicity.

The 0.1 µm membrane shows a slight increase in resistance over the 5 cycles, but the 0.8 µm membrane shows more irreversible fouling as the resistance increases from less than 1 x 10^{11} m^{-1} to nearly 6 x 10^{11} m^{-1} over 5 cycles. The resistances were then broken down into rinsible fouling resistance ($R_{F(rinse)}$; fouling removed by water rinsing), cleanable fouling resistance ($R_{F(clean)}$; fouling removed by cleaning with NaOH) irreversible fouling resistance ($R_{F(irr)}$) ; the resistance of deposits not removed by cleaning with NaOH) and membrane resistance (R_m) and the data for cycles 1-3 for all three pore sized membranes are shown in Figures 4.20, 4.21 and 4.22. Concentration polarisation was found to contribute insignificantly to the total resistance. This was determined by turning off the pump during filtration of gum arabic (after 20 min filtration) for 1 min. No increase in flux was seen when the pump was turned back on indicating that no concentration polarisation occurs. This is likely to be due to the high MW of the gum arabic species making diffusion rates slow.

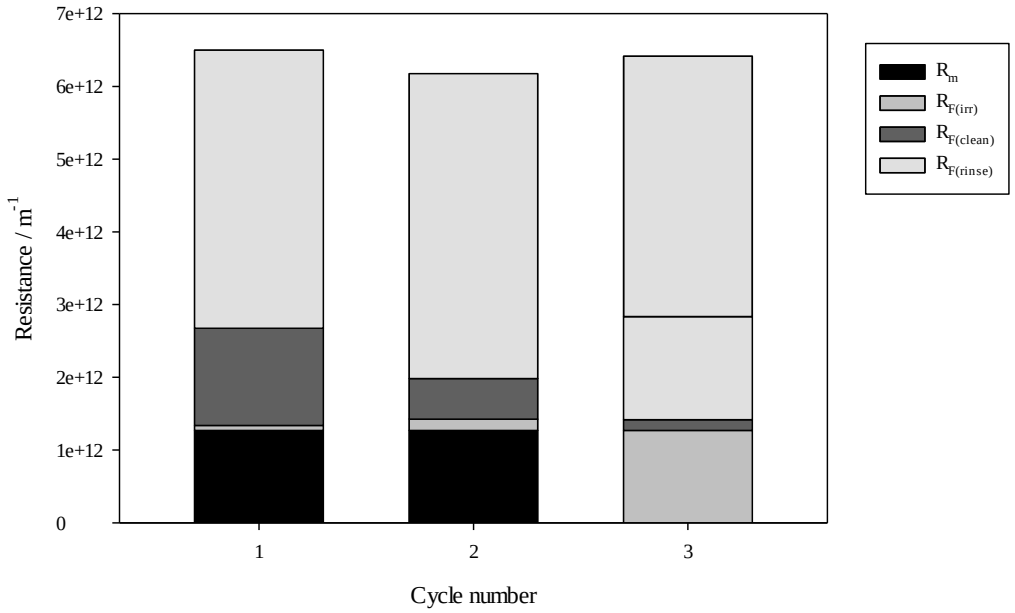

Figure 4.20: Resistance breakdown for the cycles 1 – 3 filtration of 2 wt% gum arabic using 0.1 µm PS membranes at 40 ºC, 0.5 bar TMP and 1.7 m s^{-1} CFV

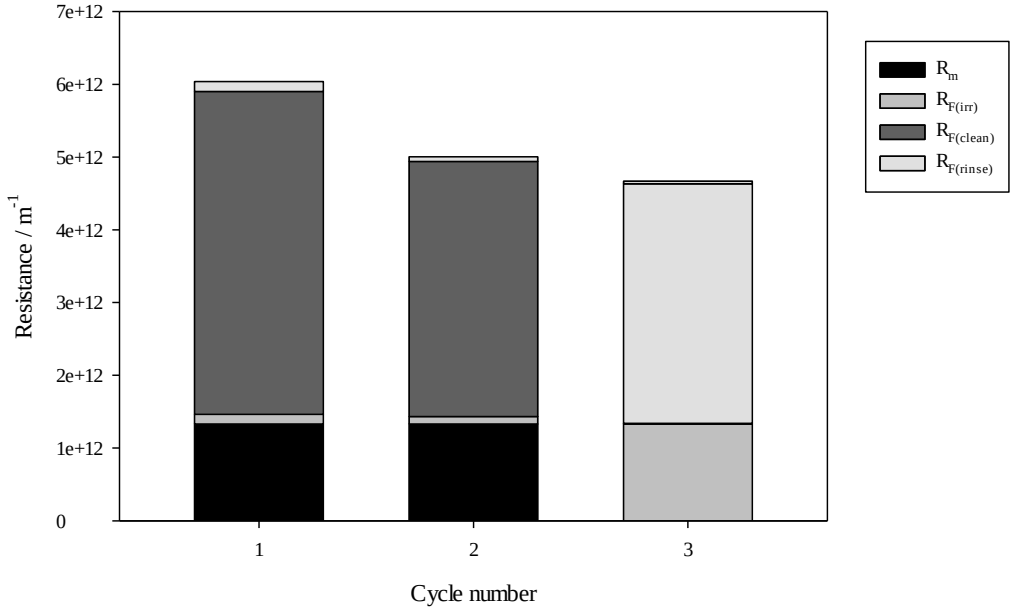

Figure 4.21: Resistance breakdown for the cycles 1 – 3 filtration of 2 wt% gum arabic using 0.5 µm PS membranes at 40 ºC, 0.5 bar TMP and 1.7 m s^{-1} CFV

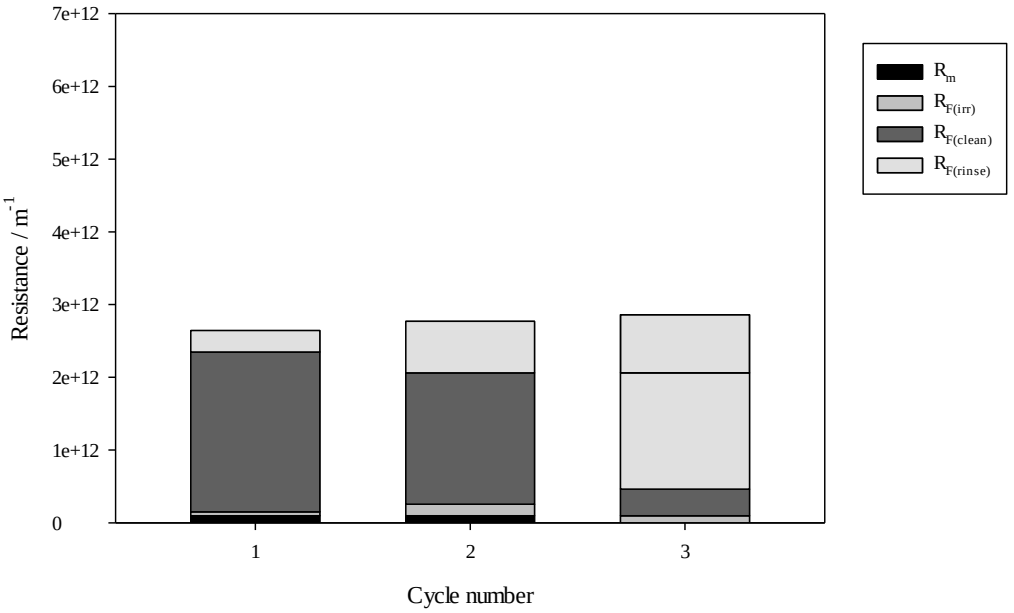

Figure 4.22: Resistance breakdown for the cycles 1 – 3 filtration of 2 wt% gum arabic using 0.8 µm PS membranes at 40 ºC, 0.5 bar TMP and 1.7 m s^{-1} CFV

The resistance profiles shown above differ greatly indicating different fouling mechanisms for the different pore sized membranes. The 0.1 µm membrane shows a fairly constant resistance profile over the three cycles and a membrane resistance of 1.27 x 10^{12} m^{-1}. Over 50 % of the total resistance is due to rinsible fouling, suggesting that this is caused by surface fouling removed during the water rinse stage. Approximately 20 % of the resistance is due to fouling that can be removed by caustic cleaning, suggesting that more of the surface fouling and potentially a small amount of pore blocking is removed. The irreversible fouling is small, but increases slightly after each cycle. Due to the small pore size and low solids transmission observed with this membrane, there is unlikely to be very much in pore fouling. Hermia modelling of the flux decline curves is presented below.

The 0.5 µm PS membrane resistance is 1.33 x 10^{12} m^{-1} and the resistance profile is very different. There is very little fouling that is removed by rinsing alone, as the difference in total resistance and resistance after water rinsing is very small. This suggests that either there is very

little surface fouling, that it is harder to remove by rinsing or that the amount of surface fouling is much less severe than in pore fouling that cannot be removed by rinsing alone. The irreversible fouling, however, is minimal as the fouling is virtually all removed by the caustic cleaning process. This suggests a different fouling mechanism to the 0.1 µm PS membrane and is perhaps pore constriction / blocking. The caustic cleaning can cause hydrolysis of the proteinaceous components within gum arabic, meaning that the AGP and GP fractions may be hydrolysed.[25] This lowers the gum viscosity as the MW of the AGP is reduced. This is likely to allow more efficient removal from the membrane pores due to increased solubility of the lower MW species and increased efficacy of removal by hydraulic action due to the reduction in viscosity.

A similar profile is seen for the 0.8 µm PS membranes but the membrane resistance is much lower at 9.8×10^{12} m^{-1}. A slightly greater rinsible fouling layer is seen with this pore size, but the majority of the fouling is still removed by caustic cleaning rather than just by water rinsing. The irreversible fouling is greater with the 0.8 µm PS membranes than with the other two pore sizes, indicating that the fouling will build up over a number of cycles and affect the filtration properties, as seen in Section 4.5.3.

Researchers previously in the group also used this resistance breakdown technique. Jones *et al*. studied molasses filtration using 1.5 µm PS membranes for the purpose of clarification.[131] They found that the molasses was not easily removed from the surface of the membrane by rinsing with water but that a large proportion of the fouling was effectively remove by cleaning with NaoH and citric acid. These data are similar to the findings in this thesis for gum arabic fouling using 0.5 and 0.8 µm PS membranes.[131]

Hermia modelling

The blocking laws developed by Hermia (1982) have been modified by a number of authors to linearise the blocking laws.[81, 83, 85, 86] Using this method, the fouling mechanism can be

attributed to either cake filtration, complete pore blocking or standard blocking. The methods for determining which mechanism is prevalent is given in the Section 4.2.3. and are based on the explanation given in Nataraj *et al.* (2008).[81] If the plot of the filtration flux vs permeate volume (V) is linear, this means that complete pore blocking is the dominant mechanism. If time (t) / V vs time is linear, standard blocking is dominant and if t/V vs permeate volume is linear, cake formation is dominant. The R^2 value for the graph must be greater than 0.99 for the mechanism of fouling to be dominant. These graphs were plotted for the first 5 min and 10-60 mins of the filtration of 2 wt% gum arabic at 40 ºC, 0.5 bar and 1.7 m s^{-1} and the R^2 values for each mechanism are given in Tables 4.11 and 4.12. The graphs are shown in Appendix C.

Table 4.11: R^2 values for the linearisation of blocking laws for the filtration of 2 wt% gum arabic using 0.1, 0.5 and 0.8 µm PS membranes. The models were fitted to the graphs of the first 5 min of filtration

Membrane	**R^2 value (1st 5 min)**		
	Complete pore blocking	**Standard pore blocking (constriction)**	**Cake formation**
0.1 µm PS	0.2498	0.9152	0.9277
0.5 µm PS	0.0118	0.9923	0.9893
0.8 µm PS	0.8266	0.9754	0.9700

Table 4.12: R^2 values for the linearisation of blocking laws for the filtration of 2 wt% gum arabic using 0.1, 0.5 and 0.8 µm PS membranes. The models were fitted to the graphs of minute 10 – 60 of filtration

Membrane	**R^2 value (min 10-60)**		
	Complete pore blocking	**Standard pore blocking (constriction)**	**Cake formation**
0.1 µm PS	0.2301	0.9326	0.9380
0.5 µm PS	0.3420	0.9496	0.9582
0.8 µm PS	0.2872	0.9882	0.9899

Table 4.11 shows the R^2 values for the different pore blocking mechanisms during the first 5 min of filtration with the 3 pore sized membranes. Table 4.12 shows the mechanisms for the rest of the filtration. For the 0.1 µm PS membranes, no mechanism is dominant in the first 5 min, but both standard pore blocking and cake formation have similar values of 0.9152 and 0.9277, respectively. This shows that both mechanisms are occurring in the first 5 min but that cake formation is slightly more prevalent. In the filtration from 10 – 60 min, the same mechanisms appear to be occurring, again with cake formation slightly dominant as the R^2 value is slightly higher than that for standard blocking. The degree of fouling by each mechanism is not known but these data support the hypothesis that cake formation is dominant during filtration with 0.1 µm PS membranes.

The modelling of the 0.5 µm PS flux decline shows that the dominant fouling mechanism in the first 5 min of filtration is standard pore blocking as the R^2 value is greater than 0.99. Cake formation is also occurring as the R^2 value is 0.9893. In the second stage of filtration, after 10 min, both standard blocking and cake formation mechanisms are occurring as both have similar R^2 values of 0.9496 and 0.9582, respectively. This modelling supports the theory that pore constriction occurs with the 0.5 µm PS membranes due to the larger pore size than the 0.1 µm membranes, but the constriction occurs mainly in the first 5 min of filtration.

The 0.8 µm PS membranes demonstrate no dominant mechanism in the first 5 min filtration but both standard pore blocking and cake filtration are important. Standard pore blocking (or constriction) is slightly more prevalent as the R^2 value is 0.9754 compared to 0.9700 for cake formation. In the second stage of filtration, both standard pore blocking and cake formation are almost equal with R^2 values of 0.9882 and 0.9899, respectively. These data show that the 0.8 µm PS membranes are also prone to pore constriction in the first 5 min, with cake formation becoming slightly more dominant in the second stage of filtration.

Overall, these data support the theory that cake formation is most dominant with the 0.1 µm PS membranes due to the small pore size, although some pore constriction occurs as well. The 0.5 and 0.8 µm PS membranes are subject to more pore constriction in the first 5 min of filtration, after which formation of a cake layer occurs.

4.5.4. Membrane cleaning

Hot water cleaning

Fouling and cleaning cycles were carried out with the three PS membranes to test the efficacy of cleaning with only hot water and no cleaning agents. Membranes were fouled with 2 wt% gum arabic at 40 ºC, 0.5 bar and 1.7 m s^{-1} CFV for 1 h. The membranes were then rinsed and PWF was recorded at 40 ºC. Membranes were then cleaned with 60 ºC water for 20 min at 0.5 bar and 1.7 m s^{-1} and the PWF recorded afterwards at 40 ºC. The membranes were then cleaned with the usual 0.5 wt% NaOH protocol and rinsed and final PWF was recorded. This was repeated for 3 cycles with each membrane and averages were taken. Table 4.13 shows the percentage flux recovery from the hot water clean and the NaOH clean for each membrane. These were calculated by dividing the post-hot water clean PWF value or the post NaOH clean PWF value by the initial PWF for that cycle and multiplying by 100.

Table 4.13: Percentage flux recovery during the cleaning of 0.1, 0.5 and 0.8 µm PS membranes with hot water and NaOH

Membrane	**Percentage flux recovery from 60 ºC water cleaning**	**Percentage recovery from 0.5 wt% NaOH cleaning (40 ºC)**
0.1 µm PS	67 ± 2	98 ± 2
0.5 µm PS	44 ± 1	96 ± 3
0.8 µm PS	9 ± 4	55 ± 7

Table 4.13 shows that cleaning the membranes with 60 ºC water is not as effective as cleaning with 0.5 wt% NaOH, necessitating the use of cleaning agents to restore the membrane flux. The hot water is more effective the smaller the pore size, but the same is true of the NaOH clean, which only restores 55 % of the flux with the 0.8 µm PS membrane. This was observed in Section 4.5.3. and is hypothesised to be due to a greater proportion of in-pore fouling, which is harder to remove by the cleaning protocols used in this work.

Effect of the NaOH clean

A full foul / clean cycle experiment was carried out for each membrane where the NaOH clean was not performed in the membrane module but by soaking the membranes in the NaOH solution instead. The purpose of this experiment was to determine whether the cleaning mechanism was hydraulic or if soaking of the membrane in NaOH was more effective. Table 4.14 shows the percentage flux recovery during a normal 20 min, 40 ºC 0.5 wt% NaOH clean in the membrane module (CFV = 1.7 m s^{-1}, TMP = 0.5 bar) and during a 20 min soak of the membranes in 5 L 0.5 wt% NaOH at 40 ºC for all three membranes. The NaOH clean in module values are from 3 repeats as shown above and the NaOH flux are from 2 repeats.

Table 4.14: Flux increase from post-foul PWF to post-clean PWF for 0.1, 0.5 and 0.8 µm PS membranes from both in-module cleaning and NaOH soak cleaning

Membrane	**Percentage flux recovery from NaOH soak**	**Percentage recovery from NaOH clean in module**
0.1 µm PS	87 ± 6	98 ± 2
0.5 µm PS	93 ± 5	96 ± 3
0.8 µm PS	95 ± 3	55 ± 7

Table 4.14 shows that the NaOH soak provides similar flux recovery for the 0.1 and 0.5 µm membranes as the cleaning-in-place procedure. The NaOH soak is more effective at restoring

the flux in the 0.8 µm PS membrane. This is perhaps due to the TMP during the in-module cleaning causing compaction of the fouling layer and forcing the gum arabic further into the pores. The NaOH soak removes this additional pressure and the NaOH acts to swell and break down the gum arabic on the surface and within the pores of the 0.8 µm PS membrane, as discussed in 4.4.3.

4.5.5. Membrane characterisation

FTIR

FTIR was used to analyse the surface of a 0.1, 0.5 and 0.8 µm PS membranes in virgin (but conditioned to remove the glycerol), fouled and soaked and fouled and cleaned condition.

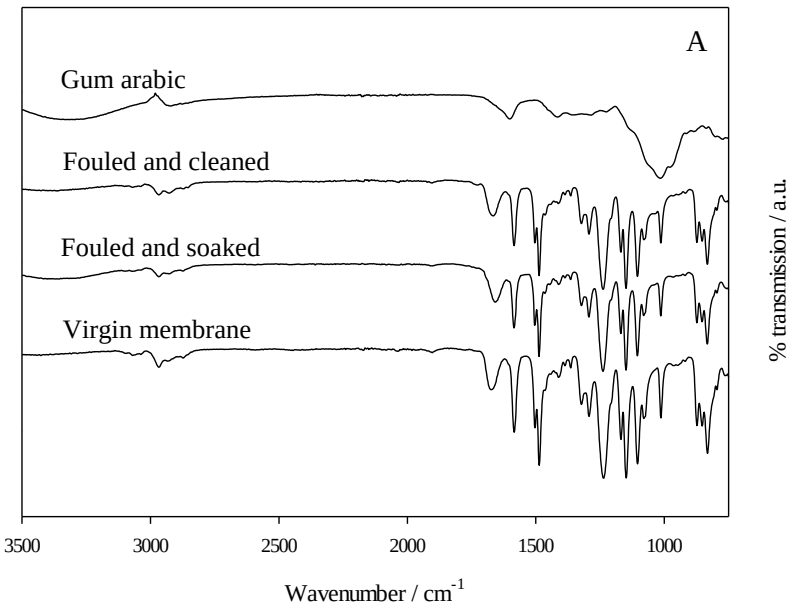

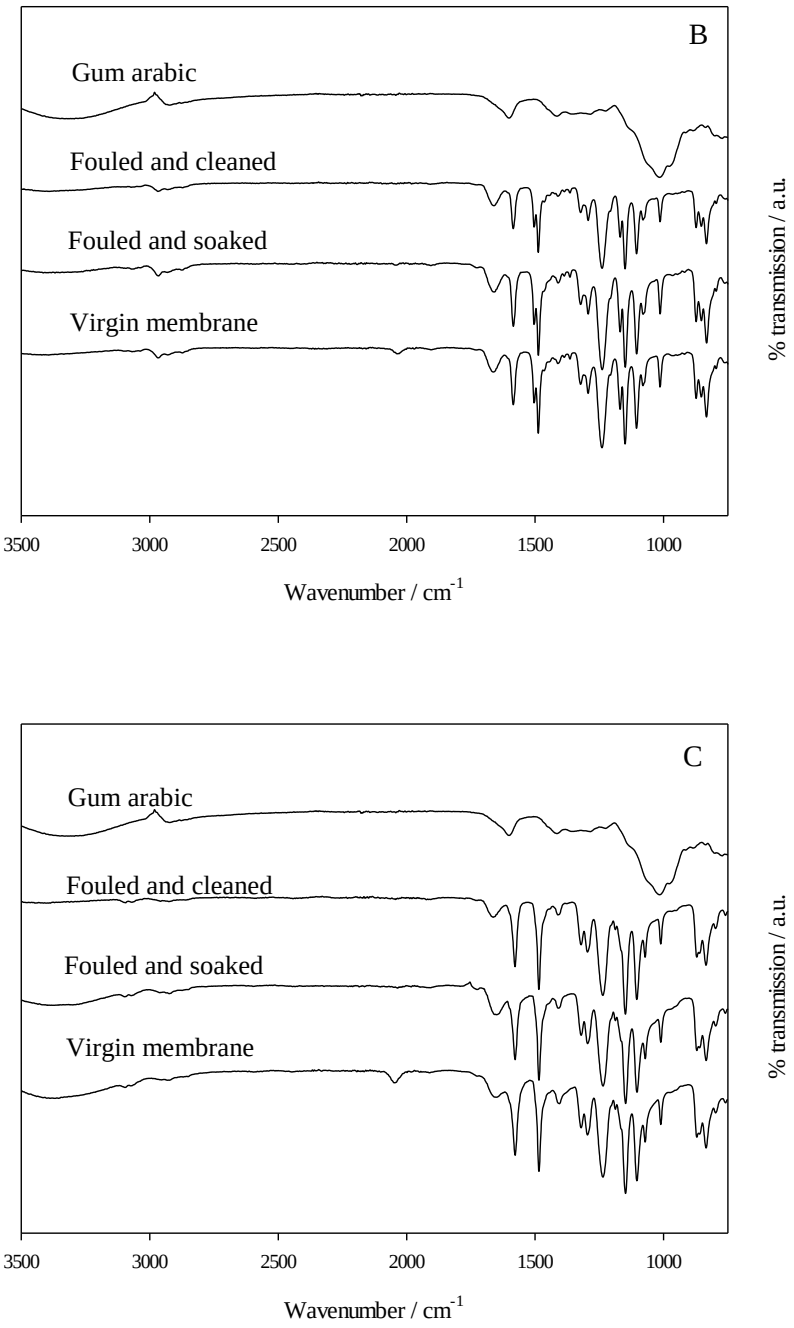

Figure 4.23: FTIR spectra for gum arabic, membranes fouled with 2 wt% gum arabic and soaked for 10 min in RO water, membrane cleaned after a foul and clean cycle and a virgin membrane conditioned to remove glycerol for 0.1 µm PS (A), 0.5 µm PS (B) and 0.8 µm PS (C)

Gum arabic displays typical O-H peaks at 3400 and 1600 cm^{-1}, C-H vibrations between 1400 and 1200 cm^{-1} and intense C-O peaks at 1020 and 976 cm^{-1} as can be seen from Figure 4.23.[42]

The virgin membrane spectra show the peaks present from the polysulfone membrane structure. In all three pore sizes, the fouled and cleaned membrane spectra are identical to the virgin membrane spectra, suggesting that no gum is present on the surface of the membrane. The majority of the gum therefore is likely to readily dissolve away from the surface during the 10 min soaking in RO water. Gum arabic is soluble in water and the 10 min soaking is sufficient for most of the surface gum arabic to diffuse away. The FTIR can only determine gum arabic on the surface of the membrane and cannot give information of any foulant within the membrane pores.

Further experiments were carried out by setting the virgin membrane in each case as the background and repeating the FTIR spectra. The results are shown in Figure 4.24.

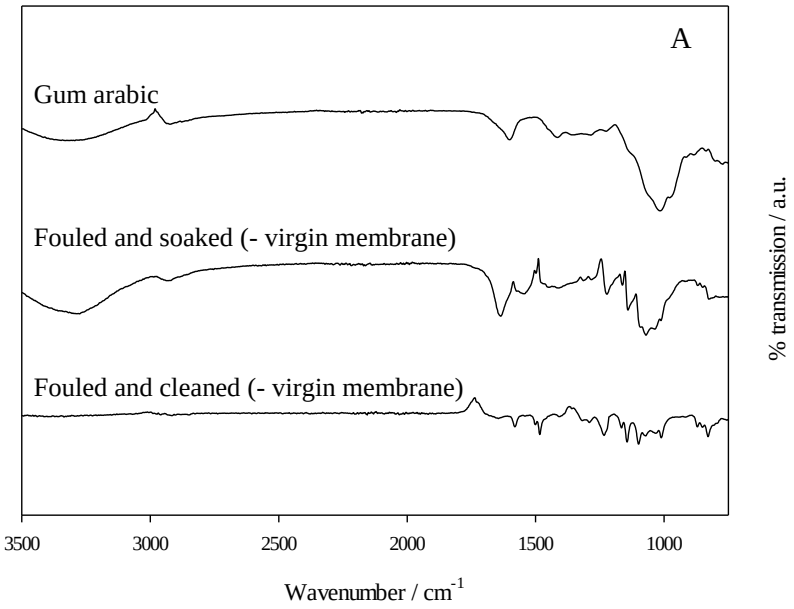

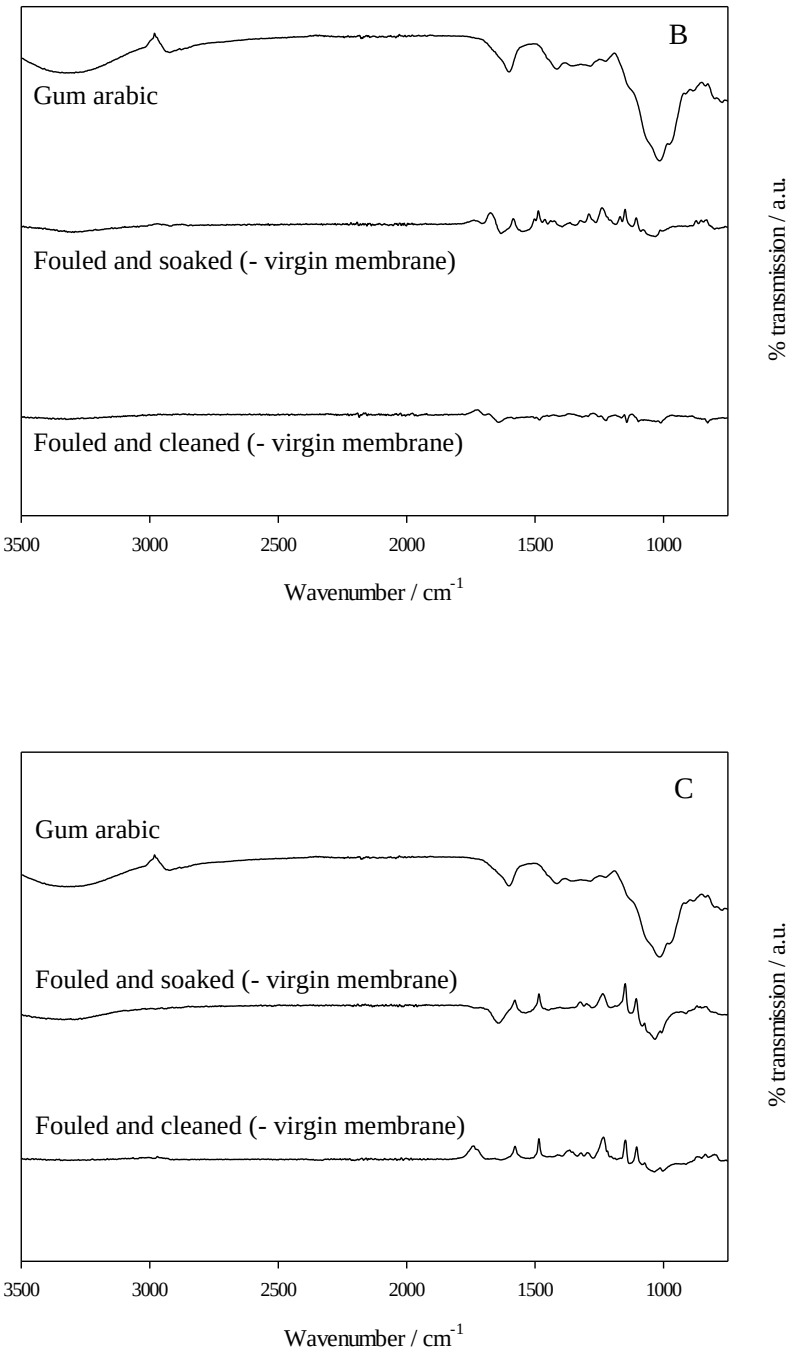

Figure 4.24: FTIR spectra for gum arabic, membranes fouled with 2 wt% gum arabic and soaked for 10 min in RO water (with virgin membrane background removed) and membranes cleaned after a foul and clean cycle (with the virgin membrane background removed) for 0.1 µm PS (A), 0.5 µm PS (B) and 0.8 µm PS (C)

Figure 4.24 shows the presence of gum arabic peaks clearly on the surface of the 0.1 and 0.8 µm PS membranes in the fouled and soaked state. The low intensity of the 0.5 µm PS fouled and soaked spectrum means that it is hard to be sure but there appears to be a small peak at about 1000 cm^{-1} where the large gum arabic peak lies. This peak is broad in the case of all three membranes, indicating that it comes from the gum arabic and not from the polysulfone, which displays sharp peaks as seen in Figure 4.23. The fouled and cleaned spectra for all three membranes show a reduction or loss of this broad peak at 1000 cm^{-1}, suggesting that there is less gum arabic on the surface. This method is not quantitative, however, so the reduction may be due to differences in intensity between samples.

SEM

SEM images were taken of the same 3 virgin, fouled and cleaned membranes. The membranes were freeze-dried prior to analysis. Figure 4.25 shows the images for 0.1 µm PS membranes and no evidence of fouling on the surface can be seen. The same was true of the 0.5 and 0.8 µm PS membranes; these images are not shown.

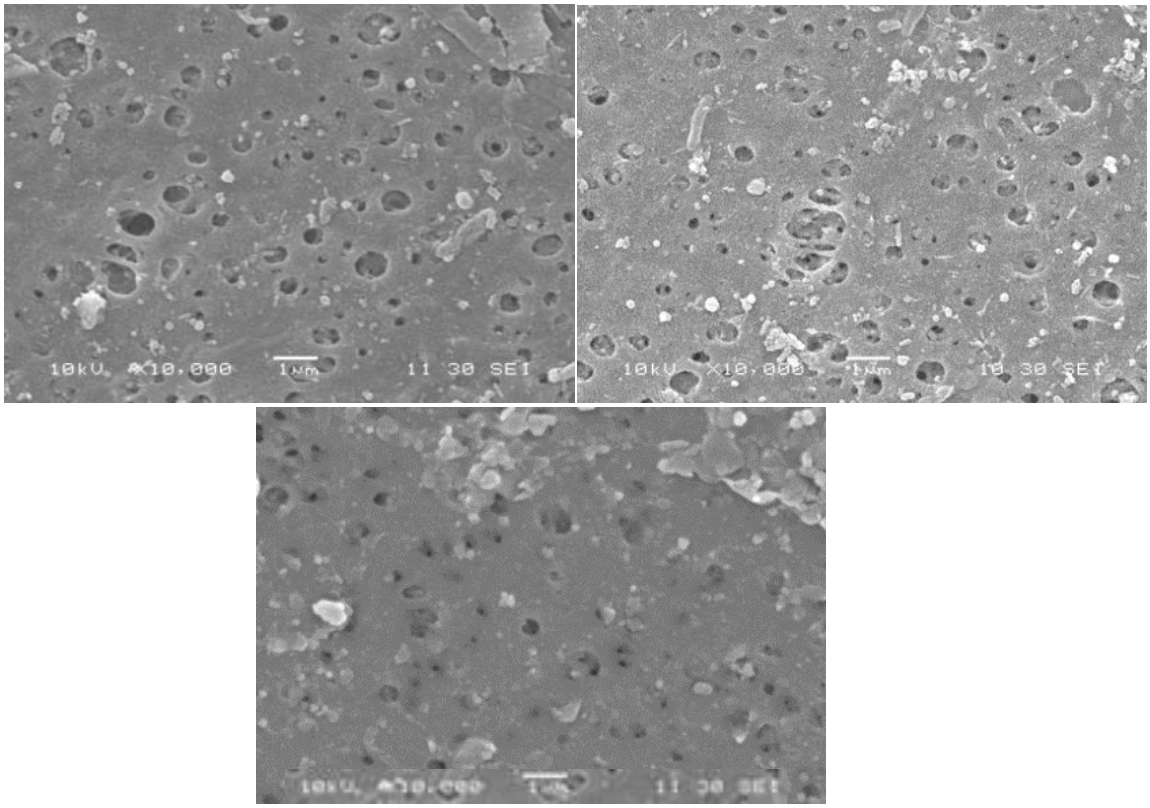

Figure 4.25: SEM images of 0.1 µm PS membranes in virgin (top, left), fouled and soaked (top, right) and fouled and cleaned (bottom) condition

Figure 4.25 shows the top of the membrane surface after conditioning treatment, after fouling and soaking for 10 min in RO water and after cleaning. There are no obvious signs of gum arabic on the surface of the membrane, suggesting that majority of the gum arabic dissolves away rapidly in the soaking process. The gum arabic seen in the FTIR must be a very fine layer that is not obvious in the SEM images

Figure 4.26, shows cross-sectional images of the active layer of the 0.5 µm PS membranes. The other pore sizes are not shown as no difference between the 3 conditions can be observed.

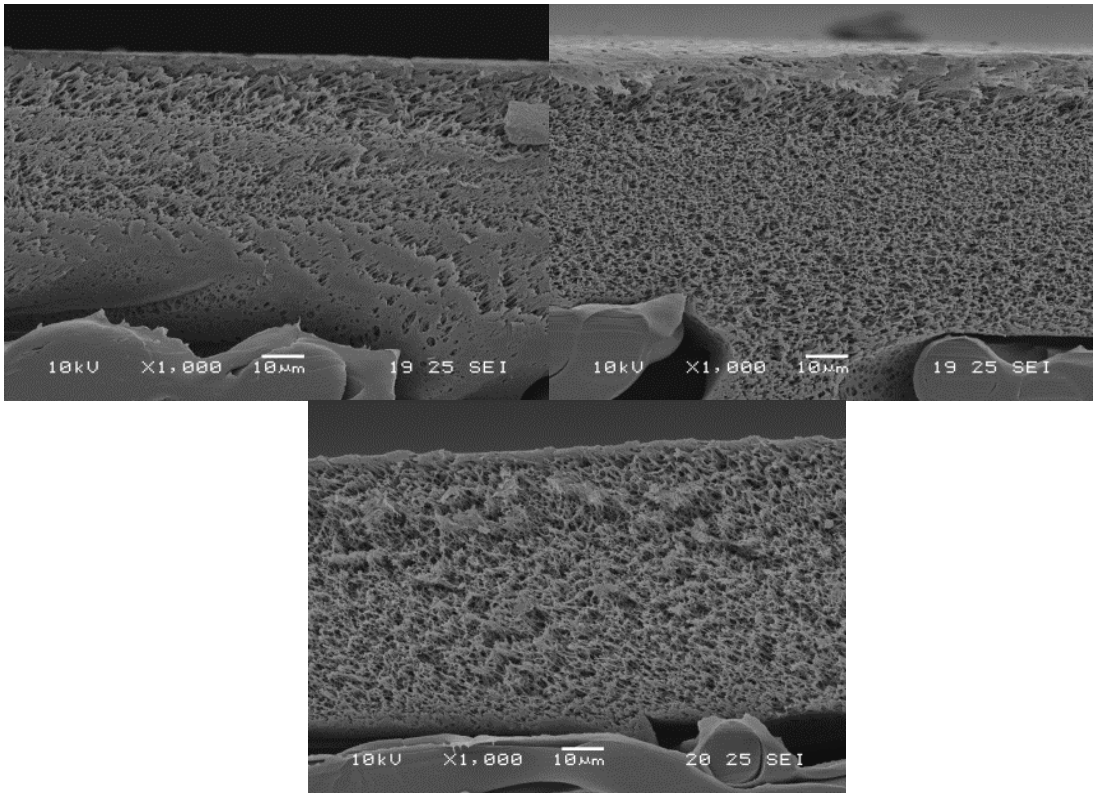

Figure 4.26: Cross-sectional SEM images of the active layer of 0.5 µm PS membranes in virgin, conditioned (top, left), fouled and soaked (top, right), and fouled and cleaned (bottom) state

The cross-sectional images of the 3 membrane pore sizes in virgin, fouled and soaked and fouled and cleaned condition showed no obvious signs of pore blocking or constriction. However, the gum arabic is likely to form a thin layer in the pores, which may not be obvious from the SEM images.

Porosity

Capillary pore porometry was used on freeze dried virgin, fouled and cleaned membranes. The bubble point diameters (largest pore size) and mean flow pore diameters (average pores size) are shown in Table 4.15 as an average of 5 samples. Standard deviations are also shown. This work was carried out during an internship at Nanyang Technological University, Singapore.

Table 4.15: The measured bubble point and mean flow pore diameter for 0.1, 0.5 and 0.8 µm PS membranes under different conditions

Membrane	Bubble point pore diameter / µm	Mean flow pore diameter / µm
0.1 µm PS virgin	0.19 ± 0.03	0.15 ± 0.03
0.1 µm PS fouled	0.11 ± 0.03	0.09 ± 0.02
0.1 µm PS cleaned	0.2 ± 0.06	0.18 ± 0.06
0.5 µm PS virgin	0.68 ± 0.14	0.44 ± 0.19
0.5 µm PS fouled	1.1 ± 0.34	0.57 ± 0.25
0.5 µm PS cleaned	0.61 ± 0.08	0.29 ± 0.02
0.8 µm PS virgin	1.62 ± 0.15	0.92 ± 0.07
0.8 µm PS fouled	1.26 ± 0.36	0.52 ± 0.1
0.8 µm PS cleaned	1.62 ± 0.05	0.85 ± 0.05

Table 4.15 shows how the mean flow pore diameter for the three pore sized membranes changes after being fouled and cleaned. The 0.1 µm PS membranes displays a slight reduction in mean flow pore diameter from 0.15 to 0.09 µm as the membrane is fouled. Considering the errors, however, the minimum pore size for the virgin membrane is 0.12 µm and the maximum mean flow pore diameter for the fouled membrane is 0.11 µm, making the reduction in pore size very small. This is consistent with the theory that little in-pore fouling is seen with the 0.1 µm membranes due to the pores being too small. The pore size appears to be restored in the cleaned membrane, as the pore diameter is statistically the same size as the virgin membrane and slightly larger than the fouled membrane pore size. This agrees with the theory that the 0.1 µm membrane does not suffer irreversible fouling from internal pore blocking. The bubble point of the fouled membrane is slightly lower than that of the virgin membrane, indicating that only the very largest of the pores are subject to pore blocking.

The 0.5 µm mean flow pore diameter appears to increase with membrane fouling but the virgin, fouled and cleaned membranes all have the same mean flow pore diameter, within the error. No conclusion can therefore be drawn from these data, except that the errors are larger than with the 0.1 µm PS membranes. The same is true of the bubble point diameters of the 0.5 µm PS membranes – there is no statistical difference between the virgin, fouled and cleaned membranes.

The bubble point diameters for the three 0.8 µm PS membranes are not statistically different. The mean flow pore diameters, however, do change. The fouled membrane has an average mean flow pore diameter of only 0.52 µm compared to 0.92 µm in the virgin membrane. This shows that the 0.8 µm PS membrane is subject to pore constriction during the fouling with gum arabic, and that the pore size is restored after cleaning as the pore size returns to that of the virgin membrane (within error).

Contact angle measurements

Measuring the contact angle by the sessile drop method can give an indication of the hydrophobicity of a surface. This was carried out for all three pore sized membranes in virgin conditioned, fouled and soaked and fouled and cleaned states. The results are shown in Figure 4.27.

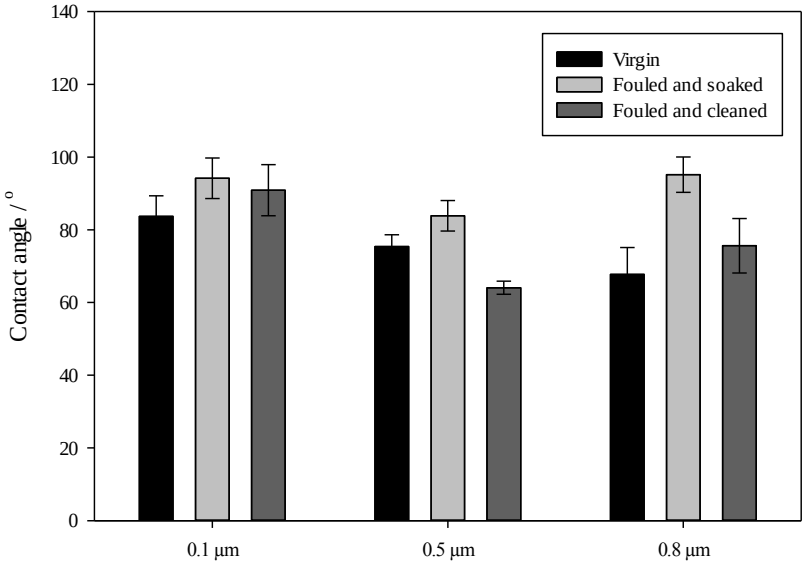

Figure 4.27: Contact angle measurements for virgin, fouled and soaked and fouled and cleaned 0.1, 0.5 and 0.8 µm PS membranes

All three membranes in virgin, freeze dried state display contact angles of between 65 - 85º. The contact angle of the 0.1 µm PS membranes are all the statistically the same and no conclusions can be drawn from the results without carrying out further experiments to reduce the error. The results are the average of 10 contact angles (left and right angles of 5 different sections of membrane), however, so the data are reliable. This suggests that any fouling layer on the membrane was dissolved away during the soaking process, or the quantity on the surface was too small to affect the contact angle. This is supported by the low intensity of gum arabic peaks seen in the FTIR and the absence of gum in the SEM images as seen above.

The 0.5 µm and 0.8 µm membranes show an increase in hydrophobicity (very slight for the 0.5 µm PS membrane) from the virgin to the fouled membrane. It is possible that during the soaking process, the majority of the gum arabic diffuses away from the surface, except for hydrophobic species, which remain bound to the hydrophobic membrane surface in an entropically favoured state. As the only hydrophobic species within gum are certain amino acid groups within gum proteins, it follows that some protein may be bound to the surface of the

membranes. AGP and GP are both protein containing fractions, but only small quantities must be present as these were not detected by FTIR or seen in the SEM images. The three pore sized membranes are all made of the same material, so gum should not bind differently to the different membranes, but the larger pore sizes of the 0.5 and 0.8 µm membranes may trap gum particles in surface pore openings that are too small in the 0.1 µm membranes. Figure 4.28 shows how the larger pore sized membranes may trap gum species on the surface more than the smaller pore sized membranes.

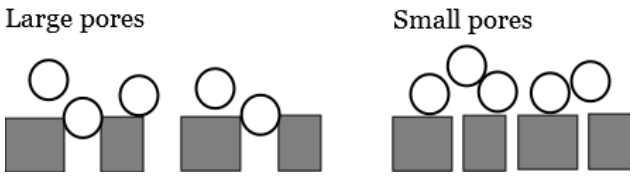

Figure 4.28: Diagram demonstrating how pores of similar size to foulant particles can trap species on the surface

There is then a reduction in contact angle in the membrane that has been fouled and cleaned. The surface has been cleaned of any residual gum species and the contact angle is brought back to that of the virgin membrane.

4.5.6. Discussion

It is postulated that in the 0.1 µm PS, the membrane pore diameter is too small to allow transmission of most of the gum species. It is therefore likely that pore blocking within the active layer is minimal, and that cake formation is the dominant fouling mechanism. This is supported by the porosity tests and Hermia modelling. Evidence of a thick cake layer was not seen upon the surface after 10 min soaking in RO water so this layer must not be tightly bound and readily diffuses away from the surface and redissolves in bulk water. Gum is readily soluble in water due to the large (approximately 80 %) arabinogalactan fraction that is a hydrophilic carbohydrate species.

Despite the low solids transmission observed with the 0.1 µm PS membranes, fractionation of the gum arabic occurred. The protein content of the dried permeate samples was higher than the feed, indicating that the small MW GP was passing through the membrane and the AGP content of the permeate was close to zero. It follows that the fractionation occurred by a size exclusion method as the AGP is the highest MW species and GP is the smallest. It is expected also that some of the lowest MW AG species also passed through the membrane, although in order to achieve better fractionation, larger quantities of these AG species need to be removed from the feed, whilst maintaining the high rejection of AGP.

The 0.5 µm PS membranes demonstrated similar fouling fluxes and solids transmission to the 0.1 µm PS membranes, which is surprising considering the much larger pore size. Although these factors were very similar to the 0.1 µm membranes, the resistance profile observed in Figure 4.21 is very different to that of the 0.1 µm. It is therefore hypothesised that the pore constriction is a more prominent fouling mechanism. The pores are large enough to allow more gum arabic into the pores but small enough that the gum particles constrict and block the pores, this may occur at pore entrances at the surface and also within the active layer. This would account for the very low rinsible resistance seen in Figure 4.21, as if a similar quantity of gum was entering the pores as with the 0.1 µm PS, the rinsible resistance would mimic that seen in Figure 4.20. The Hermia modelling shows that pore constriction is dominant in the first 5 min of filtration with pore constriction and cake formation both operating in the rest of the filtration.

The 0.8 µm PS membranes demonstrate a higher fouling flux and a much greater initial solids transmission. There is, however, little or no fractionation at these early stages of filtration, as shown in Table 4.10. Over time, however, this solids rejection increases and more fractionation is seen, indicating that the fouling layer, either on the surface or due to pore constriction, is responsible for the separation of gum species. Figure 4.19 shows that the cleaning protocol is not effective at completely restoring the membrane flux and that some fouling remains after the cycle is complete. This results in lower solids transmission but improved fractionation after

several foul-clean cycles, as seen in Figure 4.14 and Table 4.10. The larger pore size suggests that this membrane is subject to more in pore fouling that is not removed by the cleaning protocol. Hermia modelling and the porosity studied show that pore constriction occurs with this membrane.

4.6. Increasing the feed concentration

For this work, a different 25 kg sack of gum arabic was used, which had a lower AGP mass fraction of 0.146 ± 0.009 due to natural batch-to-batch variation. The exact AGP content was measured for each experiment.

The effect of increasing the gum arabic feed concentration on flux and fractionation was assessed to determine the effectiveness of this process on a more industrially relevant feed. Gum arabic is processed by *Kerry Ingredients and Flavours* at between 15 and 20 wt%. Here, up to 8 wt% gum arabic was able to be filtered under the same conditions as the 2 wt% gum using 0.8 µm PS membranes. 6 wt% feed was also filtered with 0.5 µm PS membranes.

4.6.1. 0.8 µm PS cycle 1

New, conditioned 0.8 µm PS membranes were used to filter 4, 6 and 8 wt% gum arabic at 40 ºC, 0.5 bar and 1.7 m s^{-1}. The flux data are shown in Figure 4.29 and average flux vs feed concentration is shown in Figure 4.30.

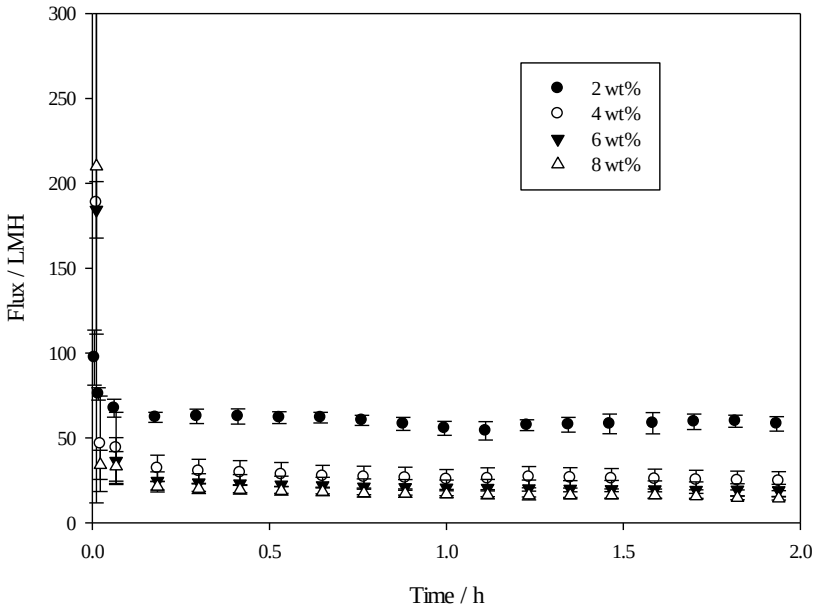

Figure 4.29: Flux decline curves for the filtration of different concentrations of gum arabic using 0.8 µm PS membranes at 0.5 bar TMP, 1.7 m s^{-1} CFV and 40 ºC. Three repeats were carried out using new, conditioned membranes for each and averages are shown. The error bars represent ± one standard deviation

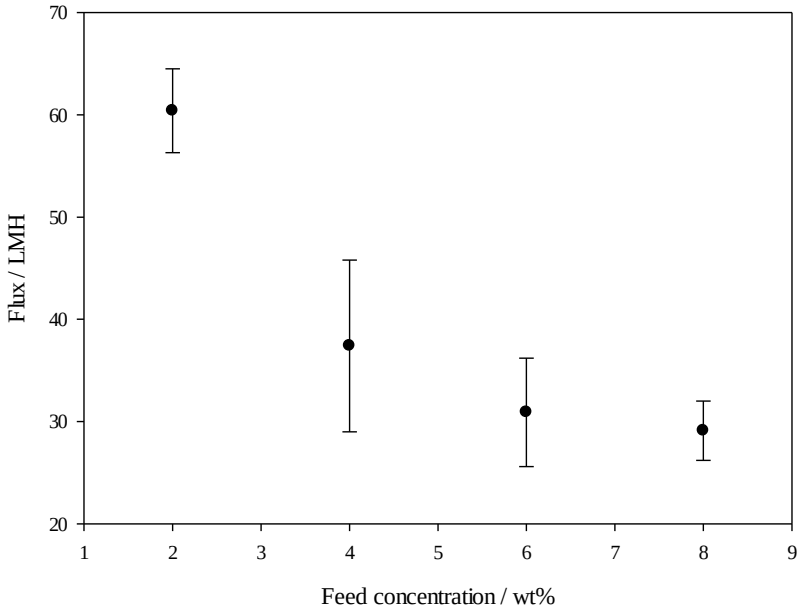

Figure 4.30: Flux against feed concentration for the filtration of gum arabic using 0.8 µm PS membranes

The average flux decreases exponentially with increasing feed concentration. As the feed concentration increases, as does the concentration of rejected species within the boundary layer at the surface, resulting in a greater barrier to flux.

Table 4.16 shows the total resistance during fouling and the solids rejection. The resistance values take into account the difference in viscosity of the permeate, which increases with the feed concentration.

Table 4.16: Total resistance and solids rejection coefficients for the filtration of different concentrations of gum arabic with 0.8 μm PS membranes

Feed wt%	**Total resistance during fouling / m^{-1}**	**Solids rejection coefficient (Cycle 1)**
2	$2.9 \times 10^{12} \pm 2.1 \times 10^{11}$	0.69 ± 0.18
4	$4.7 \times 10^{12} \pm 1.2 \times 10^{12}$	0.74 ± 0.06
6	$3.6 \times 10^{12} \pm 9.3 \times 10^{11}$	0.67 ± 0.09
8	$3.5 \times 10^{12} \pm 4.5 \times 10^{11}$	0.56 ± 0.07

No fractionation was observed with the cycle 1 filtration at different feed concentrations as seen in Table 4.17. This is not unexpected, however, as the importance of fouling to aid fractionation with the large pore sized 0.8 μm membranes was seen in Section 4.5.2.

Table 4.17: The AGP content of dried feed and permeate samples from the filtration of different concentrations of gum arabic using 0.8 μm PS membranes (cycle 1)

Feed concentration / wt%	**Feed AGP mass fraction**	**Permeate AGP mass fraction**
4	0.145 ± 0.001	0.144 ± 0.005
6	0.151 ± 0.008	0.14 ± 0.009
8	0.149 ± 0.002	0.147 ± 0.003

4.6.2. Multiple cycles

The filtration of 6 wt% gum arabic was repeated in 3 foul-clean cycles with 0.8 and 0.5 µm PS membranes to see if the trend of increasing fractionation with increasing number of cycles is also seen with the higher feed concentration. Table 4.18 shows the solids rejection coefficients and AGP content of the feed and permeate from filtration with 0.8 µm PS membranes and the same data for filtration with 0.5 µm PS membranes are shown in Table 4.19.

Table 4.18: The AGP mass fractions of dried feed and permeate samples from the filtration of 6 wt% gum arabic using 0.8 µm PS membranes (cycles 1-3)

Membrane and cycle number	**Solids rejection coefficient**	**AGP mass fraction of feed**	**AGP mass fraction of permeate**
0.8 µm PS Cycle 1	0.57	0.16	0.146
0.8 µm PS Cycle 2	0.85	0.151	0.129
0.8 µm PS Cycle 3	0.86	0.155	0.123

Table 4.19: The AGP mass fractions of dried feed and permeate samples from the filtration of 6 wt% gum arabic using 0.5 µm PS membranes (cycles 1-3)

Membrane and cycle number	**Solids rejection coefficient**	**AGP mass fraction of feed**	**AGP mass fraction of permeate**
0.5 µm PS Cycle 1	0.93	0.147	0.091
0.5 µm PS Cycle 2	0.9	0.12	0.078
0.5 µm PS Cycle 3	0.94	0.148	0.059

Table 4.18 shows there is a slight reduction in AGP from the feed to the permeate seen with the filtration of 6 wt% gum arabic using 0.8 µm PS membranes after 2 and 3 foul-clean cycles. The effect is less pronounced than with 2 wt% as seen in Table 4.9, however, indicating that the higher feed concentration reduces the fractionating performance with 0.8 µm membranes.

Table 4.19 shows the improvement in the fractionation performance during the filtration of 6 wt% gum arabic using 0.5 µm PS membranes over 3 cycles. Here, the build-up of fouling after each filtration cycle results in greater rejection of the AGP, as observed with 2 wt% gum in Figure 4.8. This shows that fractionation is possible at higher feed concentrations.

4.7. Conclusions

Dead end filtration studies using 2 wt% gum arabic and 0.1 µm PS membranes have shown that some fractionation of gum arabic is possible. During 30 min filtrations in a stirred cell, rejection of nearly all of the gum arabic AGP was seen, with higher quantities of protein observed in the permeate than in the feed. This indicates that low MW GP is passing through the membrane more easily than the higher MW AG and AGP species.

The same results were seen during crossflow filtration. CFV was shown to increase the flux and increasing the TMP above 0.5 bar only slightly increases the flux. Filtration at 40 ºC showed a higher flux than filtration at 25 ºC so conditions of 0.5/1 bar TMP, 1.7 m s^{-1} CFV and 40 ºC were adopted as standard filtration conditions. Under these conditions, a filtration flux of 77 LMH was achieved although overall solids rejection was high (> 95%).

Filtration was performed under these conditions using 0.5 and 0.8 µm PS membranes for comparison and it was observed that greater solids transmission occurred but lower rejection of AGP; this improved over filtration time and after several foul-clean cycles, however.

Breakdown of the filtration resistances together with surface analysis of the membranes, Hermia modelling and porosity studies indicates that fouling with the 0.1 µm PS membrane is primarily cake formation on the surface due to the pores being too small for the majority of gum species to enter, and this is effectively removed during the cleaning steps. The 0.5 µm PS displays lower fluxes than expected for its pore size, and this is due to pore constriction being the more dominant fouling mechanism, particularly in the first 5 min filtration. The 0.8 µm PS membranes produce a higher flux and greater solids transmission initially, due to the larger pore

size. Pore constriction over time, however, reduces the solids transmission but improves the rejection of AGP.

Studies into filtration of up to 8 wt% gum arabic show that there is some flux decline at higher feed concentrations, but that fractionation also occurs after several foul-clean cycles. The challenge now is to achieve greater transmission of the lower MW GP and AG species whilst maintaining a high rejection of AGP.

5. Critical flux of gum arabic

5.1. Introduction

The work in this chapter details experiments to determine the critical flux of 2 wt% gum arabic filtered using 0.1, 0.5 and 0.8 μm PS membranes. The flux-stepping method was used and the critical flux was determined from three different methods and averaged. Diafiltration experiments were then carried out above and below the determined critical fluxes in each case to see the effect of operating with minimal or no fouling on filtration and fractionation performance of the membranes. This work was done at the Singapore Membrane Technology Centre at Nanyang Technological University by the author of this thesis.

5.2. Experimental methods

5.2.1. Feed preparation

The 2 wt% feed was prepared in the same way as in Chapter 4 but the prefiltration was done by gravity filtration through the same 50 μm stainless steel filter rather than under N_2 pressure.

5.2.2. Critical flux measurements

The flux-stepping method was used to determine the critical flux of 2 wt% gum arabic using 0.1, 0.5 and 0.8 μm PS membranes.[105] New, conditioned membranes were used for each experiment. Conditioning was done by passing Milli-Q water through the membrane for 90 min at 60 ºC and a CFV of 0.37 m s^{-1}. First, the TMP readings were recorded every 20 s for Milli-Q water over a range of fluxes. The operating conditions for this membrane pure water permeability were the same as for the fouling experiment of 2 wt% gum arabic. Standard filtration conditions were set at 40 ºC, a crossflow velocity of 0.37 m s^{-1}, and 15 minute flux steps were carried out from 2 LMH until a flux where TMP increase over the step period was significant, which indicates serious membrane fouling. For the 0.8 μm membranes, the flux-

stepping started at 10 LMH. Permeate and retentate were cycled back to the feed tank to maintain constant feed volume and concentration.

The effect of altering CFV was investigated by carrying out flux-stepping experiments using 0.1 µm PS membranes at varying crossflow velocities (0.18, 0.37, 0.56 and 0.67 m s^{-1}). A total of 3 repeats of the critical flux measurement of 2 wt% gum arabic with 0.1 µm PS membranes at 0.37 m s^{-1} CFV were carried out to test the reproducibility of the experiments.

5.2.3. The effect of operation below critical flux

After determination of the critical flux of 2 wt% gum arabic with the 3 membrane pore sizes under standard conditions, longer diafiltration experiments were performed both above and below the critical flux in order to study the effect of fouling on the filtration and fractionation performance of the membrane.

5.2.4. Data analysis

The critical flux of 2 wt% gum arabic at 40 ºC and 0.37 m s^{-1} CFV was determined using the flux-stepping method. There are several approaches for estimating the critical flux in this flux-stepping method and each of these techniques was employed and compared. Figure 3.4, modified from Le Clech *et al.* (2003), explains the different parameters based on TMP used to identify the point at which membrane fouling occurred.[1] The first parameter is the change in TMP over the step period (15 minutes). This can be observed visually from the graphs of TMP vs. time. The critical flux is defined as the flux above which dTMP/ $dt > 0$. This is also calculated using Equation 3.3.

$$\frac{d\mathrm{TMP}}{dt} = \frac{(\mathrm{TMP}_{final} - \mathrm{TMP}_{initial})}{(t_{final} - t_{initial})} \qquad \text{Equation 5.1}$$

$TMP_{initial}$ is the average TMP over the first minute of the flux step, excluding the first data point and TMP_{final} is the average TMP over the last minute of the flux step. Time is represented by *t*.

A second parameter, the initial TMP increase (ΔTMP_0) between each step can also be calculated and the point at which this value stops being proportional to the step size can be defined as the critical flux. Finally, the average TMP in each step (TMP_{av}) can be plotted against flux and the point at which the two are no longer proportional is a third method for determining the critical flux.

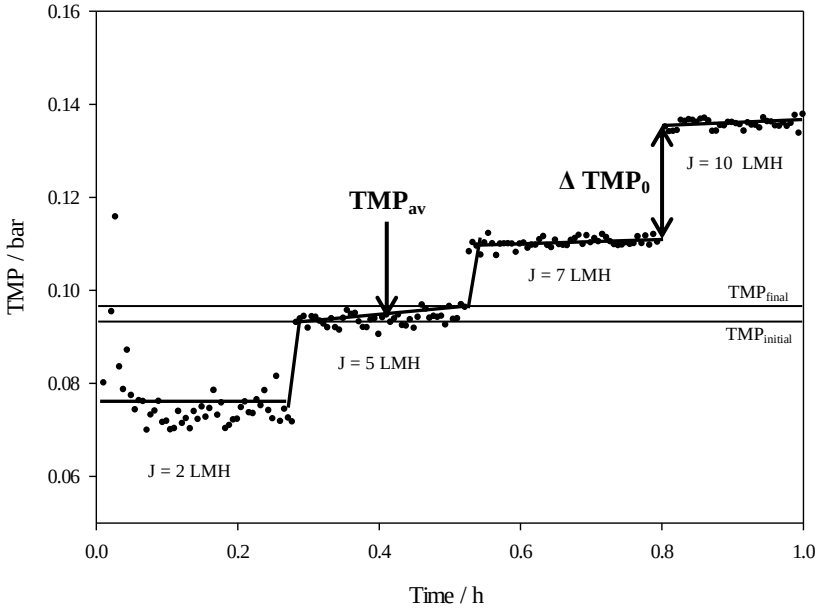

Figure 5.1: Explanation of the different parameters used to determine critical flux using the flux-stepping method. Modified from Le Clech *et al*. (2003)[1]

5.3. Pure water filtration

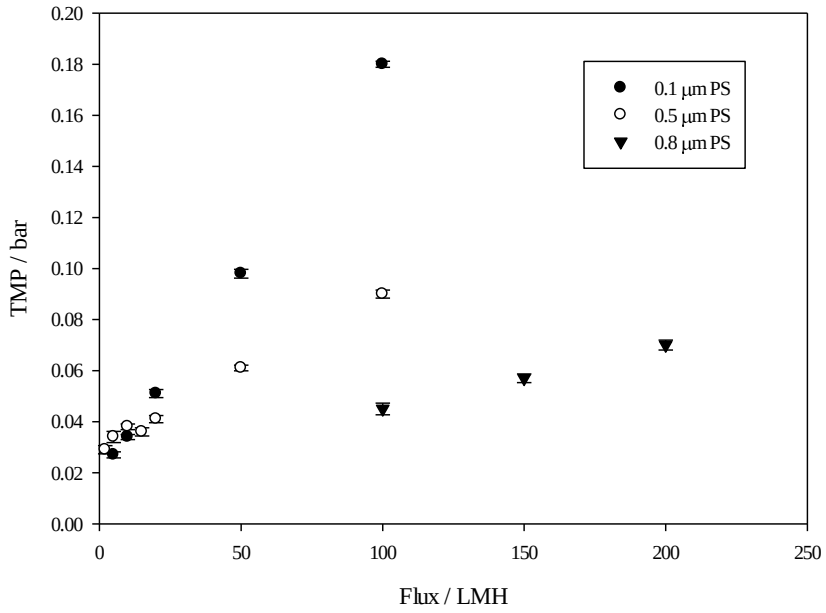

Figure 5.2: The relationship between flux and TMP during the filtration of Milli-Q water through 0.1, 0.5 and 0.8 μm PS membranes at 40 ºC and a CFV of 0.37 m s^{-1}

Figure 5.2 shows the TMP for the flow of Milli-Q water through 0.1, 0.5 and 0.8 μm PS membranes over a range of fluxes. The TMP was recorded every 20 s for 5 min at each flux and the points represent the mean value. The error bars represent ± one standard deviation. The membrane resistances were calculated from pure water flux measurements to be 1.05 x 10^{12}, 4.96 x 10^{11} and 2.48 x 10^{11} m^{-1} for 0.1, 0.5 and 0.8 μm PS membranes, respectively.

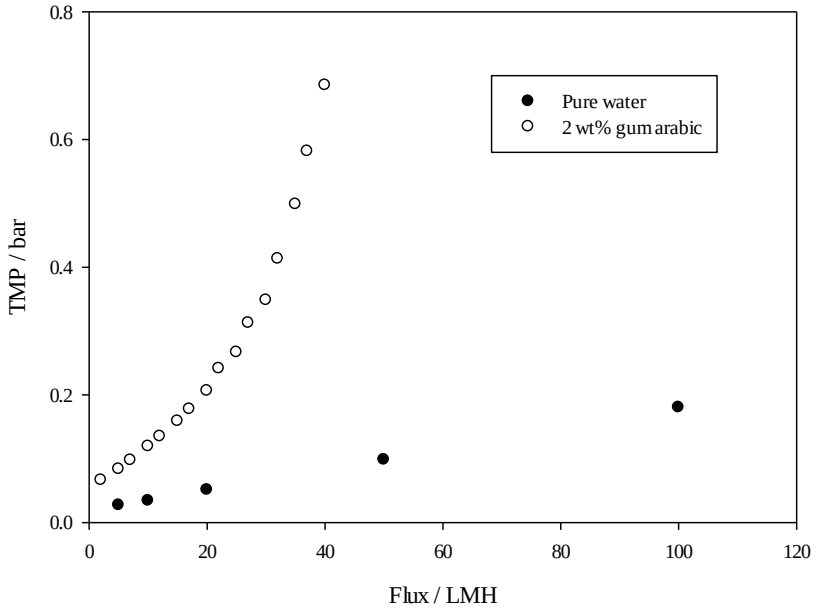

Figure 5.3: TMP as a function of flux for Milli-Q water and 2 wt% gum arabic filtration using 0.1 µm PS membrane. The filtration temperature was 40 ºC and the CFV was 0.37 m s^{-1}

Figure 5.3 shows that the critical fluxes considered in this work are weak forms of the critical flux, where the fouling flux is not equal to the pure water flux but there still exists a flux below which no TMP rise is seen. A critical flux in its strict form does not exist under the conditions studied here. Figure 5.3 shows the data for 0.1 µm membranes but the same applies for the 0.5 and 0.8 µm membranes. Critical flux measurements

5.3.1. The effect of membrane pore size

Figures 5.4, 5.5 and 5.6 show the TMP profile of the flux-stepping for the filtration of 2 wt% gum arabic using 0.1, 0.5 and 0.8 µm PS membrane at 40 ºC and a CFV of 0.37 m s^{-1}. The step intervals were 15 min and the step size is indicated in the Figure caption below each graph. The flux-stepping was repeated 3 times with 0.1 µm PS membranes using new 0.1 µm PS membranes each time and data shown for this membrane represent the mean values with error bars showing ± one standard deviation.

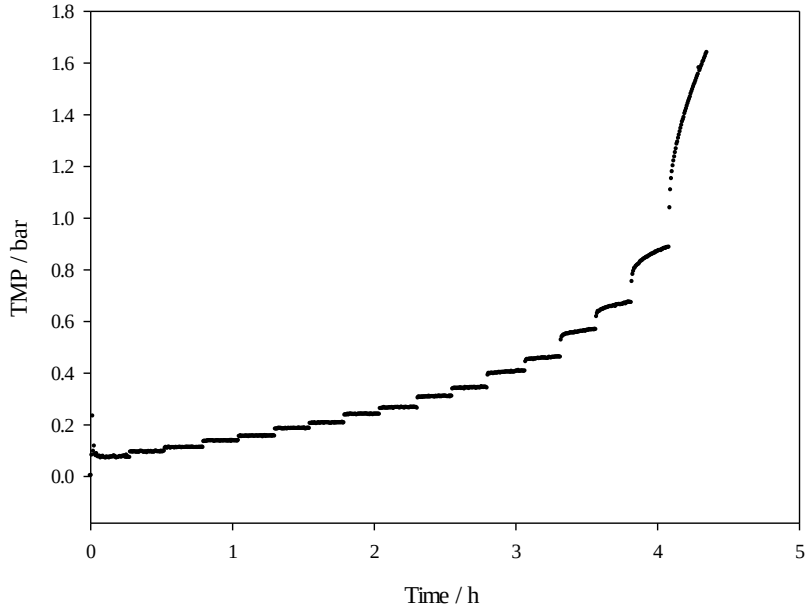

Figure 5.4: Flux steps of 15 minute duration of 2 wt% gum arabic filtration using a 0.1 µm PS membrane at 40 ºC, 0.37 m s^{-1} CFV. The steps are 2, 5, 7, 10, 12, 15, 17, 20, 22, 25, 27, 30, 32, 35, 37, 40 and 45 LMH

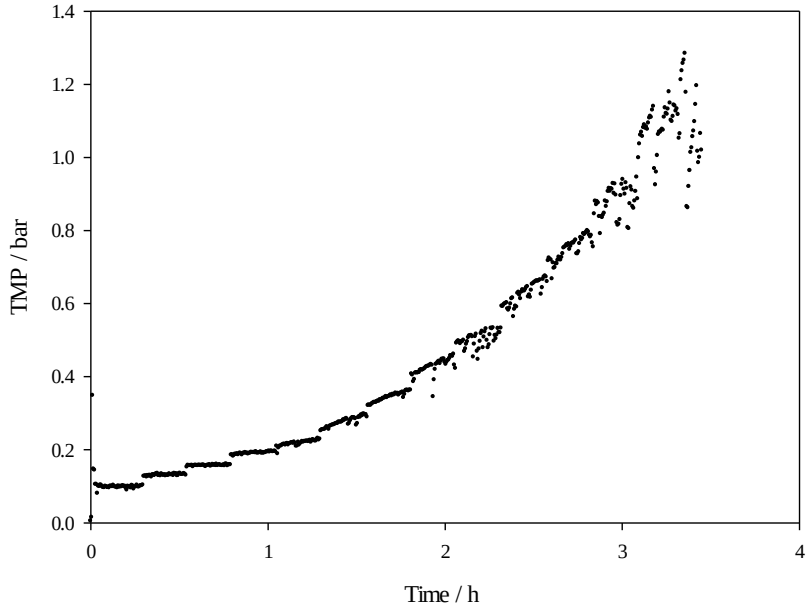

Figure 5.5: Flux steps of 15 minute duration of 2 wt% gum arabic filtration using a 0.5 µm PS membrane at 40 ºC, 0.37 m s^{-1} CFV. The steps are 2, 5, 7, 10, 12, 15, 17, 20, 22, 25, 27, 30 and 35 LMH

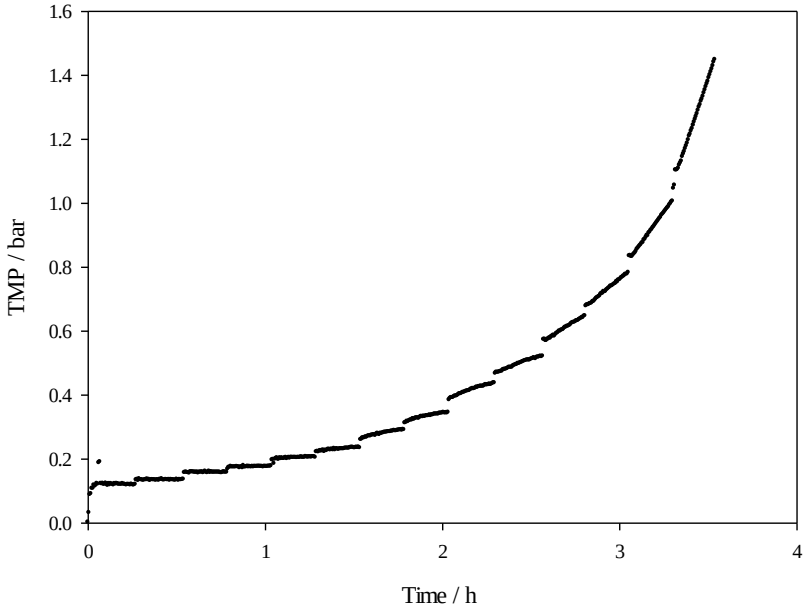

Figure 5.6: Flux steps of 15 minute duration of 2 wt% gum arabic filtration using a 0.8 µm PS membrane at 40 ºC, 0.37 m s^{-1} CFV. The steps are 2, 5, 7, 10, 12, 15, 17, 20, 22, 25, 27, 30 and 35 LMH

The weak form of the critical flux can be estimated from the graphs as the point at which the TMP no longer remains constant during the 15 minute flux step. These appear to be about 27 LMH, 10 LMH and 15 LMH for the 0.1, 0.5 and 0.8 µm membranes, respectively, from visual observation. The fouling rate is represented graphically in Figure 5.7 as a plot of dTMP/dt vs flux. Figure 5.8 shows the average TMP as a function of flux and Figure 5.9 shows the change in TMP between each flux step, normalised for step size. The critical fluxes determined by each method are summarised in Table 5.1.

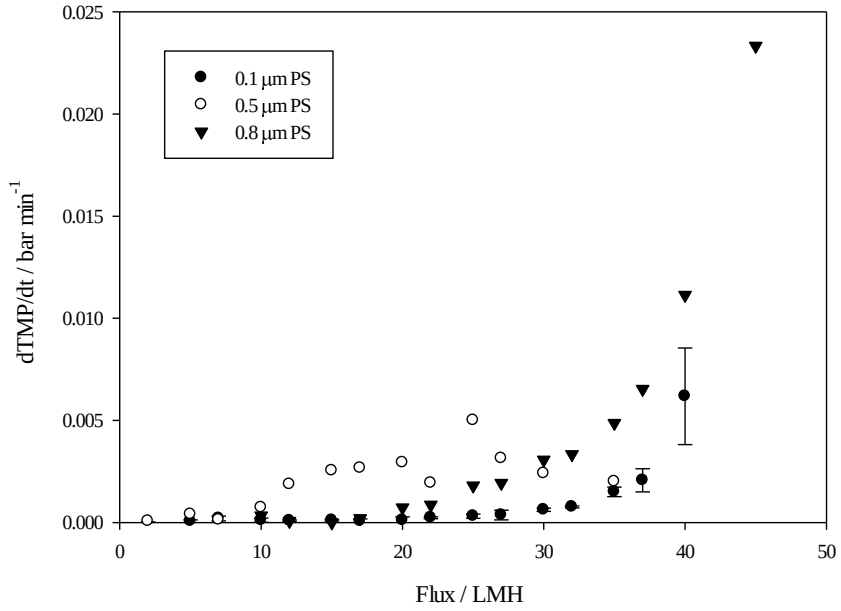

Figure 5.7: Fouling rate for 2 wt% gum arabic using 0.1, 0.5 and 0.8 µm PS membranes. The filtration temperature was 40 ºC and the CFV was 0.37 m s^{-1}

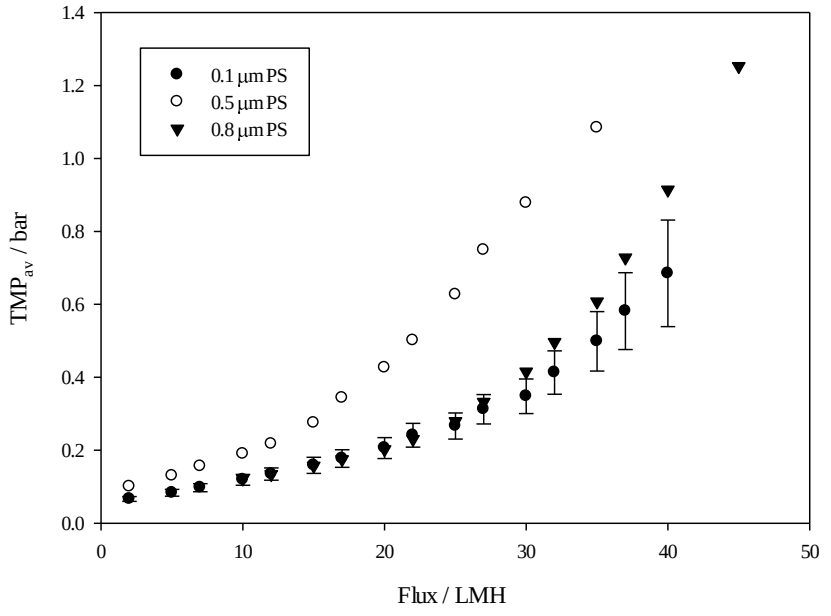

Figure 5.8: TMP_{av} for the filtration of 2 wt% gum arabic with 0.1, 0.5 and 0.8 µm PS membranes as a function of flux. The temperature was 40 ºC and CFV 0.37 m s^{-1}

The critical flux can be defined as maximum flux at which the permeability remains linear.[79]

$$\text{Permeability} = \frac{J}{TMP_{av}} \qquad \text{Equation 5.2}$$

From Figure 5.8, the permeability can be calculated as 113.6, 75.8, and 93.5 L m^{-2} h^{-1} bar^{-1} for 0.1, 0.5 and 0.8 µm membranes, respectively. These values are all lower than the corresponding permeability for pure water (625, 1667 and 3333 L m^{-2} h^{-1} bar^{-1}), which shows that the weak form of the critical flux is observed.

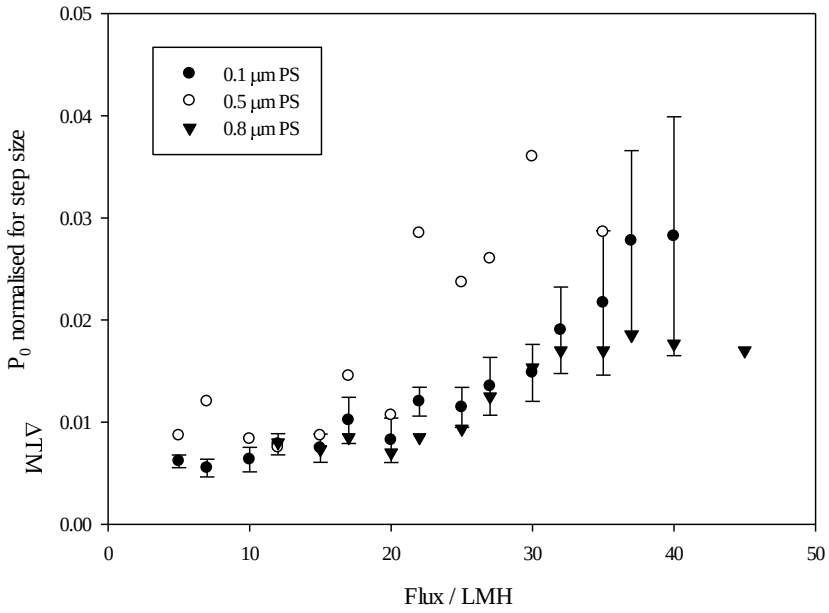

Figure 5.9: ΔTMP_0 for the filtration of 2 wt% gum arabic with 0.1, 0.5 and 0.8 µm PS membranes as a function of flux. The temperature was 40 ºC and CFV 0.37 m s^{-1}

Figure 5.9 shows ΔTMP_0 to be fairly constant up to a certain flux (20, 15 and 25 LMH for 0.1, 0.5 and 0.8 µm membranes, respectively), at which point the initial increase between each step increases.

Table 5.1: Critical flux values for the filtration of 2 wt% gum arabic using 0.1, 0.5 and 0.8 µm PS membranes determined by different methods

Criterion	**Critical flux / LMH for 0.1 µm membrane**	**Critical flux / LMH for 0.5 µm membrane**	**Critical flux / LMH for 0.8 µm membrane**
Visual	27	10	15
dTMP / dt < 0.001 bar min^{-1}	32	10	22
dTMP / dt (Fig 5.6)	27	10	22
TMP_{av} (Fig 5.7)	30	12	27
ΔTMP_0 (Fig 5.8)	20	15	25

Table 5.1 summarises the different values of the critical flux measured in this work. The weak form of the critical flux can be defined as the point at which TMP no longer remains constant over time at a constant flux. This can be determined by a plot of dTMP/dt vs. flux alone, however the other TMP-based parameters are used to also determine the critical flux and the values are averaged. The initial rapid increase in TMP between flux steps should relate directly to the membrane resistance for pure water filtration, but here, the step size is greater than that of pure water indicating that some fouling does occur at each step increase. The TMP does not continue to rise however and therefore the point at which ΔTMP_0 begins to increase can be considered the weak form of the critical flux. Another form of the critical flux can be determined as the point at which the plot of TMP_{av} vs. flux moves from a linear to non-linear relationship.

Membranes with a higher porosity should demonstrate an overall higher critical flux for the same feed under the same conditions due to a better distribution of the permeate flux across the membrane surface, which minimises fouling build up in certain areas.[75] The pure water flux for

the three pore sized membranes (virgin) increases with pore size (Figure 5.2), but it was shown in Chapter 4 that the total resistance for the filtration of 2 wt% gum was 5.8 x 10^{12}, 6.1 x 10^{12} and 3.3 x 10^{12} m^{-1} for 0.1, 0.5 and 0.8 µm PS membranes, respectively. This suggests that the 0.5 µm membrane is more prone to fouling than the other two pore sized membranes. This is perhaps due to a large proportion of the gum particles being of a similar size to the pores and the membrane being susceptible to pore blocking or pore constriction. It was concluded in Chapter 4 that the 0.5 and 0.8 µm membranes were fouled initially by pore constriction and then by formation of a cake layer on the surface. The pores of the 0.1 µm membrane were too small to allow any great quantities of gum arabic into the internal structure (this was seen by > 97% solids rejection and evidence from Hermia modelling) and less pore blocking occurred.

The values for critical flux observed here show that the 0.5 µm membrane has a lower critical flux than 0.8 µm. This is likely to be due to the higher porosity in the larger pore sized membrane and the higher fouling propensity observed with the 0.5 µm membrane as discussed above. The 0.1 µm membrane demonstrates a higher critical flux than expected, based on the membrane pore size. This can be explained by a lack of pore blocking, which occurs with the 0.5 and 0.8 µm membranes. Cake formation is the main fouling mechanism, which starts to become significant at higher fluxes than the pore constriction mechanism, as the effect of surface shear caused by the CFV adds to the movement of particles away from the surface by lateral migration.

5.3.2. The effect of CFV

The effect of CFV on the critical flux was measured by carrying out flux-stepping of 2 wt% gum arabic with 0.1 µm PS membranes at 0.18, 0.37, 0.56 and 0.67 m s^{-1} CFV. The same three TMP-based parameters as explained above were used to determine critical flux values and these are shown in Figures 5.10, 5.11 and 5.12.

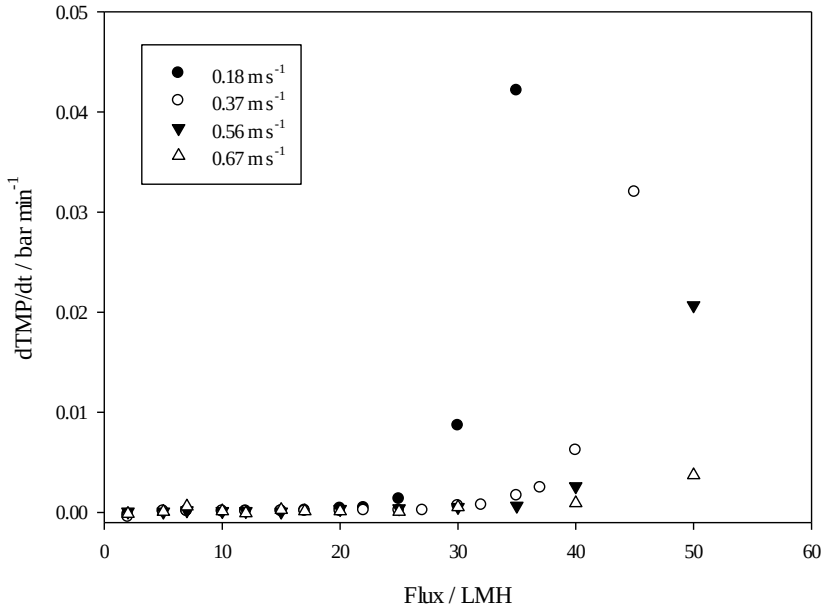

Figure 5.10: dTMP/dt for the filtration of 2 wt% gum arabic with 0.1 µm PS membranes at different CFVs as a function of flux. The temperature was 40 ºC

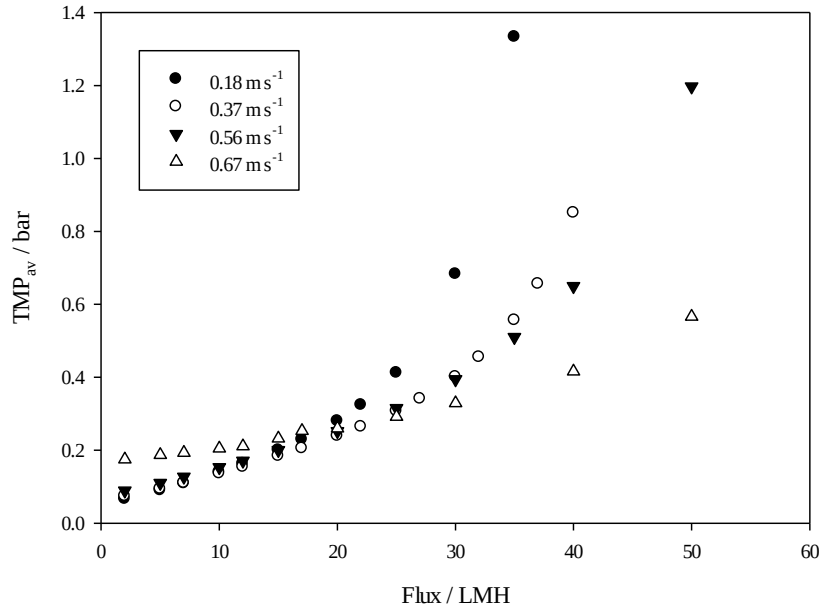

Figure 5.11: TMP_{av} for the filtration of 2 wt% gum arabic with 0.1 µm PS membranes at different CFVs as a function of flux. The temperature was 40 ºC

The critical fluxes determined from Figure 5.11 as the point at which permeability is no longer linear are 20, 27, 30 and 40 LMH for 0.18, 0.37, 0.56 and 0.67 m s^{-1} CFV, respectively.

The subcritical permeability for these 4 CFVs (85.5, 113.6, 93.4 and 161.2 L m^{-2} h^{-1} bar $^{-1}$, respectively) were observed to be lower than the corresponding constants for pure water (769.2, 625.0, 416.7 and 714.3 L m^{-2} h^{-1} bar^{-1}, respectively), indicating the weak form of the critical flux.

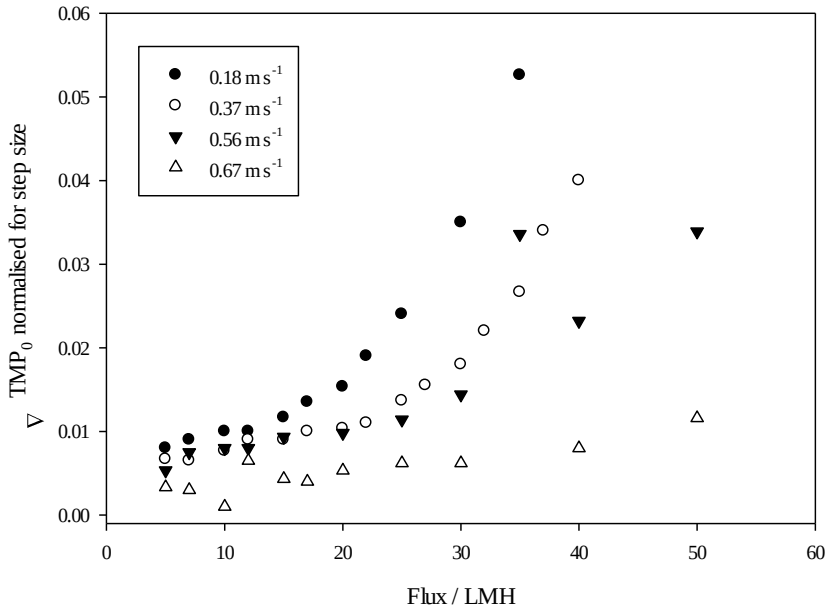

Figure 5.12: ΔTMP_0 for the filtration of 2 wt% gum arabic with 0.1 µm PS membranes at different CFVs as a function of flux. The temperature was 40 ºC

Table 5.2: The critical flux of 2 wt% gum arabic using 0.1 µm PS membranes at different CFVs determined by different methods

Criterion	**Critical flux / LMH 0.18 m s^{-1} CFV**	**Critical flux / LMH 0.37 m s^{-1} CFV**	**Critical flux / LMH 0.56 m s^{-1} CFV**	**Critical flux / LMH 0.67 m s^{-1} CFV**
dTMP / dt < 0.001 bar min^{-1}	22	32	35	40
dTMP / dt (Fig 5.9)	22	32	35	40
TMP_{av} (Fig 5.10)	17	27	30	40
ΔTMP_0 (Fig 5.11)	15	22	25	40

The average critical fluxes were determined and plotted against CFV shown in Figure 5.13.

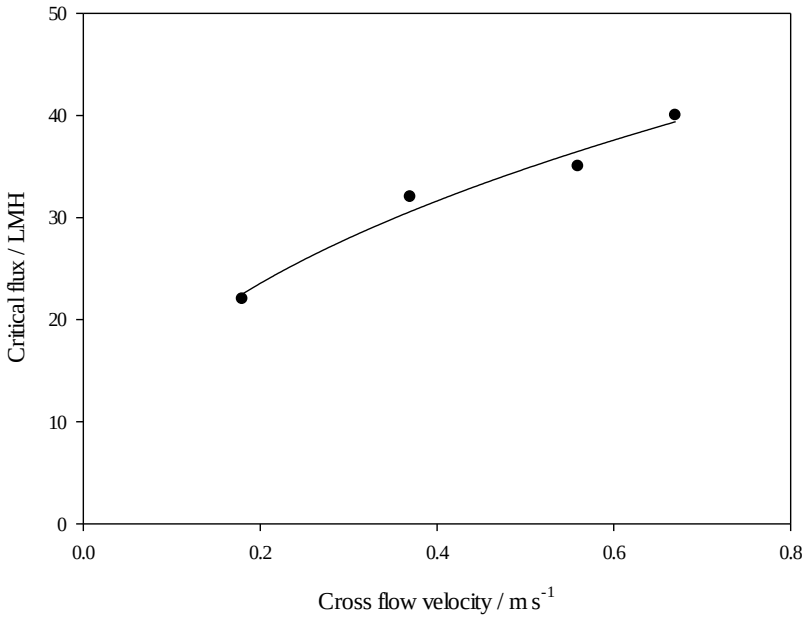

Figure 5.13: Critical flux values for 2 wt% gum arabic at varying CFVs with 0.1 µm PS membranes

The relationship between flux and CFV can be described using the following equation:

$$J = f(V)^{\alpha} \qquad \text{Equation 5.3}$$

The value of α varies depending on the system conditions but is typically between 0.3 – 1.33 for laminar flow, with the most common values lying between 0.3 and 0.6 [62]. The α value for this system was found to be 0.425, confirming that the system operates in laminar flow.The graph displays a power law, whereby the higher the CFV, the less beneficial effect this has on increasing the critical flux. This is discussed below.

Increasing the CFV had the effect of increasing the critical flux. The values determined by dTMP/dt are 22 LMH, 32 LMH, 35 LMH and 40 LMH for 0.18, 0.37, 0.56 and 0.67 m s^{-1}, respectively, as shown in Table 5.2

These experiments into the effect of CFV on the critical flux show that the flux at which fouling becomes significant increases quite considerably within the range studied. The largest increase occurs towards the lower end of the CFVs. The increase in CFV creates a greater shear across the surface of the membrane, reducing the boundary layer thickness and minimising the risk of fouling at low permeate fluxes. The CFV creates lateral migration of particles, which is a mechanism counteracting the convective transport of particles towards the membrane. As the CFV is increased, however, a greater pressure drop across the membrane is seen and this results in a higher TMP at the inlet. This higher TMP may be super-critical, even if the average over the membrane is sub-critical. This can result in increases in CFV having smaller effects on the critical flux increase at higher CFV values. Table 5.3 shows the average pressure drop across the membrane for each of the experiments.

Table 5.3: The average pressure drops across a 0.1 μm PS membrane during the filtration of 2 wt% gum arabic at different CFVs

Experiment crossflow velocity / m s^{-1}	**Average pressure drop across the membrane / bar**
0.18	0.018
0.37	0.053
0.56	0.1
0.67	0.25

Gesan-Guiziuo *et al.* (1999) studied the effect of hydrodynamic conditions on critical flux of skimmed microfiltration.[132] They found that the limiting flux – the flux above which significant and irreversible fouling occurred - depended on the wall shear stress. A critical ratio of flux : wall shear stress was defined below which performance was satisfactory. Above this critical ratio, consolidation of the deposit occurred due to compression under the high TMP. This is likely to be similar with gum arabic, where increasing the CFV increases the wall shear stress, thereby allowing a greater operation flux before significant fouling occurs.

5.4. Fouling above and below the critical flux

Fouling experiments of 4 h duration were carried out in diafiltration mode with 2 wt% gum arabic, both above and below the critical fluxes determined above and the TMP vs flux curves for the three membranes are shown in Figures 5.14, 5.15 and 5.16. Feed and permeate samples were collected and analysed for total solids, AGP and protein rejection.

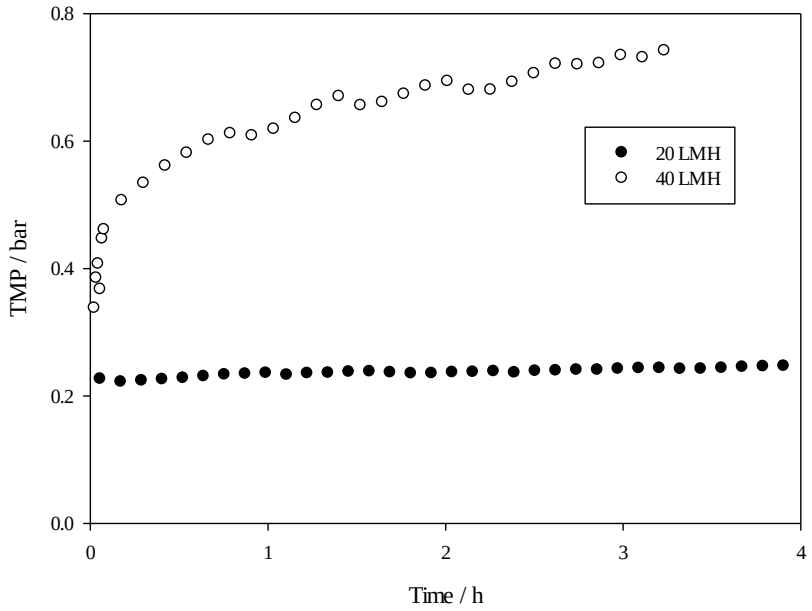

Figure 5.14: TMP fouling curves for the filtration of 2 wt% gum arabic using 0.1 µm PS membrane above and below the critical flux. Filtration temperature was 40 ºC and the CFV was 0.37 m s^{-1}

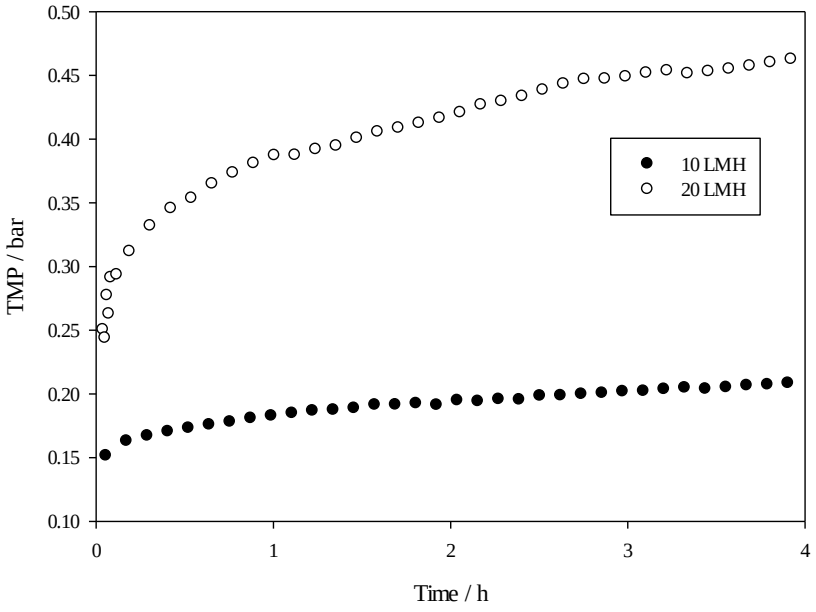

Figure 5.15: TMP fouling curves for the filtration of 2 wt% gum arabic using 0.5 µm PS membrane above and below the critical flux. Filtration temperature was 40 ºC and the CFV was 0.37 m s^{-1}

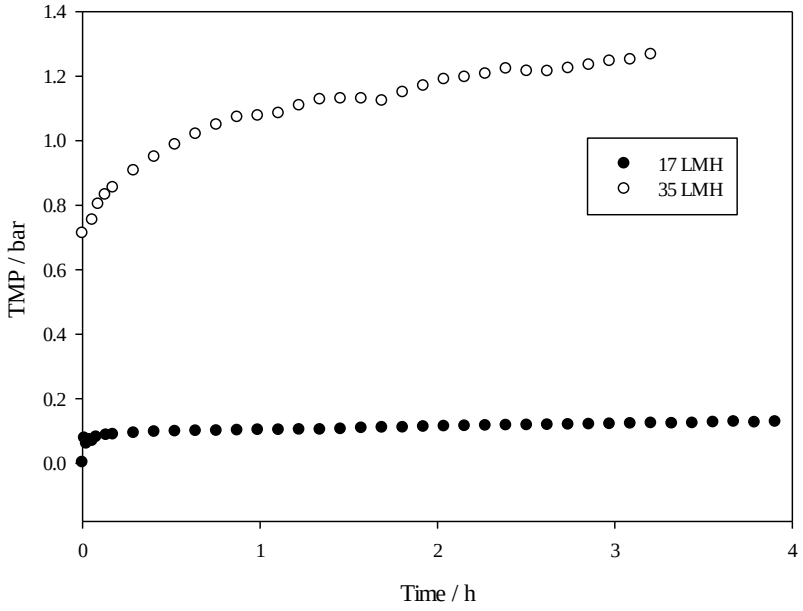

Figure 5.16: TMP fouling curves for the filtration of 2 wt% gum arabic using 0.8 µm PS membrane above and below the critical flux. Filtration temperature was 40 ºC and the CFV was 0.37 m s^{-1}

Tables 5.4 and 5.5 display the solids rejection and the protein and AGP content of the permeate from the filtration of 2 wt% gum arabic using 0.1, 0.5 and 0.8 µm PS membranes at fluxes above and below the critical flux. The protein mass fraction of the feed was 0.052 ± 0.01 and all protein values were calculated from elemental analysis by multiplying the %N by a conversion factor of 6.6.[13] The feed AGP mass fraction was 0.146 ± 0.009.

Table 5.4: Solids content, protein mass fraction and AGP mass fraction of the permeate for filtration of 2 wt% gum arabic with 0.1, 0.5 and 0.8 µm PS below critical flux

Membrane	**Rejection**	**Permeate protein mass fraction**	**Permeate AGP mass fraction**
0.1 µm	0.99	*Insufficient sample mass*	*Insufficient sample mass*
0.5 µm	0.96	0.083	0.087
0.8 µm	0.6	0.035	0.133

Table 5.5: Solids content, protein mass fraction and AGP mass fraction of the permeate for filtration of 2 wt% gum arabic with 0.1, 0.5 and 0.8 µm PS above critical flux.

Membrane	**Rejection**	**Permeate protein mass fraction**	**Permeate AGP mass fraction**
0.1 µm	0.95	0.095	0.009
0.5 µm	0.97	0.082	0.085
0.8 µm	0.92	0.07	0.108

The solids rejection values are plotted against membrane pore size in Figure 5.17.

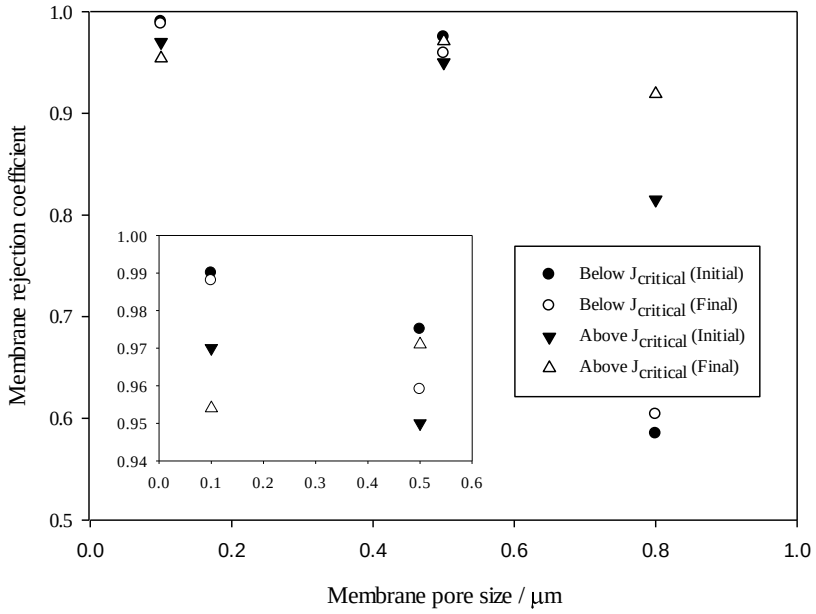

Figure 5.17: Rejection coefficients for the filtration of 2 wt% gum arabic using 0.1, 0.5 and 0.8 µm PS membranes above and below the critical flux. Rejection coefficients are shown for the first 100 mL permeate (initial) and an average of the rest of the permeate (final)

Figures 5.14, 5.15 and 5.16 show how the TMP changes over time during the diafiltration of 2 wt% gum arabic, both above and below the critical flux. For the 0.1 µm PS membrane, there is no TMP rise over 4 h of filtration at 20 LMH whereas at 40 LMH, a rapid initial increase is seen over the first 30 minutes, followed by a more gradual yet still substantial increase after that. For the 0.5 µm membranes, (Figure 5.15) a slight increase in TMP over time at 10 LMH indicates that the critical flux is in fact lower than determined above. The curve at 20 LMH shows the same rapid increase in TMP followed by a more gradual increase. This trend is also seen for the 0.8 µm membrane, with the flux of 17 LMH being sub-critical as no TMP rise is seen.

Le Clech *et al.* also found there to be no strong form of the critical flux during their study of synthetic and real sewage filtration.[1] A weak form of the critical flux was found, however, which defined the flux below which very little fouling occurred and above which significant fouling was observed. They found that the flux stepping method was sufficient to define the critical flux for short term fouling, but that after a critical time period, fouling increased significantly as well. In this work, the critical flux was found to be accurate for up to 4 h fouling, but longer studies would be needed to confirm its long-term validity.

In all three fouling curves during operation above the critical flux, 2 distinct phases can be observed. The first is an initial, rapid rise in TMP due to concentration polarisation (although this is suspected to be minimal for gum arabic), the adsorption of species to the surface of the membrane and pore constriction. The second phase is a slower, steadier rise in TMP caused by the build-up of a cake layer together with some pore constriction for the larger pore sized membranes.[133] A higher super critical operation TMP is seen for the 0.8 µm membrane than for the other two membranes. This is likely to be due to the larger pore size of the membrane allowing for greater pore blocking or constriction as a larger proportion of the gum species are able to enter the pores. This is clear from the solids rejection, which is lowest for the 0.8 µm membrane, but increases rapidly over time due to fouling (Figure 5.17). This is in agreement with the work in Chapter 4.

From Tables 5.4 and 5.5, it can be seen that both the 0.5 and 0.8 µm PS membranes show the expected trend of the 0.5 µm permeate sample having a lower solids content that the 0.8 µm permeate sample due to the larger pore size of the 0.8 µm membrane allowing a greater proportion of the gum arabic through. In the cases of filtration above the critical flux, the solids content drops from the first 100 mL of permeate to the average over the whole filtration (between 400 – 600 mL permeate). This is because fouling of the internal membrane structure as well as cake formation on the surface effectively reduces the membrane pore size, reducing the % of gum that can be transmitted by the membrane. In the case of the filtration below the critical flux, the solids content of the first 100 mL permeate is very similar to the average of the full permeate. This is because significant fouling of the membrane does not occur and so the filtration capability of the membrane is not affected.

The results from the 0.1 µm filtrations, however, are inconclusive. This is possibly due to the high error associated with the very small solids content of the permeate. Repeats of this experiment are needed in order to obtain more reliable data.

Elemental analysis and GPC were carried out on permeate samples to determine the protein and AGP mass fractions (Tables 5.4 and 5.5). The protein and AGP mass fractions for the 0.5 µm membranes above and below the critical flux are almost identical. This is likely to be due to the 'sub-critical' experiment in fact not being below the critical flux, as discussed above. Although the fouling was certainly more severe in the experiment at 20 LMH than the experiment at 10 LMH, this seems to have had little effect on the fractionation. The permeate is depleted in AGP compared to the feed, however, showing that AGP is rejected by the membrane.

The 0.8 µm data show that a greater proportion of the AGP is rejected by the membrane at 35 LMH, i.e. above the critical flux. This is because the fouling enhances the fractionation performance of the membrane, which was also observed in Chapter 4. However, the permeate still contains about 10 wt% AGP, so this membrane alone is not sufficient for good gum arabic fractionation. Some feed or membrane modification is required to improve the AGP rejection.

The 0.1 µm membrane at super-critical flux shows almost complete rejection of AGP, which is very positive, however a high rejection of all gum solids is also seen, meaning the use of this membrane for fractionation would be very time consuming and both energy and water intensive.

5.5. Conclusion

The weak form of the critical flux of 2 wt% gum arabic using 0.1, 0.5 and 0.8 µm PS membranes was determined by a flux-stepping method to be 27, 12 and 22 LMH, respectively, at 40 ºC and a CFV of 0.37 m s^{-1}. Experiments performed at different CFVs showed the critical flux to increase with increasing CFV. Longer fouling tests were carried out both above and below the determined critical flux and showed that the flux-stepping method is effective at estimating the critical flux over short (several hour) fouling runs. Analysis of the permeate shows that operating below the critical flux removes the membrane fouling and therefore, in the case of the 0.8 µm membrane, reduces the fractionation capability of the membrane. To further improve the fractionation of gum arabic using membranes, the use of other membrane materials and feed modification need to be investigated.

6. The effect of membrane material on the filtration and fractionation performance

6.1. Introduction

This chapter details the work carried out with different membrane materials. 0.5 µm polysulfone (PS) was compared with 0.5 µm fluoropolymer (FP) and 0.45 µm cellulose acetate (CA). The filtration performance using 2 wt% gum arabic was compared as was the extent of fouling and the fractionation performance. The membrane surfaces were analysed by contact angle, AFM, zeta potential, FTIR and SEM to explain the trends seen.

6.2. Experimental methods

6.2.1. Diafiltration experiments

Feed preparation and use of the M10 module were as explained above for Chapter 4. 0.5 µm PS and FP membranes were conditioned with RO water at 60 ºC prior to use. PWF measurements were recorded at 40 ºC, 0.5 bar and 1.7 m s^{-1} CFV. Diafiltration fouling experiments were then run for 2 h and the membranes were then rinsed and cleaned as detailed above for Chapter 4. Feed and permeate samples were dried by rotary evaporation and analysed for total solids, AGP and protein content.

6.2.2. Membrane characterisation

Membranes were air dried at different stages of the foul-clean cycle. Virgin membranes were conditioned (for PS and FP) and the PWF was recorded (for all three materials) and then dried. 'Fouled and soaked' membranes were removed from the filtration rig after fouling and soaked in 5 L RO water for 10 minutes before being air dried. For the zeta potential measurements the

membranes were fouled and rinsed with RO water in the M10 rig. 'Fouled and cleaned' membranes were air dried after the full foul-clean cycle.

All membranes were analysed by FTIR, SEM and AFM; the contact angle with water was recorded and the surface charge was measured.

6.3. Membrane structure

Figure 6.1 shows cross-sections of 0.5 µm PS (A), 0.5 µm FP (B) and 0.45 µm CA (C). The PS and FP skin layers are clear in images A and B, respectively. The backing layer is made of polypropylene. The CA membrane in image C is of symmetric structure, the denser areas are areas that were compressed by the cross-sectioning process. Higher magnification images of the skin layers are shown below each image.

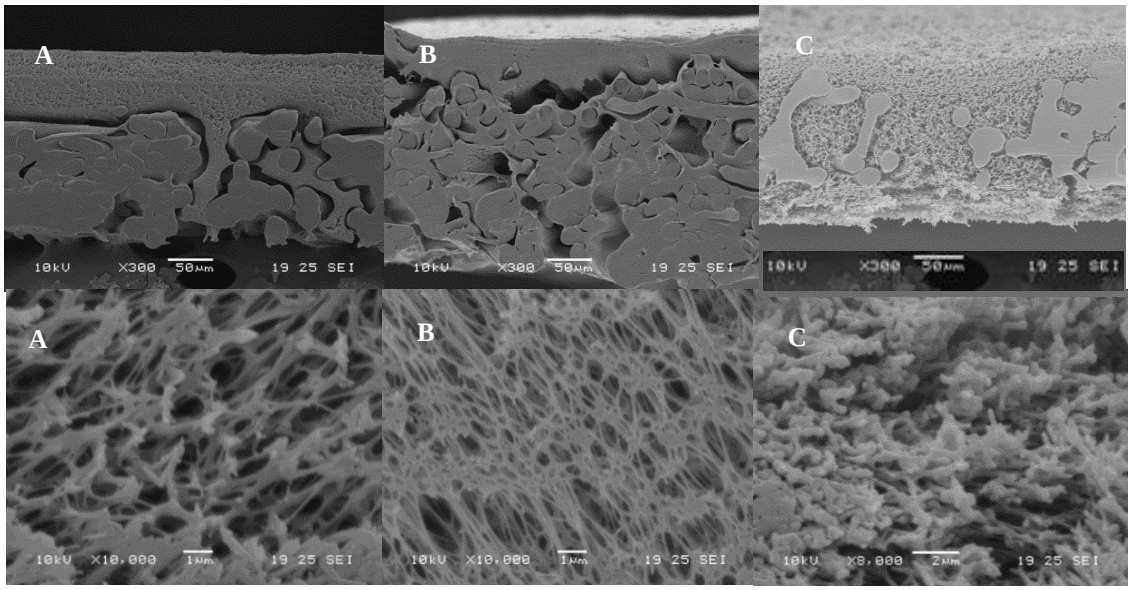

Figure 6.1: Cross-sectional SEM images of 0.5 µm PS (A), 0.5 µm FP (B) and 0.45 µm CA (C) membrane showing the whole cross section (top) and a higher magnification image of the active layer (bottom)

6.4. The filtration behaviour of PS, FP and CA

6.4.1. Water permeability

The water permeability of the three membranes was measured for each membrane after the PS and FP membranes had been conditioned to remove the glycerol coating. The CA membranes were uncoated and therefore not conditioned. The TMP vs flux plots are shown in Figure 6.2. Permeability is the gradient of a pressure-flux graph and this is shown in Table 6.1 for all three membranes at 40 ºC.

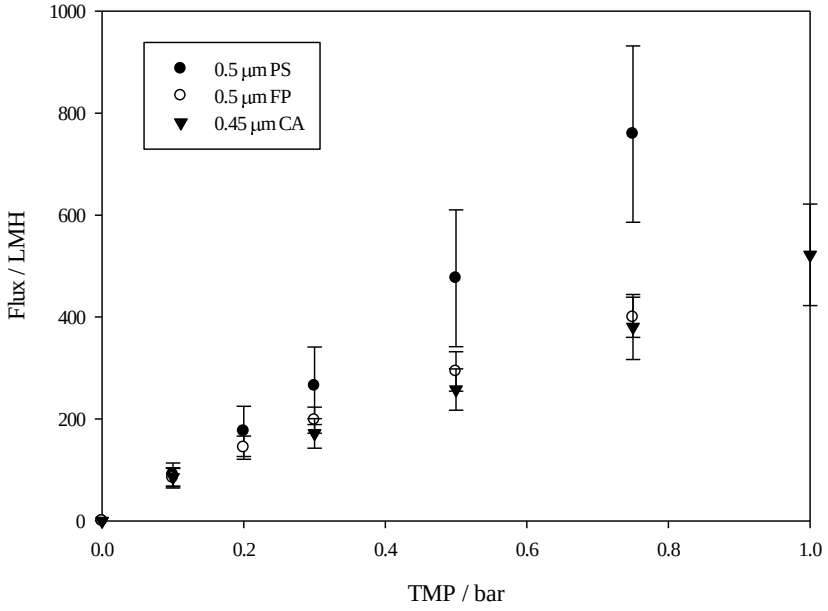

Figure 6.2: Flux vs TMP plots for 0.5 µm PS, 0.5 µm FP and 0.45 µm CA membranes measured at 40 ºC and 1 m s^{-1} CFV

Table 6.1: Permeability and membrane resistances for 0.5 µm PS, 0.5 µm FP and 0.45 µm CA membranes

Membrane	**Membrane resistance / x 10^{12} m^{-1}**	**Permeability / L m^{-2} h^{-1} bar^{-1}**
0.5 µm PS	0.55 ± 0.15	997 ± 269
0.5 µm FP	0.97 ± 0.15	570 ± 86
0.45 µm CA	1.06 ± 0.19	521 ± 94

6.4.2. Filtration flux

Figure 6.3 shows the flux of 2 wt% gum arabic under the conditions set as standard as a TMP of 0.5 bar, a CFV of 1.7 m s^{-1} and an operating temperature of 40 ºC. The average total solids rejection coefficient for each membrane is shown in Table 6.2.

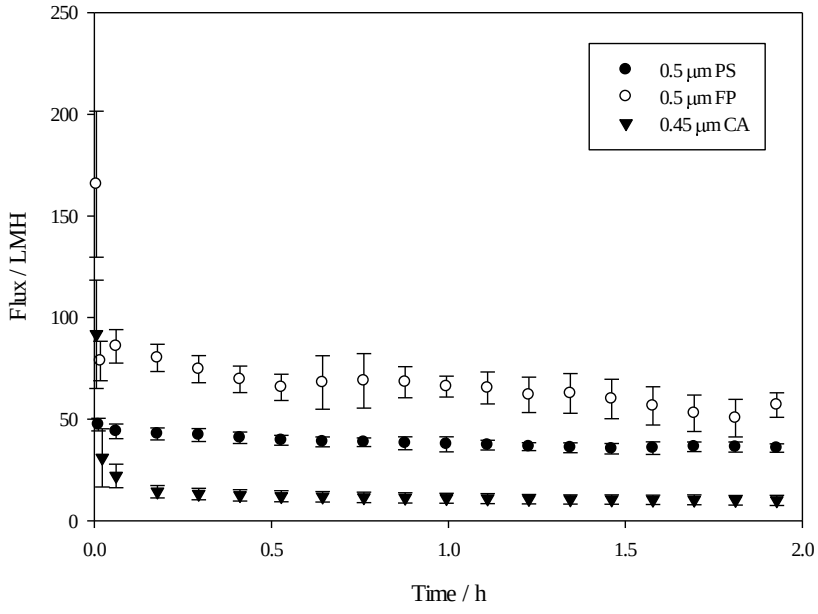

Figure 6.3: The permeate flux of 2 wt% gum arabic filtered through 0.5 µm PS, 0.5 µm FP and 0.45 µm CA membranes at 40 ºC, 0.5 bar TMP and 1.7 m s^{-1} CFV

Table 6.2: The total solids rejection coefficients for the filtration of 2 wt% gum arabic using 3 membrane materials

Membrane	**Solids rejection coefficient**
0.5 µm PS	0.95 ± 0.05
0.5 µm FP	0.96 ± 0.007
0.45 µm CA	0.28 ± 0.03

The difference in permeate flux between the different membrane materials is quite significant, with the FP displaying the highest flux (72 LMH average). The PS has a lower average flux of 36 LMH and the CA has an average flux of only 17 LMH. Both the PS and FP membranes display greater than 95 % rejection of solids whereas the CA membrane rejects only 28 % of the solids, which represents a huge difference in performance for membranes of approximately the same nominal pore size.

Due to the vast difference in rejection coefficient between the CA membrane and the PS and FP membranes, the gum concentration and therefore the viscosity of the permeate will differ greatly. It is important, therefore, to also look at the total membrane resistance for the 3 materials. This is shown in Figure 6.4.

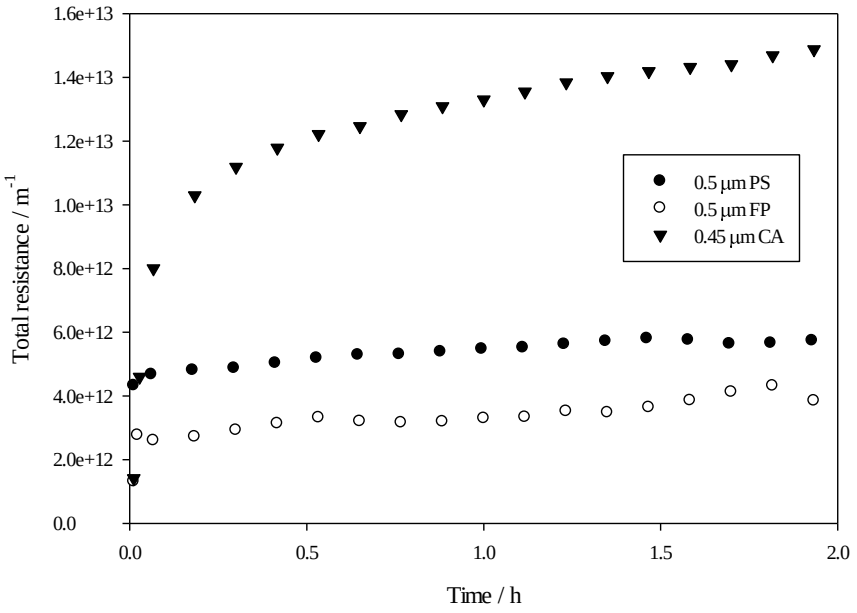

Figure 6.4: The total resistance for the filtration of 2 wt% gum arabic using 0.5 µm PS, 0.5 µm FP and 0.45 µm CA membranes at 40 ºC, 0.5 bar TMP and 1.7 m s^{-1} CFV

Figure 6.4 shows that, although the permeate concentration and viscosity of the CA membranes is much higher than the other two materials, this does not entirely account for the greater resistance during fouling, as the resistance normalises for viscosity.

Nataraj *et al*. studied the fouling effects of model polysaccharides including xanthan gum, which is a high MW polysaccharide containing large amounts of glucuronic acid, similar to gum arabic.[81] They found that deposition of small quantities of the xanthan gum onto regenerated cellulose membranes resulted in severe flux decline, similar to that experienced here.

The 3 membranes behave very differently during the filtration of gum arabic and it is necessary to analyse the membrane surface to determine whether the surface charge, hydrophobicity or surface roughness are the cause of the differences.

6.5. Membrane characterisation

6.5.1. FTIR

All three dried membranes in virgin, fouled and soaked and fouled and cleaned condition were analysed by FTIR to determine whether there was gum arabic fouling on the surface and the efficacy of its removal during cleaning. The spectra for all three membranes are shown in Figure 6.5.

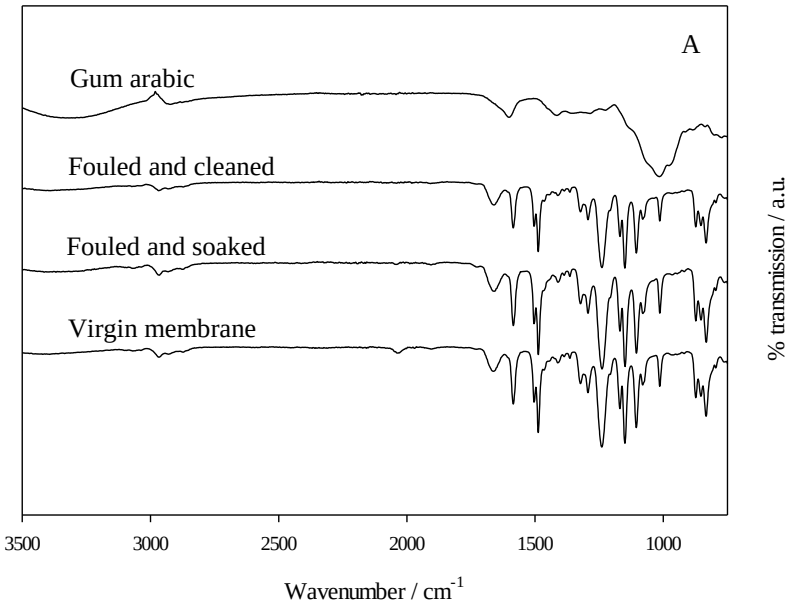

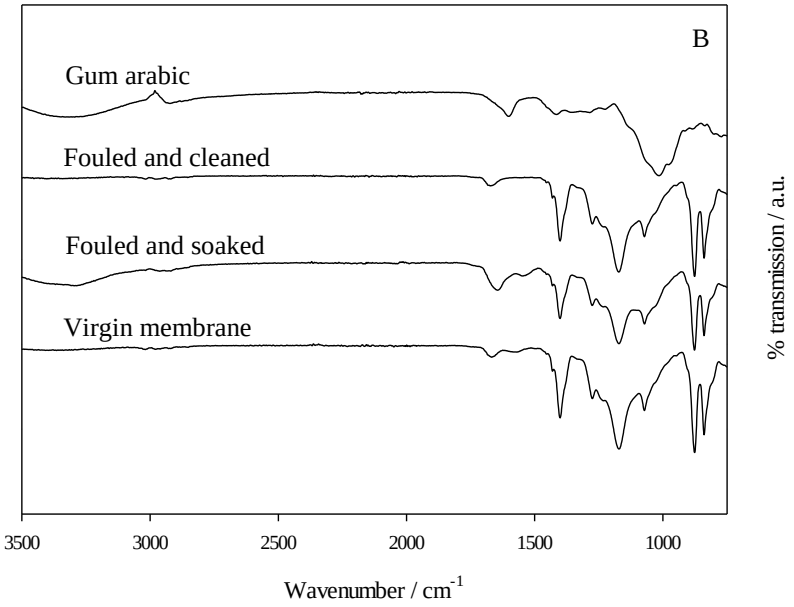

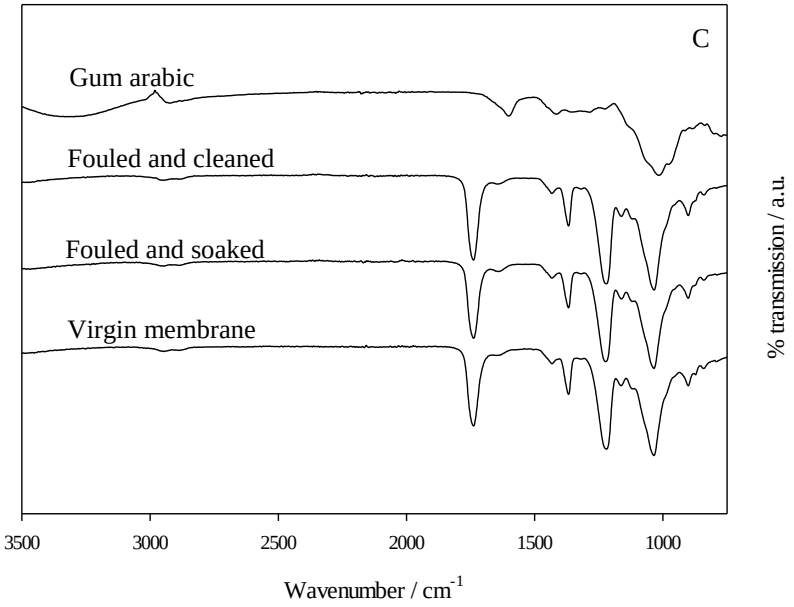

Figure 6.5: FTIR traces of virgin, fouled and soaked and fouled and cleaned 0.5 µm PS (A), 0.5 µm FP (B) and 0.45 µm CA (C) membranes with the FTIR trace of gum arabic in each case

In all three membranes no clear evidence of gum arabic peaks is seen in the fouled and soaked spectra. It is suspected, therefore, that the 10 min soaking process was sufficient for all of the surface fouling, or sufficient to be undetectable by FTIR, to redissolve and be removed from the

surface, as seen in Chapter 4. A slight shoulder peak is seen in the fouled and soaked spectrum of the 0.5 µm FP membrane (B) at just below 1000 cm^{-1}, which fits with the large gum arabic peak at the same wavelength. This is possibly due to some residual gum on the surface. Large peaks in the cellulose acetate spectra (C) at about 1000 cm^{-1} could be masking gum arabic peaks in this case so definite conclusions cannot be drawn from these data. Background removal of the virgin membrane spectrum for each material was carried out, as in Chapter 4, but the intensity of the peaks was too low to confirm the presence or absence of gum arabic on the surface. It is presumed that due to the soluble nature of the gum, the majority of the cake layer is dissolved away in the soaking process, leaving too little gum on the surface to be detected by FTIR.

6.5.2. Contact angle measurements

Air-dried PS, FP and CA membranes in virgin, fouled and soaked and fouled and cleaned states were analysed for hydrophobicity by measuring the surface contact angle with water. Figure 6.6 shows the average contact angles for the PS and FP membranes each taken from 5 repeats with left and right contact angles recorded for each. The error bars represent ± 1 standard deviation.

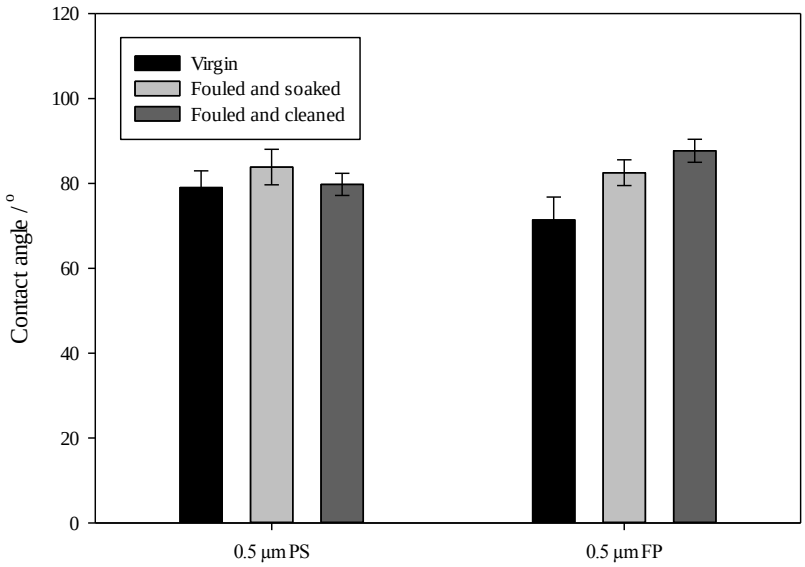

Figure 6.6: Contact angle values for 0.5 µm PS and 0.5 µm FP in virgin, fouled and soaked and fouled and cleaned condition

The PS and FP membranes display contact angles of between 70 and 90º in virgin, fouled and cleaned states. The PS membranes show no statistical difference in contact angle between the virgin, fouled and cleaned membranes. The FP membranes show a slight increase in contact angle upon fouling, meaning that the membrane hydrophobicity has increased. This is perhaps due to hydrophobic amino acid groups within the gum protein binding to the fairly hydrophobic membrane surface.

The CA membranes demonstrated very high contact angles, which were not expected as the material is described as hydrophilic by the manufacture but this was due to a change in the membrane properties upon drying. The membranes were kept wet for all filtrations and only dried for analysis purposes. The contact angle was measured with material straight from the packet and the membrane 'wetted out' immediately making it impossible to measure the contact angle accurately. It can be said that the material is highly hydrophilic, however. Hydrophilic membranes are often less prone to fouling with feeds containing proteinaceous or lipid material than hydrophobic membranes. Lockley *et al.* (1988) found this in a study that compared protein

adsorption to hydrophobic polysulfone membranes with that to hydrophilic cellulose acetate membranes. They found that fouling was much more severe in the case of the hydrophobic membranes.

Approximately 90 % of the gum arabic is made of hydrophilic carbohydrate material, which is likely to hydrogen bond with the hydrophilic cellulose acetate. This could explain the very high resistance during fouling seen with the CA membranes.

6.5.3. Surface charge measurements

The membrane surface charge over a range of pHs was measured and the data for the three membrane materials in virgin condition are shown in Figure 6.7. Three measurements were taken at each pH and error bars represent ± one standard deviation.

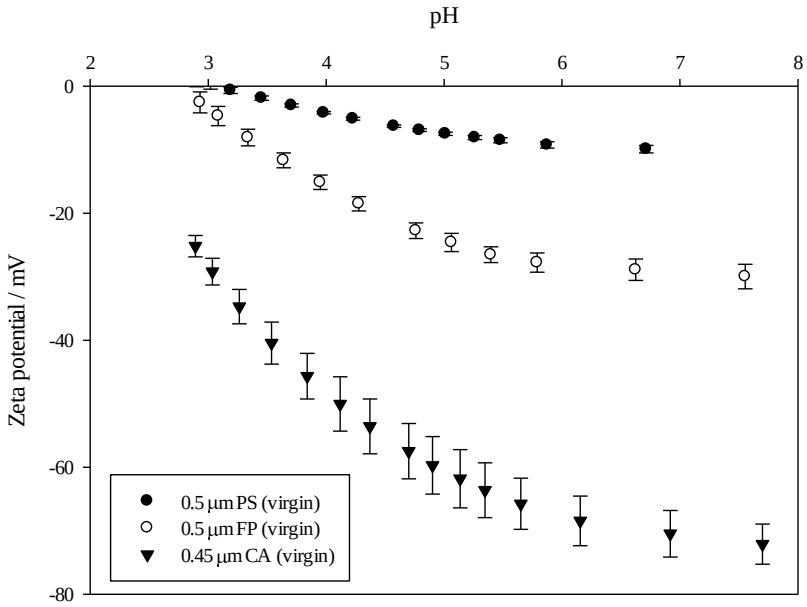

Figure 6.7: Zeta potential curves for 0.5 µm PS, 0.5 µm FP and 0.45 µm CA in virgin condition over pH range of 3 - 8

The virgin membrane curves (Figure 6.7) show that all three membranes are negatively charged in the pH range of 3 – 8 but to different degrees. The PS has a maximum charge of about -10 mV at pH 7 - 8. This deceases to an isoelectric point at approximately pH 3. At the natural pH

of 2 wt% gum arabic (~ pH 4.5), the membrane displays a charge of about -7 mV. The FP is more negatively charged with a maximum charge of about -30 mV at pH 7 – 8. The membrane charge is fairly constant as the pH is dropped until pH 5 where the charge then rapidly decreases, reaching a charge of about -5 mV at pH 3. The isoelectric point is therefore estimated to be at approximately pH 2.5. The membrane charge is approximately -20 mV at the natural pH of 2 wt% gum arabic. The CA membrane is more negatively charged still, approximately -70 mV at pH 7 – 8. An isoelectric point is not reached or approached in the pH range tested and the membrane charge at pH 4.5 is about -55 mV.

Lim *et al.* (2011) studied the ultrafiltration of gelatin using PES membranes and found that at the IEP of the gelatin, there was no charge repulsion and the protein was able to assemble more densely in the concentration boundary layer, leading to a greater resistance to flux.[93] At the natural pH of gum arabic, all three membranes and the gum arabic will be negatively charged so this should prevent the dense build-up of deposit in the councentration boundary layer.Figure 6.8 (A, B and C) show the zeta potential curves for the 3 membrane materials in virgin, fouled and rinsed and fouled and cleaned state to show the effect of these conditions on the surface charge.

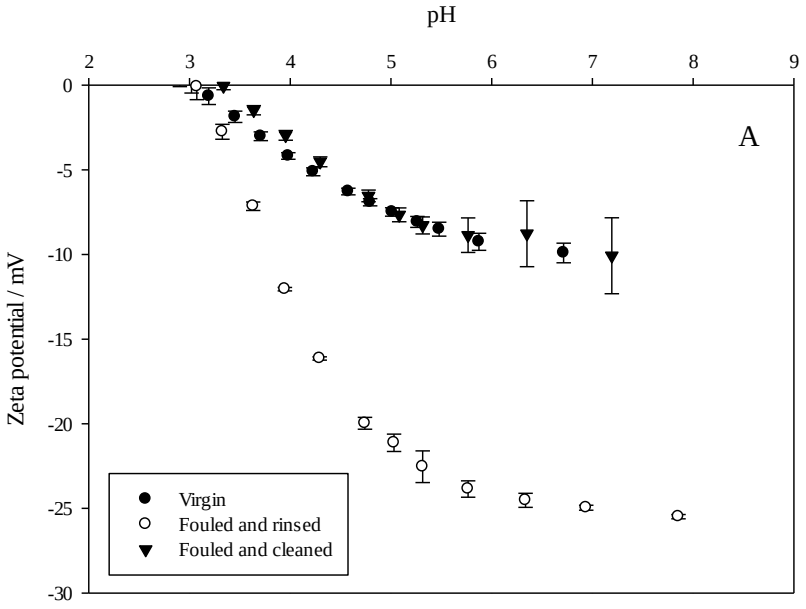

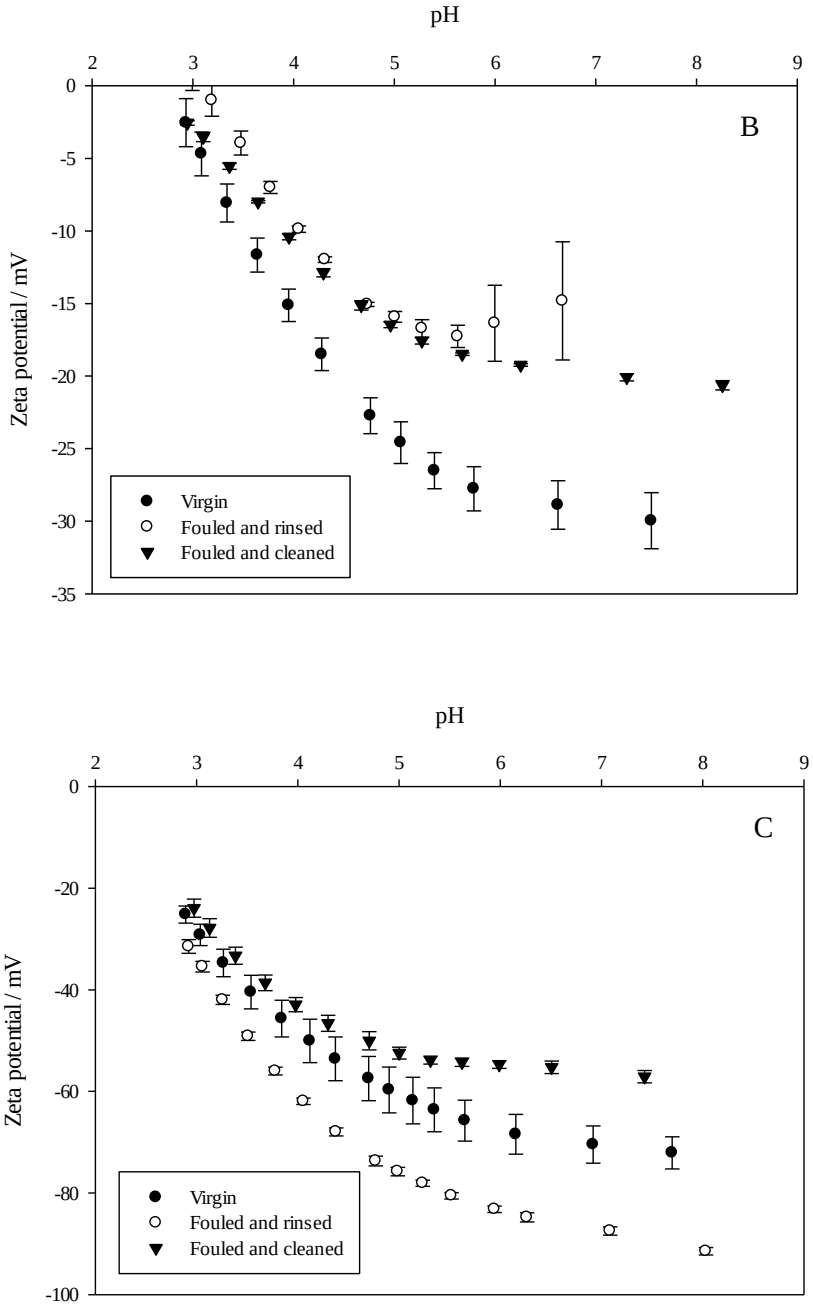

Figure 6.8: Zeta potential curves for virgin, fouled and rinsed and fouled and cleaned 0.5 µm PS (A), 0.5 µm FP (B) and 0.45 µm CA (C) membranes over pH range of 3 - 8

The PS membrane fouled and rinsed with RO water displays a considerably lower surface charge than the virgin membrane, which is returned to the original charge upon cleaning. This suggests the binding of some negatively charged species to the surface of the membrane, which is then removed during cleaning. The proteins within gum arabic will be negatively charged at

pHs above their isoelectric point (< pH 3), so it is likely that some protein has bound to the surface. As there are hydrophobic groups in the proteins, it follows that these should bind to the hydrophobic membrane surface. The NaOH cleaning is effective at returning the membrane surface to the original condition. This method does not indicate whether the membrane charge within the pores is altered by fouling and cleaning but the surface charge is effectively restored.

The FP becomes less negatively charged upon fouling of the membrane, which could be due to adhesion of positively charged species in the gum, such as metal cations. These would mask some of the negative charge on the membrane surface. The zeta potential is not restored to that of the virgin membrane in the fouled and cleaned curve, indicating that the cleaning is not effective at removing these positively charged species.

The CA membrane becomes more negatively charged upon fouling, indicating adhesion of negatively charged gum species. The charge is then reduced to values below that of the virgin membrane upon cleaning. It is hypothesised that the membrane is not cleaned by the small quantities of NaOH (CA is not tolerant of high pHs) but that the charges are masked by binding of Na^+ ions from the cleaning solution. The quantities of foulant adhering to the surface can only be small as gum species were not detected in the FTIR or observed in the SEM of any of the 3 membrane materials, but small quantities can still affect the zeta potential.

6.5.4. SEM imaging

Figure 6.9 shows SEM images of the surface of 0.5 µm PS, 0.5 µm FP and 0.45 µm CA membranes in virgin condition.

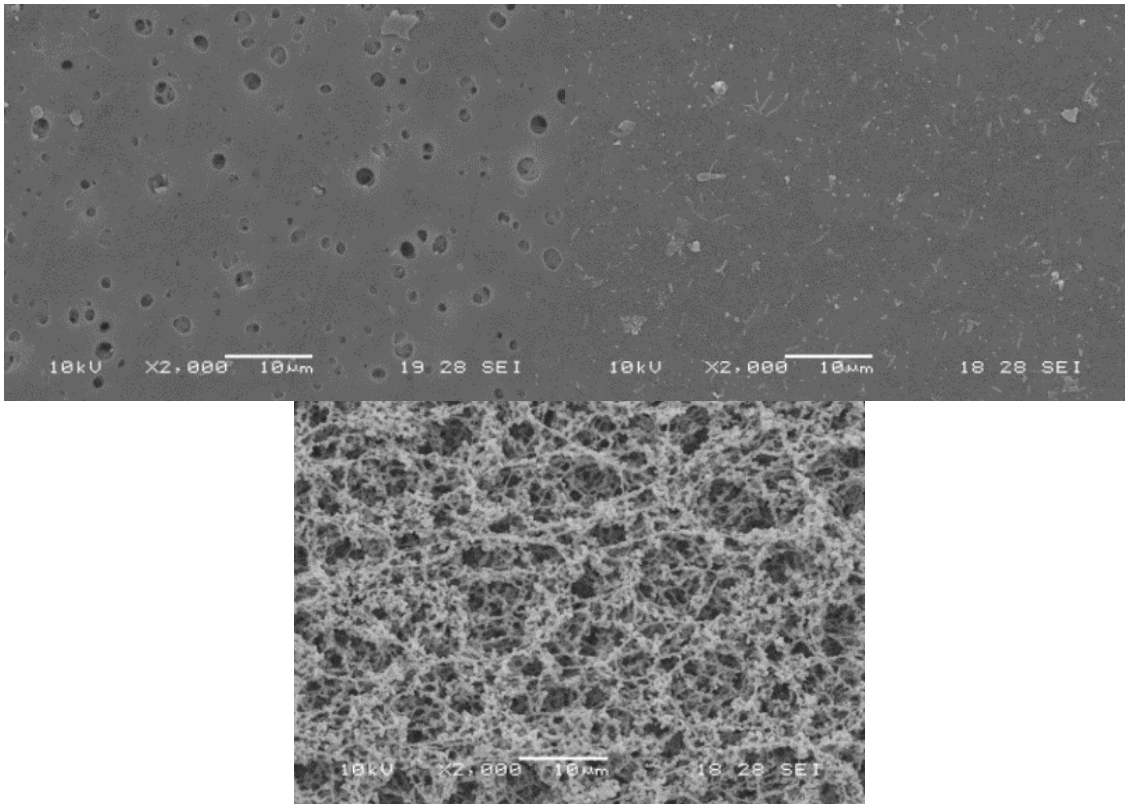

Figure 6.9: SEM images of the top surface of 0.5 µm PS (top, left), 0.5 µm FP (top, right) and 0.45 µm CA (bottom) membranes in virgin condition

None of the fouled and soaked membranes showed signs of surface fouling by gum arabic, so only virgin membrane surfaces are shown. This supports the hypothesis that the cake layer is redissolved into the bulk during the 10 min soaking.

6.5.5. Surface roughness measurements

Roughness measurements for all membranes are detailed in Table 6.3. Three different areas were imaged for each membrane and standard deviations are given.

Table 6.3: Roughness values (S_A) for 100 μm^2 areas of virgin 0.5 μm PS (A), 0.5 μm FP (B) and 0.45 μm CA (C) membranes

Membrane	**Roughness / nm**		
	Virgin	Fouled and soaked	Fouled and cleaned
0.5 μm PS	120.5 ± 17.1	119.0 ± 30.6	113.7 ± 13.1
0.5 μm FP	550.8 ± 61.2	365.8 ± 52.5	408.0 ± 57.2
0.45 μm CA	1053.8 ± 158.8	868.2 ± 28.8	889.4 ± 61.5

All three virgin membranes display very different surface roughness measurements. The PS membrane has the lowest roughness value at 120 nm, the FP is rougher at 550 nm and the CA is very rough at over 1 μm in roughness. Some studies have shown that smoother membrane surfaces are prone to greater flux declines due to the build-up of dense fouling layers that are not disrupted by localised turbulence caused by contours on the membrane.[101, 134] However, the rougher surfaces can provide 'hooks' for suspended matter in the feed, leading to increased fouling.[62] In this case, the CA displays the lowest permeate flux and the highest surface roughness, suggesting that the roughness results in greater fouling. The FP, however, with a roughness of 550 nm performs the best with the highest average permeate flux. This suggests that roughness is not the governing factor in membrane performance.

6.6. Membrane fouling

6.6.1. Resistance breakdown

Full diafiltration resistance profiles are shown in Figures 6.10, 6.11 and 6.12. The conditions for each step are detailed in 4.2.4.. The data shown are an average of 3 cycles and error bars represent ± 1 standard deviation.

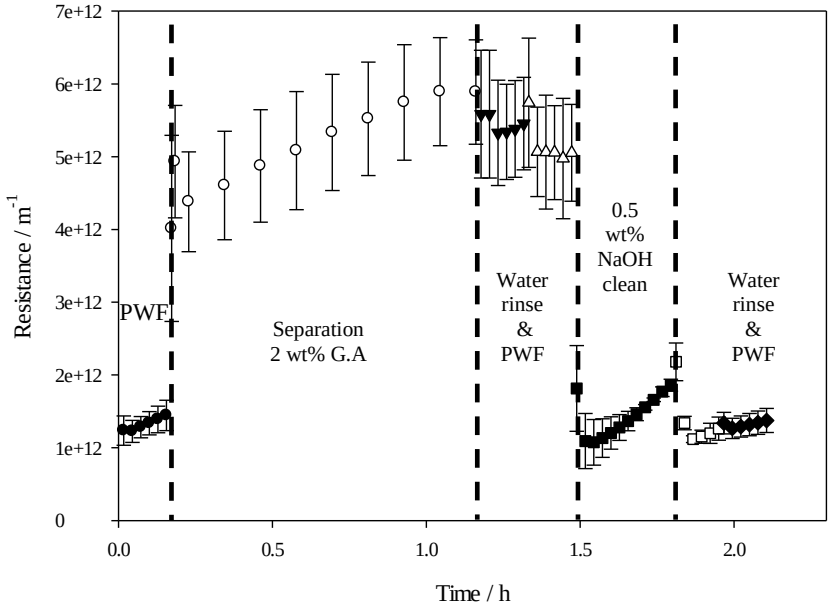

Figure 6.10: Foul-clean cycle resistance profile for 2 wt% gum arabic using a 0.5 µm PS membrane

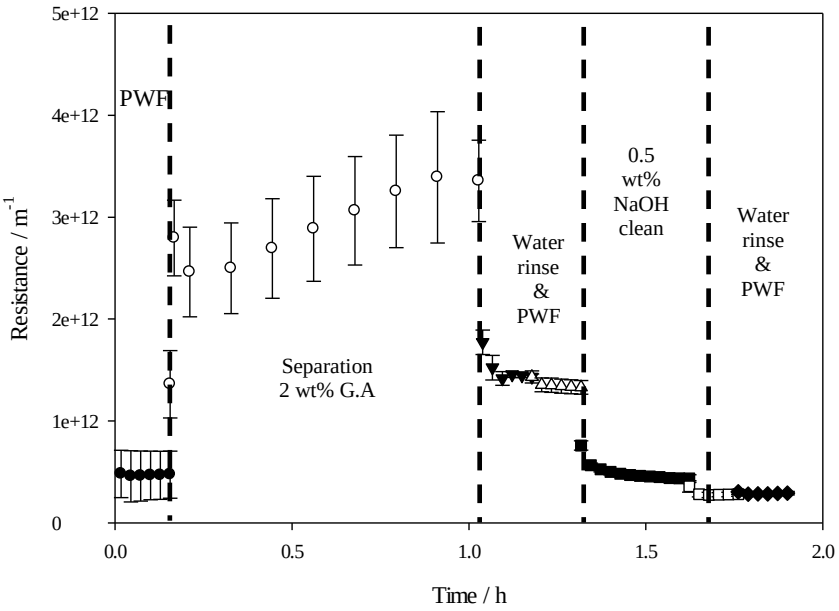

Figure 6.11: Foul-clean cycle resistance profile for 2 wt% gum arabic using a 0.5 µm FP membrane

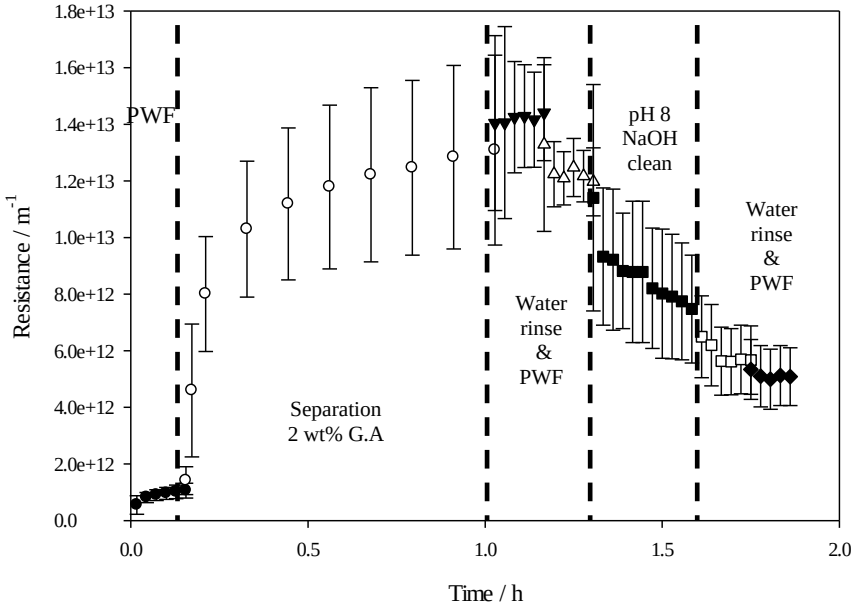

Figure 6.12: Foul-clean cycle resistance profile for 2 wt% gum arabic using a 0.45 µm CA membrane

The foul-clean cycle for 0.5 µm PS shows recovery of resistance after the foul-clean cycle. Water rinsing alone is not effective at reducing the resistance but the NaOH results in a large initial decrease in resistance followed by an increase. This was proposed in Chapter 4 to be due to gum swelling in the NaOH solution causing increased constriction of the pores or the TMP forcing more gum into the membrane pores.

The foul-clean cycle for 0.5 µm FP shows a large initial increase and then gradual increase in resistance upon fouling with gum arabic, some reduction upon rinsing with water and further reduction of the resistance on cleaning with NaOH. The resistance is restored to close that of the initial membrane resistance after the full foul-clean cycle.

The CA diafiltration profile shows the total resistance during fouling to be higher than that of the PS and FP membranes, despite the resistance accounting for the higher permeate viscosity with the CA membranes. Upon rinsing with RO water, the resistance appears to increase slightly, although this is within the error bars and shows that rinsing is ineffective at cleaning the membrane. The membrane was cleaned with NaOH but due to the sensitivity of the

membrane to high pHs, this was only conducted at pH 8 which, it can be seen, was not effective at restoring the flux. The flux did recover further, however, after being soaked in water overnight. Table 6.4 shows the PWF values for cycles 1 – 3 before and after the foul-clean cycle. 1 cycle was conducted per day and the membranes were left, wet, in the module overnight. The increase in flux seen overnight can be explained by gum redissolving in the water and diffusing out of the pores or from the surface overnight.

Table 6.4: PWF values before and after foul-clean cycles 1 – 3 using 0.45 µm CA membranes and 2 wt% gum arabic

Cycle Number	Initial PWF / LMH	Post-clean PWF / LMH
1	289	53
2	91	52
3	79	50

The resistances for each of these membranes were broken down into membrane resistance (R_m) irreversible fouling resistance ($R_{F(irr)}$), cleanable resistance ($R_{F(clean)}$) and rinsible fouling resistance ($R_{F(rinse)}$) and these values are displayed in Figures 6.13, 6.14 and 6.15 for 3 consecutive foul-clean cycles.

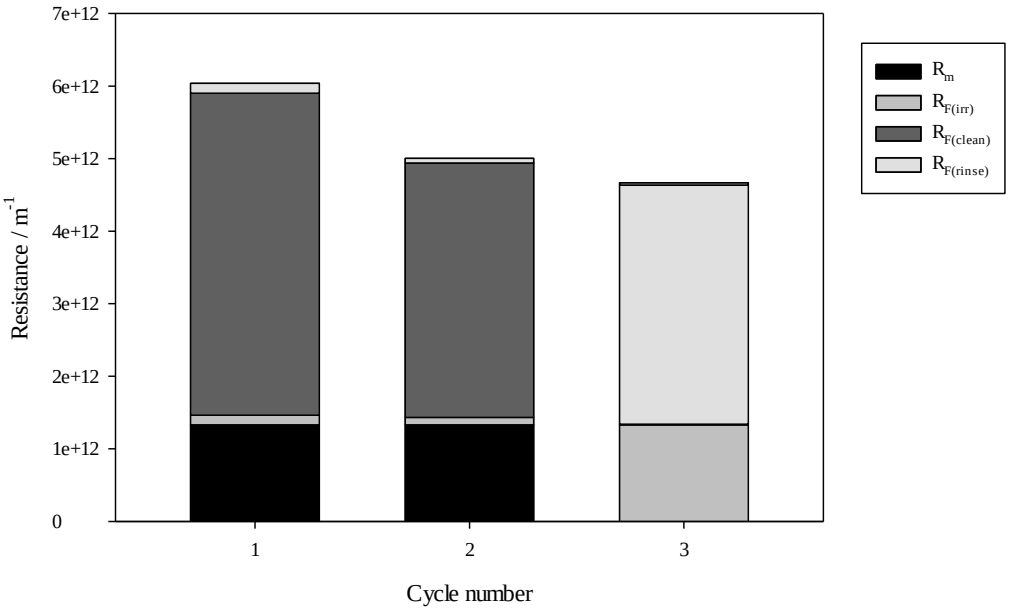

Figure 6.13: Resistance breakdown for the filtration cycles 1 – 3 of 2 wt% gum arabic using 0.5 µm PS membranes at 40 ºC, 0.5 bar TMP and 1.7 m s^{-1} CFV

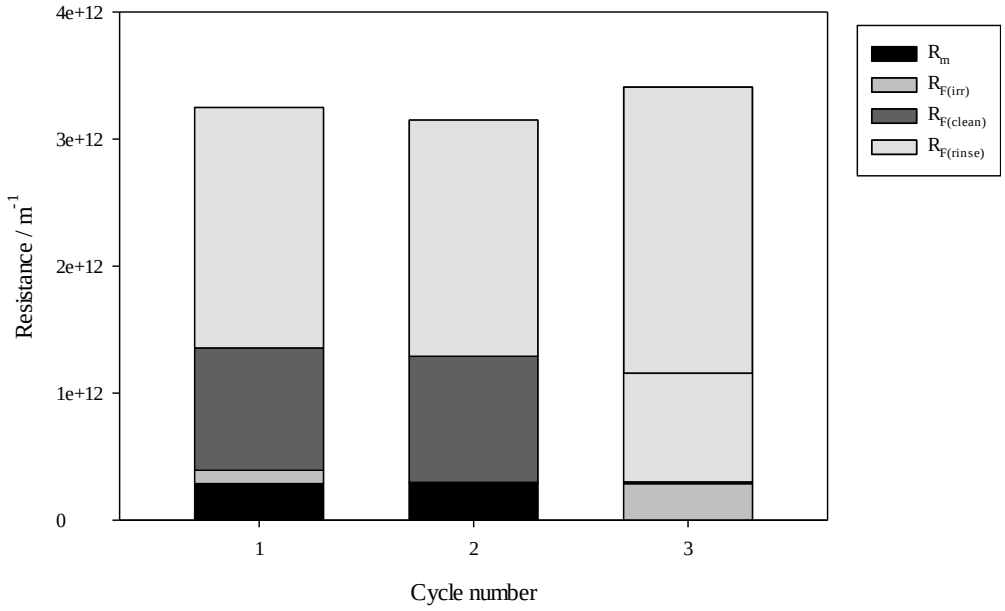

Figure 6.14: Resistance breakdowns for the filtration cycles 1 – 3 of 2 wt% gum arabic using 0.5 µm FP membranes at 40 ºC, 0.5 bar TMP and 1.7 m s^{-1} CFV

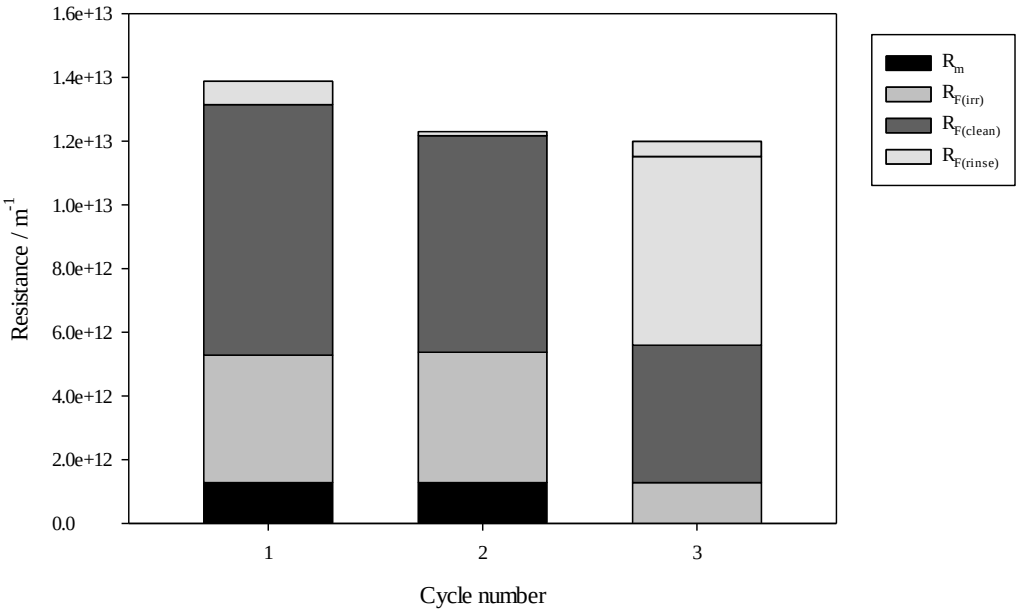

Figure 6.15: Resistance breakdowns for the filtration cycles 1 – 3 of 2 wt% gum arabic using 0.45 µm CA membranes at 40 ºC, 0.5 bar TMP and 1.7 m s^{-1} CFV

The resistance profiles for the three membrane materials are very different. The PS membrane shows very little water rinsible fouling, but this fouling is then removed upon cleaning with NaOH, returning the membrane to its initial condition. The FP membrane shows much more rinsible fouling, some fouling than can be removed by cleaning and again, very little irreversible fouling, meaning that the PWF is restored to its original value after cleaning. The CA membranes show very large amounts of irreversible fouling; the cleaning is not effective at fully restoring the PWF. Rinsing of the membrane is not effective at reducing the resistance, but some reduction is seen with the cleaning with caustic at pH 8. The membrane has limited stability at high pH so this cleaning method is not effective for CA and for sustained use, a different cleaning agent such as an oxidising agent should be investigated.

It was hypothesised in Chapter 4 that the 0.5 µm PS suffered in-pore fouling (pore blocking or pore constriction) and this fouling was not effectively removed by water rinsing alone. Rinsing was seen to be effective at removing cake layers on the surface (the 0.1 µm PS membranes with

little in-pore fouling were effectively cleaned). As the 0.5 µm FP membranes show a large reduction in resistance after rinsing, this suggests that the 0.5 µm FP has a greater proportion of cake formation than the PS membrane, rather than in pore fouling. In contrast, the CA membrane shows little reduction in resistance upon water rinsing, and as the solids transmission is very high with this membrane, it is likely that pore constriction / internal pore blocking is more prevalent.

6.6.2. Hermia modelling

Linearised Hermia modelling was carried out on flux decline curves for the three membranes in the same way as described in Sections 4.2.3. and 4.5.3. in order to determine the main fouling mechanisms. Tables 6.5 and 6.6 show the R^2 values for the different blocking mechanisms for the first 5 min and the rest of the filtration curves.

Table 6.5: R^2 values for the linearisation of blocking laws for the filtration of 2 wt% gum arabic using 0.5 µm PS, 0.5 µm FP and 0.45 µm CA membranes. The models were fitted to the graphs from the first 5 min of filtration

Membrane	**R^2 value (1st 5 min)**		
	Complete pore blocking	**Standard pore blocking (constriction)**	**Cake formation**
0.5 µm PS	0.0118	0.9923	0.9893
0.5 µm FP	0.2438	0.8466	0.8523
0.45 µm CA	0.7678	0.9662	0.9876

Table 6.6: R^2 values for the linearisation of blocking laws for the filtration of 2 wt% gum arabic using 0.5 µm PS, 0.5 µm FP and 0.45 µm CA PS membranes. The models were fitted to the graphs from minute 10 – 60 of filtration

Membrane	**R^2 value (min 10-60)**		
	Complete pore blocking	**Standard pore blocking (constriction)**	**Cake formation**
0.5 µm PS	0.342	0.9496	0.9582
0.5 µm FP	0.356	0.9736	0.9805
0.45 µm CA	0.8409	0.9484	0.9611

The 0.5 µm PS membrane displays standard pore blocking (or pore constriction) as the dominant fouling mechanism in the first 5 min (as the R^2 value is greater than 0.99). In the filtration after 10 min, however, a dominant fouling mechanism cannot be described as no mechanism has an R^2 value of 0.99. Both standard blocking and cake formation have R^2 values of approximately 0.95, suggesting that there is a combination of both mechanisms, with cake formation having the highest value so perhaps being slightly more prevalent.

Saha *et al.* (2007) found similar fouling characteristics during the ultrafiltration of sugarcane juice.[80] They found a high MW polysaccharide-rich arabinogalactan protein to be mainly responsible for the large flux decline observed using PS and PES membranes. The polysaccharide initially caused pore blocking followed by formation of a cake layer. It is likely that the large AGP fraction in gum arabic is responsible for the initial pore blocking.

The FP membrane shows no dominant fouling mechanism as no R^2 value is greater than 0.99, but both pore constriction and cake formation have the highest R^2 values. Both in the first 5 min of filtration and the rest of the filtration cake formation has the highest value so is likely to be slightly dominant. This supports the theory above that this membrane is mainly subject to cake formation.

The CA membrane also shows no dominant fouling mechanism but pore constriction and cake formation both have relatively high R^2 values, with cake formation being slightly dominant in both stages of filtration. This membrane is subject to heavy fouling, shown by the high resistances and this is likely to be both in pore and on the surface.

6.7. Membrane cleaning

6.7.1. Hot water cleaning

Cleaning tests were carried out as in Section 4.5.4. to test the efficacy of cleaning with hot water alone. Table 6.7 shows the percentage flux recovery from cleaning with 60 ºC water and cleaning with 0.5 wt% NaOH at 60 ºC. The flux recovery for NaOH clean with 0.45 µm CA membranes is not shown as the membranes are not tolerant of high pHs and cleaning with NaOH at pH 8 was shown to be ineffective (Figure 6.12).

Table 6.7: Percentage flux recovery during the cleaning of 0.5 µm PS, 0.5 µm FP and 0.45 µm CA membranes with hot water and NaOH

Membrane	**Percentage flux recovery during 60 ºC water clean**	**Percentage flux recovery during 0.5 wt% NaOH clean (40 ºC)**
0.5 µm PS	44 ± 1	96 ± 3
0.5 µm FP	47 ± 4	105 ± 6
0.45 µm CA	4.6	-

Table 6.7 shows that for the 0.5 µm PS and 0.5 µm FP membranes, cleaning with 60 ºC water is not as effective as cleaning with 0.5 wt% NaOH at 40 ºC. The cellulose acetate membrane is not resistant to the high pHs of NaOH clean and cleaning with hot water is not effective either. For future work with this membrane, an alternative cleaning agent needs to be used that can restore the PWF.

6.8. Fractionation of gum arabic

Analysis of the feed and permeate composition for the 0.45 µm CA membranes was carried out and the AGP and protein content are shown in Table 6.8. The gum concentration in the permeate of the 0.5 µm PS and 0.5 µm FP was so low that further analysis was not undertaken. Some fractionation with 0.5 µm PS was observed in Chapter 4, however.

Table 6.8: The AGP and protein mass fractions of dried feed and permeate samples from the filtration of 2 wt% gum arabic using 0.45 µm CA membranes

Sample	**AGP mass fraction**	**Protein mass fraction**
0.45 µm CA Feed	14.8 ± 0.2	4.3 ± 0.6
0.45 µm CA Permeate	14.7 ± 0.3	3.6 ± 0.04

Table 6.8 shows that there is no rejection of AGP by the CA membranes. There is no significant change in the protein mass fraction of the feed and permeate either and it can be concluded that no fractionation is occurring with the 0.45 µm CA membranes. Due to the high transmission of species, however, the pore size may be too large to reject the high molecular weight AGP. The same filtration conditions were therefore tried with 0.2 µm CA membranes to see if the tighter membrane had any effect on the fractionation.

The average permeate flux during fouling, together with the membrane resistance, solids rejection and feed and permeate AGP content are shown in Table 6.9 for the filtration of 2 wt% gum arabic using 0.2 µm CA membranes.

Table 6.9: Characteristics for the filtration of 2 wt% gum arabic using 0.2 µm CA membranes at 0.5 bar TMP, 1.7 m s^{-1} CFV and 40 ºC

Cycle number	**Membrane resistance / m^{-1}**	**Permeate flux / LMH**	**Solids rejection coefficient**	**AGP mass fraction in feed**	**AGP mass fraction in permeate**
1	1.23 x 10^{11}	19.3	0.43	14.3	13.8
2	1.23 x 10^{11}	18.4	0.42	14.2	13.8
3	1.23 x 10^{11}	16.2	0.4	14.8	14.2

The filtration of 2 wt% gum arabic with 0.2 µm CA membranes results in a very similar permeate flux to that using 0.45 µm CA membranes; the solids rejection is slightly higher. This rejection value, however is still much lower than for the PS membranes in all three pore sizes studied in Chapter 4. Unfortunately, selective rejection of AGP is not seen even with the smaller pore size. The transmission of solids being high, however, a smaller pore size still could be investigated.

6.9. Conclusions

The filtration of 2 wt% gum arabic was performed using 3 different membrane materials of approximately the same nominal pore size to observe the effect of different membrane charges, hydrophobicities and surface roughness on filtration and fractionation performance. The FP membrane was observed to have the highest permeate flux at an average of 72 LMH, the PS had an average of 36 LMH and the CA had a much lower flux of only 17 LMH. Both the PS and FP showed solids rejection of greater than 95 % but the CA allowed much more gum arabic to pass into the permeate stream at only 28 % rejection.

Analytical techniques were used to study the membrane surfaces to account for the vast differences in performance. The 3 materials had different surface roughness with CA being rougher than FP, which was rougher than PS. Both FP and PS had similar contact angles indicating fairly hydrophobic surfaces but the CA was very hydrophilic, which may explain the high transmission of gum arabic, which is approximately 90 % hydrophilic carbohydrate. The CA also displayed a much more negative surface charge than the FP or PS membranes, which would be expected to result in rejection of negatively charged protein species, but no rejection of AGP was observed. It is hypothesised that the hydrophobicity of the membrane was the governing factor in the performance difference observed with the CA membranes compared to the FP and PS membranes. The high carbohydrate content of the gum arabic means that the gum can easily hydrogen bond with the surface, resulting in high adsorption, but the species are not repelled by the membrane, explaining the low solids rejection compared to the same pore sized FP and PS membranes.

7. Conclusions, recommendations and future work

The aim of this study was to investigate the potentials of using commercial polymeric membranes to fractionate gum arabic. The study focused on using crossflow microfiltration and investigated the effects of operating conditions, membrane pore size, membrane material, fouling and cleaning on the filtration and fractionation performance. Detailed conclusions were given at the end of each results chapter so this chapter aims to draw together the overall findings of this thesis and give recommendations to future researchers in this area.

The filtration of 2 wt% gum arabic was first optimised within the range of the M10 crossflow filtration rig used in this work. It was found that low TMP (0.5 bar) and high CFV (1.7 m s^{-1}) provided the highest permeate flux, although flux decline over time was still severe. Total gum arabic solids transmission was low (< 5%) with 0.1 µm PS membranes but almost complete rejection of AGP was observed. Transmission of solids increased to between 10 and 20 % but rejection of AGP decreased as the PS pore size was increased to 0.5 and 0.8 µm. Irreversible fouling increased with the 0.5 and 0.8 µm PS membranes over 5 foul-clean cycles, but this fouling layer improved the fractionation performance of the membrane. It was hypothesised that the 0.1 µm PS membrane showed little in pore fouling and that it was mainly all cake formation that was effectively removed during the cleaning process. The 0.5 and 0.8 µm PS membranes were subject to greater in pore fouling and it was suspected that this fouling was less effectively removed by the cleaning, which led to the improved fractionation after several cycles.

The critical flux of gum arabic with the same 3 membranes was measured and these values were found to be 27, 12 and 22 LMH for 0.1, 0.5 and 0.8 µm PS membranes, respectively. The highest critical flux observed for the smallest pore size membrane was suspected to be due to the different fouling mechanisms with the 0.1 µm membrane not allowing gum arabic into the pores. The larger pore size membranes did allow gum arabic into the pores and were therefore

subject to in pore fouling at lower fluxes than the 0.1 µm membrane, where surface fouling was prevented at low fluxes due to the surface shear. Higher CFVs resulted in higher critical flux for the 0.1 µm PS membranes so it is recommended for future work that high CFVs are used together with short channel membranes to prevent high pressure drops. The range of CFVs tested in this work was from 0.18 to 0.67 m s^{-1}. It was clear from this work that operating below the critical flux resulted in much lower pressure increases over the filtration time, so that operation would be possible for much longer periods without cleaning. For the fractionation purposes, however, it was made evident that for the 0.5 and 0.8 µm PS membranes, some fouling is necessary for the rejection of AGP to occur.

Finally, three membrane materials of 0.45 or 0.5 µm nominal pore size were compared to see the effect on filtration and fractionation performance. The CA membrane displayed the highest total resistance during fouling but had a much lower solids rejection (~28 %) than the FP or PS membrane, which both displayed solids rejection of ~ 95%. This was attributed mainly to its hydrophilic nature, which caused severe fouling but high transmission of the mainly hydrophilic carbohydrate containing gum arabic. Unfortunately, no fractionation was seen with this membrane, or a 0.2 µm CA membrane.

To further improve on the fractionation of gum arabic observed in this work, a number of experiments are recommended. Improving the transmission of AG with the PS membranes whilst maintaining the good AGP rejection would make the process more viable. This could be done by surface modification such as plasma-treating the membrane surface to introduce hydrophilic functional groups[135] or bonding of hydrophilic groups such as polyethylene glycols.[136]

The hydrophilic CA membrane showed very good solids transmission overall, but no rejection of AGP, so if the membrane or conditions could be modified such that the transmission remains high but the AGP is rejected this membrane could be promising. The difficulty lies in the amphiphilic nature of the AGP meaning that it can bind to both hydrophilic and hydrophobic

surfaces. AGP contains protein, which would be negatively charged at natural gum pH but it was not seen to be repelled by the highly negatively charged CA membrane as no rejection was seen. Increasing the feed pH would make the protein more negatively charged so may increase its rejection from the CA membrane. Investigating the effect of solution ionic strength would also be interesting, as this would mask the membrane and solute charges, resulting in different filtration and fractionation properties. Alternatively, due to the higher MW of AGP compared to the other fractions, size exclusion could be employed as with the PS membranes in Chapter 4. No rejection of AGP was seen with 0.45 or 0.2 μm CA membranes but the total solids transmission was still 60% with the 0.2 μm membrane. Smaller pore sized CA membranes could be tested, with lower feed concentrations if the fluxes become too low, in order to reject the AGP by size exclusion.

Membrane chromatography could also be investigated, which involves the binding of substrate-specific ligands to a membrane surface.[137] If a ligand could be found that would reversibly bind only the protein moieties in gum arabic, a large pore sized hydrophilic membrane such as CA could be used to remove the carbohydrate fraction. The protein-containing AGP and GP fractions would be retained and could be detached from the membrane in a separate membrane wash stage.

Further materials that are more hydrophilic than PS or FP but less hydrophilic than CA could be investigated in a range of pore sizes to try and improve the AGP rejection and solids transmission. These could be other polymers such as polyethersulfone or regenerated cellulose or inorganic materials such as alumina.

To improve the filtration flux of gum arabic, a module that allows higher CFVs could be tested, as high CFVs were shown to reduce the build-up of fouling and increase the critical flux. Operating below the weak form of the critical flux was shown to minimise fouling and allow sustained operation. This means the frequency of cleaning cycles can be reduced and there would be less ‘downtime’ where the system is being cleaned. Even if it is not possible or

practical to operate below the critical flux, operating at a flux lower than the maximum possible (a 'sustainable' flux[75]) will reduce the fouling and need for cleaning. A co-current system could be employed to allow a high CFV to be used without incurring a large pressure drop along the length of the membrane channel.[59]

Flux recovery with a 0.5 wt% NaOH clean was shown to be effective at restoring the flux following fouling for the PS and FP membranes, although the 0.8 μm PS membrane and the CA showed irreversible fouling. The effects of different cleaning agents could be studied. The cleaning agents must be compatible with the food industry so the use of citric acid could be tested. Citric acid would solubilise inorganic deposits and it also acts a chelating agent, which may be important at removing Ca^{2+} ions from the fouling layer, which can act as bridges between the membranes and charged foulant species. Cellulose acetate is not tolerant to extremes of pH but can tolerate oxidising agents so the use of sodium hypochlorite would be interesting to investigate.

Bibliography

1. Le Clech, P.; Jefferson, B.; Chang, I. S.; Judd, S. J., Critical flux determination by the flux-step method in a submerged membrane bioreactor. *Journal of Membrane Science* **2003,** 227, (1–2), 81-93.

2. FAO, Compendium of Food Additive Specifications (Addendum 7). *Joint FAO/WHO Expert Committee on Food Additives (53rd Session)* **1999**.

3. Bonizzoni, L.; Bruni, S.; Guglielmi, V.; Milazzo, M.; Neri, O., Field and laboratory multi-technique analysis of pigments and organic painting media from an Egyptian coffin (26th Dynasty). *Archaeometry* **2011,** 53, 1212-1230.

4. Idris, O. H. M.; Williams, P. A.; Phillips, G. O., Characterisation of gum from Acacia senegal trees of different age and location using multidetection gel permeation chromatography. *Food Hydrocolloids* **1998,** 12, (4), 379-388.

5. Anderson, D. M.; Hirst, E.; Stoddart, J. F., Studies on uronic acid materials .17. Some structural features of Acacia Senegal gum (gum arabic). *Journal of the Chemical Society C-Organic* **1966**, (21), 1959-&.

6. Flindt, C.; Al-Assaf, S.; Phillips, G. O.; Williams, P. A., Studies on acacia exudate gums. Part V. Structural features of Acacia seyal. *Food Hydrocolloids* **2005,** 19, (4), 687-701.

7. Goodrum, L. J.; Patel, A.; Leykam, J. F.; Kieliszewski, M. J., Gum arabic glycoprotein contains glycomodules of both extensin and arabinogalactan-glycoproteins. *Phytochemistry* **2000,** 54, (1), 99-106.

8. Renard, D.; Lavenant-Gourgeon, L.; Ralet, M.-C.; Sanchez, C., Acacia senegal gum: Continuum of molecular species differing by their protein to sugar ratio, molecular weight, and charges. *Biomacromolecules* **2006,** 7, (9), 2637-2649.

9. Akiyama, Y.; Eda, S.; Kato, K., Gum arabic is a kind of arabinogalactan protein. *Agricultural and Biological Chemistry* **1984,** 48, (1), 235-237.

10. Anderson, D. M. W.; Stoddart, J. F., Studies on uronic acid materials: XV. The use of molecular-sieve chromatography in studies on Acacia Senegal gum (gum arabic). *Carbohyd Res* **1966,** 2, ((2)), 104-114.

11. Randall, R. C.; Phillips, G. O.; Williams, P. A., The role of the proteinaceous component on the emulsifying properties of gum arabic. *Food Hydrocolloids* **1988,** 2, (2), 131-140.

12. Randall, R. C.; Phillips, G. O.; Williams, P. A., Fractionation and characterization of gum from Acacia senegal. *Food Hydrocolloids* **1989,** 3, (1), 65-75.

13. Anderson, D. M. W.; McDougall, F. I., The composition of the proteinaceous gums exuded by Acacia gerrardii and Acacia goetzii subsp goetzii. *Food Hydrocolloids* **1987,** 1, (4), 327-331.

14. Islam, A. M.; Phillips, G. O.; Sljivo, A.; Snowden, M. J.; Williams, P. A., A review of recent developments on the regulatory, structural and functional aspects of gum arabic. *Food Hydrocolloids* **1997,** 11, (4), 493-505.

15. Nishino, M.; Katayama, T.; Sakata, M.; Al-Assaf, S.; Phillips, G. O., Effect of AGP on emulsifying stability of Gum Arabic. In *Gum Arabic*, The Royal Society of Chemistry: 2012; pp 269-274.

16. Yadav, M. P.; Manuel Igartuburu, J.; Yan, Y.; Nothnagel, E. A., Chemical investigation of the structural basis of the emulsifying activity of gum arabic. *Food Hydrocolloids* **2007,** 21, (2), 297-308.

17. Churms, S. C.; Merrifield, E. H.; Stephen, A. M., Some new aspects of the molecular structure of Acacia senegal gum (gum arabic). *Carbohydrate Research* **1983,** 123, (2), 267-279.

18. Sanchez, C.; Schmitt, C.; Kolodziejczyk, E.; Lapp, A.; Gaillard, C.; Renard, D., The acacia gum arabinogalactan fraction is a thin oblate ellipsoid: A new model based on small-angle neutron scattering and ab initio calculation. *Biophysical Journal* **2008,** 94, (2), 629-639.

19. Nie, S.-P.; Wang, C.; Cui, S. W.; Wang, Q.; Xie, M.-Y.; Phillips, G. O., A further amendment to the classical core structure of gum arabic (Acacia senegal). *Food Hydrocolloids* **2013,** 31, (1), 42-48.

20. Nie, S.-P.; Wang, C.; Cui, S. W.; Wang, Q.; Xie, M.-Y.; Phillips, G. O., The core carbohydrate structure of Acacia seyal var. seyal (Gum arabic). *Food Hydrocolloids* **2013,** 32, (2), 221-227.

21. Dror, Y.; Cohen, Y.; Yerushalmi-Rozen, R., Structure of gum arabic in aqueous solution. *Journal of Polymer Science Part B-Polymer Physics* **2006,** 44, (22), 3265-3271.

22. Gashua, I. B.; Williams, P. A.; Yadav, M. P.; Baldwin, T. C., Characterisation and molecular association of Nigerian and Sudanese Acacia gum exudates. *Food Hydrocolloids* **2015,** 51, 405-413.

23. Qi, W.; Fong, C.; Lamport, D. T. A., Gum arabic glycoprotein is a twisted hairy rope - A new model based on O-galactosylhydroxyproline as the polysaccharide attachment site. *Plant Physiology* **1991,** 96, (3), 848-855.

24. Fincher, G. B.; Stone, B. A.; Clarke, A. E., Arabinogalactan-proteins - Structure, biosynthesis and function. *Annual Review of Plant Physiology and Plant Molecular Biology* **1983,** 34, 47-70.

25. Mahendran, T.; Williams, P. A.; Phillips, G. O.; Al-Assaf, S.; Baldwin, T. C., New insights into the structural characteristics of the Arabinogalactan−Protein (AGP) fraction of Gum Arabic. *Journal of Agricultural and Food Chemistry* **2008,** 56, (19), 9269-9276.

26. Al-Assaf, S.; Phillips, G. O.; Aoki, H.; Sasaki, Y., Characterization and properties of Acacia senegal (L.) Willd. var. senegal with enhanced properties (Acacia (sen) SUPER GUM (TM)): Part 1 - Controlled maturation of Acacia senegal var. senegal to increase viscoelasticity, produce a hydrogel form and convert a poor into a good emulsifier. *Food Hydrocolloids* **2007,** 21, (3), 319-328.

27. Al-Assaf, S.; Sakata, M.; McKenna, C.; Aoki, H.; Phillips, G. O., Molecular associations in acacia gums. *Structural Chemistry* **2009,** 20, (2), 325-336.

28. Williams, P. A.; Phillips, G. O.; Stephen, A. M., Spectroscopic and molecular comparisons of three fractions from Acacia senegal gum. *Food Hydrocolloids* **1990,** 4, (4), 305-311.

29. Lopez-Torrez, L.; Nigen, M.; Williams, P.; Doco, T.; Sanchez, C., Acacia senegal vs. Acacia seyal gums – Part 1: Composition and structure of hyperbranched plant exudates. *Food Hydrocolloids* **2015,** 51, 41-53.

30. Renard, D.; Garnier, C.; Lapp, A.; Schmitt, C.; Sanchez, C., Structure of arabinogalactan-protein from Acacia gum: From porous ellipsoids to supramolecular architectures. *Carbohydrate Polymers* **2012,** 90, (1), 322-332.

31. Panda, H., *The Complete Technology Book On Natural Products (Forest Based)*. National Institute of Industrial Research: 2002.

32. Mothé, C. G.; Rao, M. A., Rheological behavior of aqueous dispersions of cashew gum and gum arabic: effect of concentration and blending. *Food Hydrocolloids* **1999,** 13, (6), 501-506.

33. Li, X.; Fang, Y.; Al-Assaf, S.; Phillips, G. O.; Nishinari, K.; Zhang, H., Rheological study of gum arabic solutions: Interpretation based on molecular self-association. *Food Hydrocolloids* **2009,** 23, (8), 2394-2402.

34. Dickinson, E.; Elverson, D. J.; Murray, B. S., On the film-forming and emulsion-stabilizing properties of gum arabic: dilution and flocculation aspects. *Food Hydrocolloids* **1989,** 3, (2), 101-114.

35. Jayme, M. L.; Dunstan, D. E.; Gee, M. L., Zeta potentials of gum arabic stabilised oil in water emulsions. *Food Hydrocolloids* **1999,** 13, (6), 459-465.

36. Nakauma, M.; Funami, T.; Noda, S.; Ishihara, S.; Al-Assaf, S.; Nishinari, K.; Phillips, G. O., Comparison of sugar beet pectin, soybean soluble polysaccharide, and gum arabic as food emulsifiers. 1. Effect of concentration, pH, and salts on the emulsifying properties. *Food Hydrocolloids* **2008,** 22, (7), 1254-1267.

37. Padala, S. R.; Williams, P. A.; Phillips, G. O., Adsorption of Gum Arabic, egg white protein, and their mixtures at the oil-water interface in limonene oil-in-water emulsions. *Journal of Agricultural and Food Chemistry* **2009,** 57, (11), 4964-4973.

38. Al-Assaf, S.; Andres-Brull, M.; Cirre, J.; Phillips, G. O., Structural changes following industrial processing of Acacia gums. In *Gum Arabic*, The Royal Society of Chemistry: 2012; pp 153-168.

39. Ward, F. M. Water-soluble esterified hydrocolloids (Patent US 6455512). US 6455512, Sep. 24, 2002, 2002.

40. Sarkar, S.; Gupta, S.; Variyar, P. S.; Sharma, A.; Singhal, R. S., Hydrophobic derivatives of guar gum hydrolyzate and gum Arabic as matrices for microencapsulation of mint oil. *Carbohydrate Polymers* **2013,** 95, (1), 177-182.

41. Sarkar, S.; Singhal, R. S., Esterification of guar gum hydrolysate and gum Arabic with n-octenyl succinic anhydride and oleic acid and its evaluation as wall material in microencapsulation. *Carbohydrate Polymers* **2011,** 86, (4), 1723-1731.

42. Wang, H.; Williams, P. A.; Senan, C., Synthesis, characterization and emulsification properties of dodecenyl succinic anhydride derivatives of gum Arabic. *Food Hydrocolloids* **2014,** 37, 143-148.

43. Aoki, H.; Al-Assaf, S.; Katayama, T.; Phillips, G. O., Characterization and properties of Acacia senegal (L.) Willd. var. senegal with enhanced properties (Acacia (sen) SUPER GUM (TM)): Part 2 - Mechanism of the maturation process. *Food Hydrocolloids* **2007,** 21, (3), 329-337.

44. Katayama, T.; Ido, T.; Nishino, M.; Inoue, T.; Phillips, G. O., Emulsification superiority of Super Gum(TM). In *Gum Arabic*, The Royal Society of Chemistry: 2012; pp 275-282.

45. Hayashi, H. Method of modifying gum arabic (Patent). EP 1505078 B1, 2009.

46. Sakata, M.; Katayama, T.; Ogasawara, T.; Sasaki, Y. Method of modifying gum arabic, modified gum arabic obtained by the method, and use thereof (Patent). US 08460734, Jun 11 2013, 2013.

47. Fang, Y.; Krulish, J.; Jendrysik, R. Food and beverage emulsifiers (Patent). US 08435581, May 7 2013, 2013.

48. Heidebach, T.; Sass, M.; De With, A. Enzymatic treatment of gum arabic (Patent). EP2606750-A1; WO2013091799-A1.

49. Osman, M. E.; Menzies, A. R.; Martin, B. A.; Williams, P. A.; Phillips, G. O.; Baldwin, T. C., Characterization of gum arabic fractions obtained by anion-exchange chromatography. *Phytochemistry* **1995,** 38, (2), 409-417.

50. Osman, M. E.; Menzies, A. R.; Williams, P. A.; Phillips, G. O.; Baldwin, T. C., The molecular characterization of the polysaccharide gum from Acacia-Senegal. *Carbohydrate Research* **1993,** 246, 303-318.

51. Ray, A. K.; Bird, P. B.; Iacobucci, G. A.; Clark, B. C., Functionality of gum arabic - Fractionation, characterization and evaluation of gum fractions in citrus oil emulsions and model beverages. *Food Hydrocolloids* **1995,** 9, (2), 123-131.

52. Fauconnier, M.-L.; Blecker, C.; Groyne, J.; Razafindralambo, H.; Vanzeveren, E.; Marlier, M.; Paquot, M., Characterization of two Acacia gums and their fractions using a Langmuir film balance. *Journal of Agricultural and Food Chemistry* **2000,** 48, (7), 2709-2712.

53. Vandevelde, M. C.; Fenyo, J. C., Macromolecular distribution of Acacia Senegal (gum arabic) by size-exclusion chromatography. *Carbohydrate Polymers* **1985,** 5, (4), 251-273.

54. Picton, L.; Bataille, I.; Muller, G., Analysis of a complex polysaccharide (gum arabic) by multi-angle laser light scattering coupled on-line to size exclusion chromatography and flow field flow fractionation. *Carbohydrate Polymers* **2000,** 42, (1), 23-31.

55. Andres-Brull, M.; Al-Assaf, S.; Phillips, G. O.; Jackson, K., Optimisation of asymmetrical flow-field fractionation for the characterisation of gum arabic (Acacia sengal var senegal) and comparison with gel permeation chromatography. *Analytical Methods* **2013**.

56. Kang, J.; Cui, S. W.; Chen, J.; Phillips, G. O.; Wu, Y.; Wang, Q., New studies on gum ghatti (Anogeissus latifolia) part I. Fractionation, chemical and physical characterization of the gum. *Food Hydrocolloids* **2011,** 25, (8), 1984-1990.

57. Ibrahim, O. B.; Osman, M. E.; Hassan, E. A., *Characterization and simple fractionation of Acacia Senegal*. 2013; Vol. 2.

58. Bechervaise, P. The microfiltration of high solids content gum arabic streams for the purpose of removing thermo-resistant spores. Thesis (unpublished), University of Bath, 2013.

59. Decloux, M.; Dornier, M.; Gratius, I., Crossflow microfiltration of gum arabic solutions: Comparison of the classical system with the co-current permeate flow system. *International Journal of Food Science & Technology* **1996,** 31, (2), 153-166.

60. Lakshminarayanaiah, N., Transport processes in membranes: A consideration of membrane potential across thick and thin membranes. In *Subcellular Biochemistry*, Roodyn, D., Ed. Springer US: 1979; pp 401-494.

61. Belfort, G.; Davis, R. H.; Zydney, A. L., The behaviour of suspensions and macromolecular solutions in cross-flow microfiltration. *Journal of Membrane Science* **1994,** 96, (1-2), 1-58.

62. Cheryan, M., *Ultrafiltration and Microfiltration Handbook*. 2nd ed.; CRC Press: Boca Raton, USA, 1998.

63. Belfort, G., Membrane modules: comparison of different configurations using fluid mechanics. *Journal of Membrane Science* **1988,** 35, (3), 245-270.

64. Nakao, S.-i., Determination of pore size and pore size distribution. *Journal of Membrane Science* **1994,** 96, (1), 131-165.

65. Singh, S.; Khulbe, K. C.; Matsuura, T.; Ramamurthy, P., Membrane characterization by solute transport and atomic force microscopy. *Journal of Membrane Science* **1998,** 142, (1), 111-127.

66. Chan, R.; Chen, V., Characterization of protein fouling on membranes: Opportunities and challenges. *Journal of Membrane Science* **2004,** 242, (1–2), 169-188.

67. Evans, P. J.; Bird, M. R.; Pihlajamäki, A.; Nyström, M., The influence of hydrophobicity, roughness and charge upon ultrafiltration membranes for black tea liquor clarification. *Journal of Membrane Science* **2008,** 313, (1–2), 250-262.

68. Väisänen, P.; Bird, M. R.; Nyström, M., Treatment of UF membranes with simple and formulated cleaning agents. *Food and Bioproducts Processing* **2002,** 80, (2), 98-108.

69. Nyström, M., Fouling of unmodified and modified polysulfone ultrafiltration membranes by ovalbumin. *Journal of Membrane Science* **1989,** 44, (2–3), 183-196.

70. Nyström, M.; Lindström, M.; Matthiasson, E., Streaming potential as a tool in the characterization of ultrafiltration membranes. *Colloids and Surfaces* **1989,** 36, (3), 297-312.

71. Atkins, P.; de Paula, J., *Atkins' Physical Chemistry*. 7th ed.; Oxford University Press: Oxford, 2002.

72. Brans, G.; Schroën, C. G. P. H.; van der Sman, R. G. M.; Boom, R. M., Membrane fractionation of milk: state of the art and challenges. *Journal of Membrane Science* **2004,** 243, (1–2), 263-272.

73. Mulder, M., *Basic principles of membrane technology*. 2nd ed.; Kluwer Academic Publishers: 2000.

74. Jones, S. The application of enhanced Fluid Dynamic Gauging as a fouling sensor for pressure driven membrane separations in the food industry (Thesis). University of Bath, Bath, 2012.

75. Bacchin, P.; Aimar, P.; Field, R. W., Critical and sustainable fluxes: Theory, experiments and applications. *Journal of Membrane Science* **2006,** 281, (1–2), 42-69.

76. Fane, A. G.; Fell, C. J. D., A review of fouling and fouling control in ultrafiltration. *Desalination* **1987,** 62, 117-136.

77. Li, Q.; Elimelech, M., Organic fouling and chemical cleaning of nanofiltration membranes: Measurements and mechanisms. *Environmental Science & Technology* **2004,** 38, (17), 4683-4693.

78. Mahlangu, T. O.; Thwala, J. M.; Mamba, B. B.; D'Haese, A.; Verliefde, A. R. D., Factors governing combined fouling by organic and colloidal foulants in cross-flow nanofiltration. *Journal of Membrane Science* **2015,** 491, 53-62.

79. Ye, Y.; Clech, P. L.; Chen, V.; Fane, A. G., Evolution of fouling during crossflow filtration of model EPS solutions. *Journal of Membrane Science* **2005,** 264, (1–2), 190-199.

80. Saha, N. K.; Balakrishnan, M.; Ulbricht, M., Sugarcane juice ultrafiltration: FTIR and SEM analysis of polysaccharide fouling. *Journal of Membrane Science* **2007,** 306, (1–2), 287-297.

81. Nataraj, S.; Schomäcker, R.; Kraume, M.; Mishra, I. M.; Drews, A., Analyses of polysaccharide fouling mechanisms during crossflow membrane filtration. *Journal of Membrane Science* **2008,** 308, (1–2), 152-161.

82. Susanto, H.; Arafat, H.; Janssen, E. M. L.; Ulbricht, M., Ultrafiltration of polysaccharide–protein mixtures: Elucidation of fouling mechanisms and fouling control by membrane surface modification. *Separation and Purification Technology* **2008,** 63, (3), 558-565.

83. Tracey, E. M.; Davis, R. H., Protein fouling of track-etched polycarbonate microfiltration membranes. *Journal of Colloid and Interface Science* **1994,** 167, (1), 104-116.

84. Bowen, W. R.; Calvo, J. I.; Hernández, A., Steps of membrane blocking in flux decline during protein microfiltration. *Journal of Membrane Science* **1995,** 101, (1–2), 153-165.

85. Hermia, J., Constant pressure blocking filtration laws - Application to power-law non-Newtonian fluids. *Transactions of the Institution of Chemical Engineers* **1982,** 60, (3), 183-187.

86. Madaeni, S. S.; Samieirad, S., Chemical cleaning of reverse osmosis membrane fouled by wastewater. *Desalination* **2010,** 257, (1–3), 80-86.

87. Sim, S. T. V.; Taheri, A. H.; Chong, T. H.; Krantz, W. B.; Fane, A. G., Colloidal metastability and membrane fouling – Effects of crossflow velocity, flux, salinity and colloid concentration. *Journal of Membrane Science* **2014,** 469, 174-187.

88. de Bruijn, J.; Venegas, A.; Borquez, R., Influence of crossflow ultrafiltration on membrane fouling and apple juice quality. *Desalination* **2002,** 148, (1–3), 131-136.

89. Kuo, K.-P.; Cheryan, M., Ultrafiltration of acid whey in a spiral-wound unit: Effect of operating parameters on membrane fouling. *Journal of Food Science* **1983,** 48, (4), 1113-1118.

90. Giri, S. K.; Mangaraj, S., Soymilk concentration by ultrafiltration: effects of pore size and transmembrane pressure on filtration performance. *International Journal of Food Science & Technology* **2014,** 49, (3), 666-672.

91. de Barros, S. T. D.; Andrade, C. M. G.; Mendes, E. S.; Peres, L., Study of fouling mechanism in pineapple juice clarification by ultrafiltration. *Journal of Membrane Science* **2003,** 215, (1–2), 213-224.

92. Kallioinen, M.; Pekkarinen, M.; Mänttäri, M.; Nuortila-Jokinen, J.; Nyström, M., Comparison of the performance of two different regenerated cellulose ultrafiltration membranes at high filtration pressure. *Journal of Membrane Science* **2007,** 294, (1–2), 93-102.

93. Lim, Y. P.; Mohammad, A. W., Influence of pH and ionic strength during food protein ultrafiltration: Elucidation of permeate flux behavior, fouling resistance, and mechanism. *Separation Science and Technology* **2011,** 47, (3), 446-454.

94. Marshall, A. D.; Munro, P. A.; Tragardh, G., The effect of protein fouling in microfiltration and ultrafiltration on permeate flux, protein retention and selectivity - A literature review. *Desalination* **1993,** 91, (1), 65-108.

95. Lockley, A. K.; White, W. J. P.; Hall, G. M., A method of assessing protein adsorption onto ultrafiltraion membranes. *International Journal of Food Science and Technology* **1988,** 23, (1), 11-15.

96. Chang, S.; Waite, T. D.; Schäfer, A. I.; Fane, A. G., Adsorption of trace steroid estrogens to hydrophobic hollow fibre membranes. *Desalination* **2002,** 146, (1–3), 381-386.

97. Liu, F.; Hashim, N. A.; Liu, Y.; Abed, M. R. M.; Li, K., Progress in the production and modification of PVDF membranes. *Journal of Membrane Science* **2011,** 375, (1–2), 1-27.

98. Bowen, W. R.; Doneva, T. A.; Stoton, J. A. G., Protein deposition during cross-flow membrane filtration: AFM studies and flux loss. *Colloids and Surfaces B: Biointerfaces* **2003,** 27, (2–3), 103-113.

99. Hoek, E. M. V.; Bhattacharjee, S.; Elimelech, M., Effect of Membrane Surface Roughness on Colloid−Membrane DLVO Interactions. *Langmuir* **2003,** 19, (11), 4836-4847.

100. Weis, A.; Bird, M. R.; Nyström, M.; Wright, C., The influence of morphology, hydrophobicity and charge upon the long-term performance of ultrafiltration membranes fouled with spent sulphite liquor. *Desalination* **2005,** 175, (1), 73-85.

101. Riedl, K.; Girard, B.; Lencki, R. W., Influence of membrane structure on fouling layer morphology during apple juice clarification. *Journal of Membrane Science* **1998,** 139, (2), 155-166.

102. Nyström, M.; Pihlajamäki, A.; Ehsani, N., Characterization of ultrafiltration membranes by simultaneous streaming potential and flux measurements. *Journal of Membrane Science* **1994,** 87, (3), 245-256.

103. Field, R. W.; Wu, D.; Howell, J. A.; Gupta, B. B., Critical flux concept for microfiltration fouling. *Journal of Membrane Science* **1995,** 100, (3), 259-272.

104. Bacchin, P.; Aimar, P.; Sanchez, V., Model for colloidal fouling of membranes. *AIChE Journal* **1995,** 41, (2), 368-376.

105. Chen, V.; Fane, A. G.; Madaeni, S.; Wenten, I. G., Particle deposition during membrane filtration of colloids: transition between concentration polarization and cake formation. *Journal of Membrane Science* **1997,** 125, (1), 109-122.

106. Metsämuuronen, S.; Howell, J.; Nyström, M., Critical flux in ultrafiltration of myoglobin and baker's yeast. *Journal of Membrane Science* **2002,** 196, (1), 13-25.

107. Li, H.; Fane, A. G.; Coster, H. G. L.; Vigneswaran, S., An assessment of depolarisation models of crossflow microfiltration by direct observation through the membrane. *Journal of Membrane Science* **2000,** 172, (1–2), 135-147.

108. Madaeni, S. S.; Fane, A. G.; Wiley, D. E., Factors influencing critical flux in membrane filtration of activated sludge. *Journal of Chemical Technology & Biotechnology* **1999,** 74, (6), 539-543.

109. Huisman, I. H.; Vellenga, E.; Trägårdh, G.; Trägårdh, C., The influence of the membrane zeta potential on the critical flux for crossflow microfiltration of particle suspensions. *Journal of Membrane Science* **1999,** 156, (1), 153-158.

110. Li, H.; Fane, A. G.; Coster, H. G. L.; Vigneswaran, S., Direct observation of particle deposition on the membrane surface during crossflow microfiltration. *Journal of Membrane Science* **1998,** 149, (1), 83-97.

111. Zamani, F.; Wicaksana, F.; Taheri, A. H.; Law, A. W. K.; Fane, A. G.; Krantz, W. B., Generalized criterion for the onset of particle deposition in crossflow microfiltration via DOTM – Modeling and experimental validation. *Journal of Membrane Science* **2014,** 457, 128-138.

112. Li, H.; Fane, A. G.; Coster, H. G. L.; Vigneswaran, S., Observation of deposition and removal behaviour of submicron bacteria on the membrane surface during crossflow microfiltration. *Journal of Membrane Science* **2003,** 217, (1–2), 29-41.

113. Wicaksana, F.; Fane, A. G.; Pongpairoj, P.; Field, R., Microfiltration of algae (Chlorella sorokiniana): Critical flux, fouling and transmission. *Journal of Membrane Science* **2012,** 387–388, 83-92.

114. Bowen, W. R.; Doneva, T. A.; Yin, H.-B., Separation of humic acid from a model surface water with PSU/SPEEK blend UF/NF membranes. *Journal of Membrane Science* **2002,** 206, (1–2), 417-429.

115. Gésan-Guiziou, G.; Wakeman, R. J.; Daufin, G., Stability of latex crossflow filtration: cake properties and critical conditions of deposition. *Chemical Engineering Journal* **2002,** 85, (1), 27-34.

116. Kwon, D. Y.; Vigneswaran, S.; Fane, A. G.; Aim, R. B., Experimental determination of critical flux in cross-flow microfiltration. *Separation and Purification Technology* **2000,** 19, (3), 169-181.

117. Field, R. W.; Pearce, G. K., Critical, sustainable and threshold fluxes for membrane filtration with water industry applications. *Advances in Colloid and Interface Science* **2011,** 164, (1–2), 38-44.

118. Trägårdh, G., Membrane cleaning. *Desalination* **1989,** 71, (3), 325-335.

119. Borujeni, E. E.; Li, Y.; Zydney, A. L., Application of periodic backpulsing to reduce membrane fouling during ultrafiltration of plasmid DNA. *Journal of Membrane Science* **2015,** 473, 102-108.

120. Head, L. E.; Bird, M. R., The removal of psychotrophic spores from milk protein isolate feeds using tubular ceramic microfilters (Thesis). *Journal of Food Process Engineering* **2013,** 36, (1), 113-124.

121. Evans, P. J.; Bird, M. R., Solute-membrane fouling interactions during the ultrafiltration of black tea liquor. *Food and Bioproducts Processing* **2006,** 84, (4), 292-301.

122. Daufin, G.; Escudier, J. P.; Carrère, H.; Bérot, S.; Fillaudeau, L.; Decloux, M., Recent and emerging applications of membrane processes in the food and dairy industry. *Food and Bioproducts Processing* **2001,** 79, (2), 89-102.

123. Kotsanopoulos, K. V.; Arvanitoyannis, I. S., Membrane processing technology in the food Industry: Food processing, wastewater treatment, and effects on physical, microbiological, organoleptic, and nutritional properties of foods. *Critical Reviews in Food Science and Nutrition* **2013,** 55, (9), 1147-1175.

124. Nyström, M.; Aimar, P.; Luque, S.; Kulovaara, M.; Metsämuuronen, S., Fractionation of model proteins using their physiochemical properties. *Colloids and Surfaces A: Physicochemical and Engineering Aspects* **1998,** 138, (2–3), 185-205.

125. Arunkumar, A.; Etzel, M. R., Fractionation of α-lactalbumin and β-lactoglobulin from bovine milk serum using staged, positively charged, tangential flow ultrafiltration membranes. *Journal of Membrane Science* **2014,** 454, 488-495.

126. Wallberg, O.; Jönsson, A.-S.; Wimmerstedt, R., Fractionation and concentration of kraft black liquor lignin with ultrafiltration. *Desalination* **2003,** 154, (2), 187-199.

127. Argyle, I. Synthetic membrane performance modification by selective species adsorption (Thesis). University of Bath, Bath, 2014.

128. Bartlett, M.; Bird, M. R.; Howell, J. A., An experimental study for the development of a qualitative membrane cleaning model. *Journal of Membrane Science* **1995,** 105, (1–2), 147-157.

129. Bowes, J. H.; Kenten, R. H., The swelling of collagen in alkaline solutions .1. Swelling in solutions of soldium hydroxide. *Biochemical Journal* **1950,** 46, (1), 1-8.

130. Mercade-Prieto, R.; Chen, X. D., Dissolution of whey protein concentrate gels in alkali. *AIChE Journal* **2006,** 52, (2), 792-803.

131. Jones, S. A.; Bird, M. R.; Pihlajamäki, A., An experimental investigation into the pre-treatment of synthetic membranes using sodium hydroxide solutions. *Journal of Food Engineering* **2011,** 105, (1), 128-137.

132. Gésan-Guiziou, G.; Boyaval, E.; Daufin, G., Critical stability conditions in crossflow microfiltration of skimmed milk: transition to irreversible deposition. *Journal of Membrane Science* **1999,** 158, (1–2), 211-222.

133. Ghosh, R., Study of membrane fouling by BSA using pulsed injection technique. *Journal of Membrane Science* **2002,** 195, (1), 115-123.

134. Hirose, M.; Ito, H.; Kamiyama, Y., Effect of skin layer surface structures on the flux behaviour of RO membranes. *Journal of Membrane Science* **1996,** 121, (2), 209-215.

135. Kim, K. S.; Lee, K. H.; Cho, K.; Park, C. E., Surface modification of polysulfone ultrafiltration membrane by oxygen plasma treatment. *Journal of Membrane Science* **2002,** 199, (1–2), 135-145.

136. Li, F.; Meng, J.; Ye, J.; Yang, B.; Tian, Q.; Deng, C., Surface modification of PES ultrafiltration membrane by polydopamine coating and poly(ethylene glycol) grafting: Morphology, stability, and anti-fouling. *Desalination* **2014,** 344, 422-430.

137. Saxena, A.; Tripathi, B. P.; Kumar, M.; Shahi, V. K., Membrane-based techniques for the separation and purification of proteins: An overview. *Advances in Colloid and Interface Science* **2009,** 145, (1–2), 1-22.

Appendix

A. Calibrations

Rotameter calibration

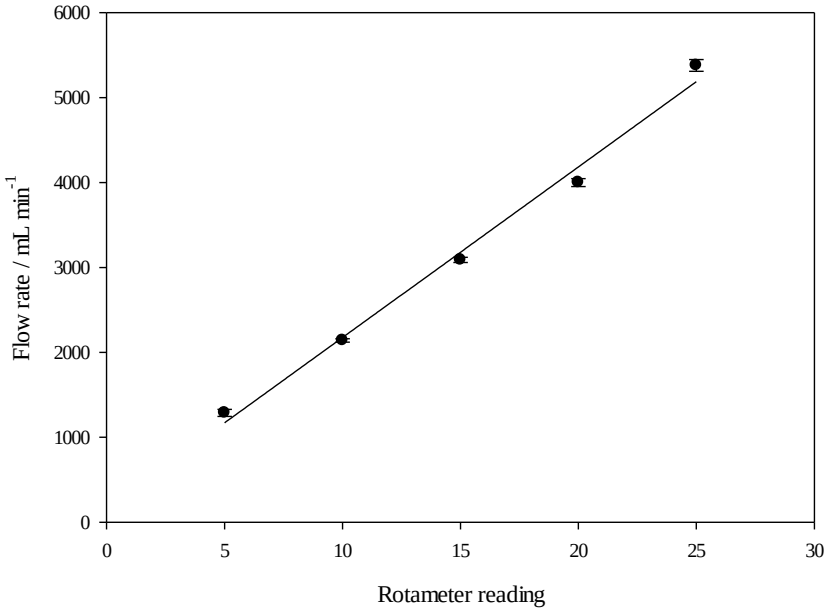

Figure A.1: Calibration of the M10 Rotameter

B. Example calculations

CFV calculations

The CFV can be calculated using Equation B.1, where Q is the volumetric flow rate, a is the channel width, b is the channel height and N is the number of channels.

$$\mathrm{CFV} = \frac{\mathrm{Q}}{\mathrm{a} \,.\, \mathrm{b} \,.\, \mathrm{N}} \qquad \text{Equation B.1}$$

An example calculation for the CFV through the critical flux rig used in this work is shown below. The calculation is for a volumetric flow rate of 2 L min^{-1}, which corresponds to 3 x 10^{-5} m^3 s^{-1}, where a = 0.03 m and b is 0.0015 m.

$$\text{CFV} = \frac{3 \text{ x } 10^{-5}}{0.03 \text{ x } 0.0015} = 0.67 \text{ m s}^{-1}$$

Flux measurement

Flux can be described as the volume of liquid passing through a membrane of known area (A_m) in a given time and can be calculated using Equation B.2.

$$J = \frac{\Delta V}{\Delta t \, . \, A_m} \qquad \text{Equation B.2}$$

An example calculation for the permeation of 0.01 L through a membrane of area 336 cm^2 in 20 s is shown below.

$$J = \frac{0.01}{(20/3600) \text{ x } 3.36 \text{ x } 10^{-2}} = 53.6 \text{ L m}^{-2}\text{h}^{-1}$$

Resistance calculations

The total resistance can be calculated from the permeate flux if the permeate viscosity (μ) is also known, as shown in Equation B.3.

$$R_m = \frac{\text{TMP}}{\mu \, . \, J} \qquad \text{Equation B.3}$$

An example calculation for the membrane resistance at 0.5 bar TMP and 40 ºC is shown below.

$$R_m = \frac{50000}{0.000653 \text{ x } (53.6/3600000)} = 5.1 \text{ x } 10^{12} \text{ m}^{-1}$$

Reynolds numbers

The Reynolds number for a system can be calculated using Equation B.4, where d is the channel diameter and ρ is the fluid density.

$$\mathrm{Re} = \frac{\mathrm{CFV} \,.\, \mathrm{d} \,.\, \rho}{\mu} \qquad \text{Equation B.4}$$

Where the channel cross-section is not circular, Equation B.5 can be used to calculate the equivalent diameter from the channel width (a) and height (b).

$$\mathrm{d} = \frac{2\mathrm{a} \,.\, \mathrm{b}}{\mathrm{a}+\mathrm{b}} \qquad \text{Equation B.5}$$

For the M10, of channel width 0.017 m and channel height 0.0007 m, at a CFV of 1.7 m s^{-1} and filtration temperature of 40 ºC, an example calculation is shown below

$$\mathrm{d} = \frac{(2 \text{ x } 0.0007) \,.\, 0.017}{0.0007+0.017} = 0.0013 \text{ m}$$

$$\mathrm{Re} = \frac{1.7 \text{ x } 0.0013 \text{ x } 992.2}{0.000653} = 3358$$

C. Linearised Hermia Modelling

The graphs plotted to determine the mechanisms for fouling in Chapters 4 (Section 4.5.3.) and 6 (Section 6.6.2..) are shown in Figures 10.1 - 10.5 with the R^2 values labelled in each case.

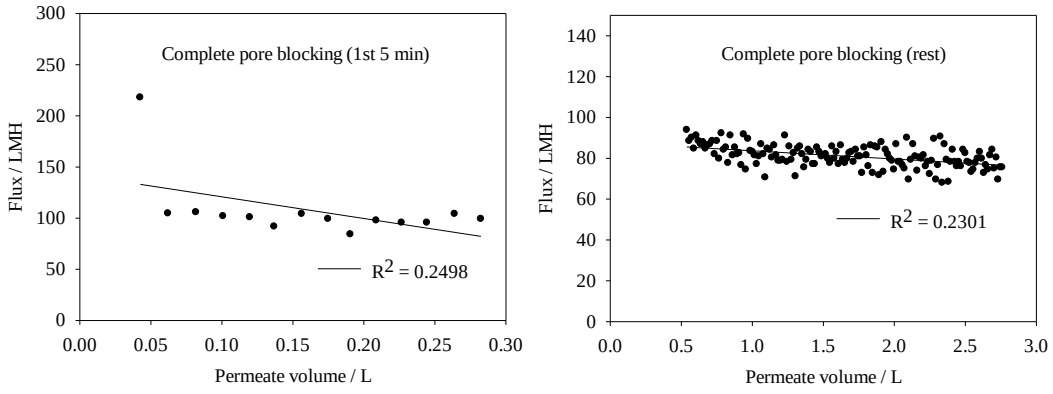

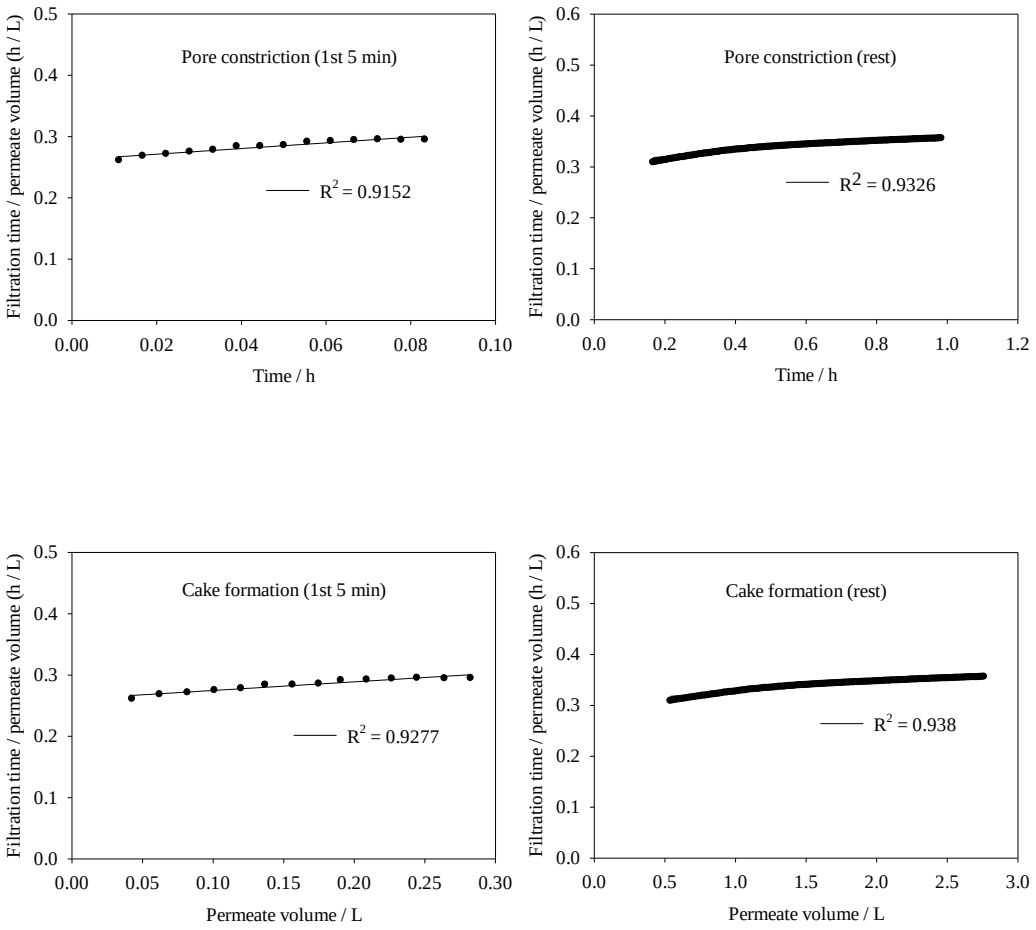

Figure C.1: Linearised Hermia modelling plots for the filtration of 2 wt% gum arabic using 0.1 µm PS membranes

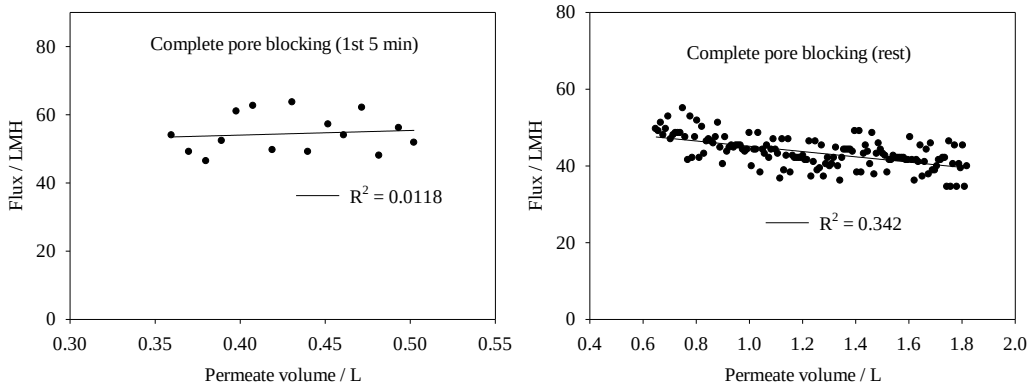

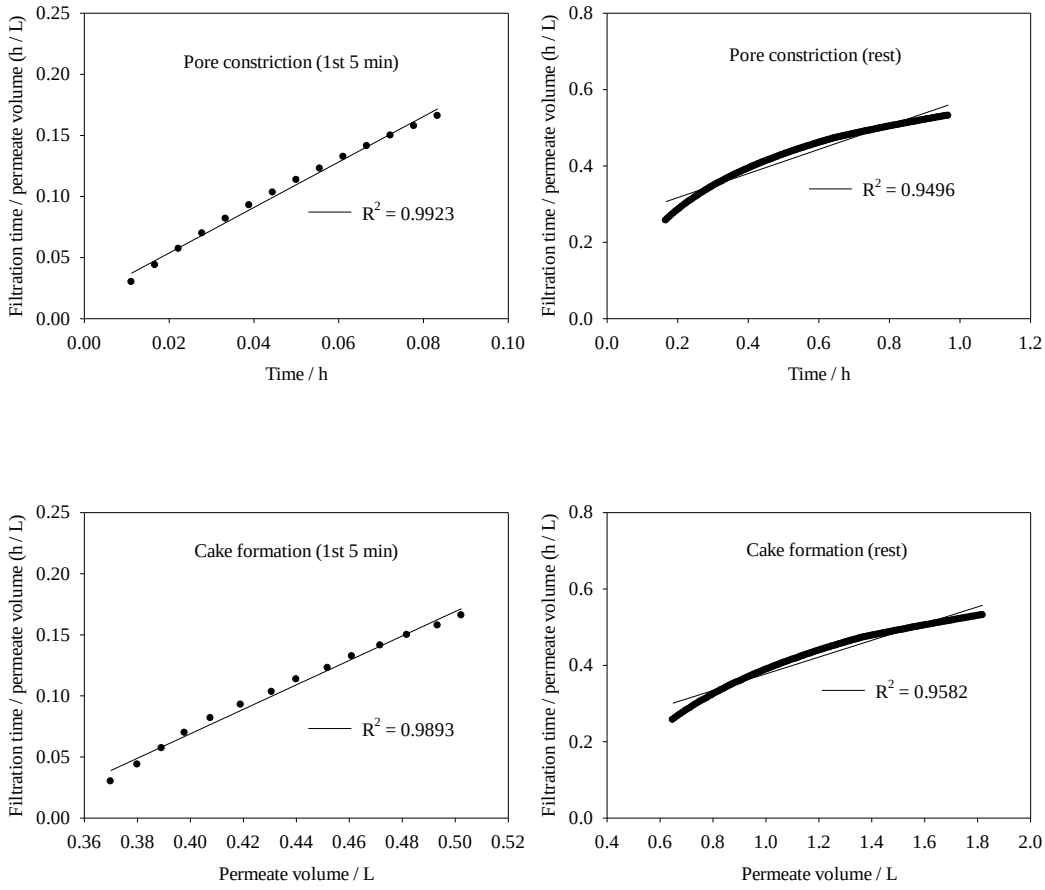

Figure C.2: Linearised Hermia modelling plots for the filtration of 2 wt% gum arabic using 0.5 µm PS membranes

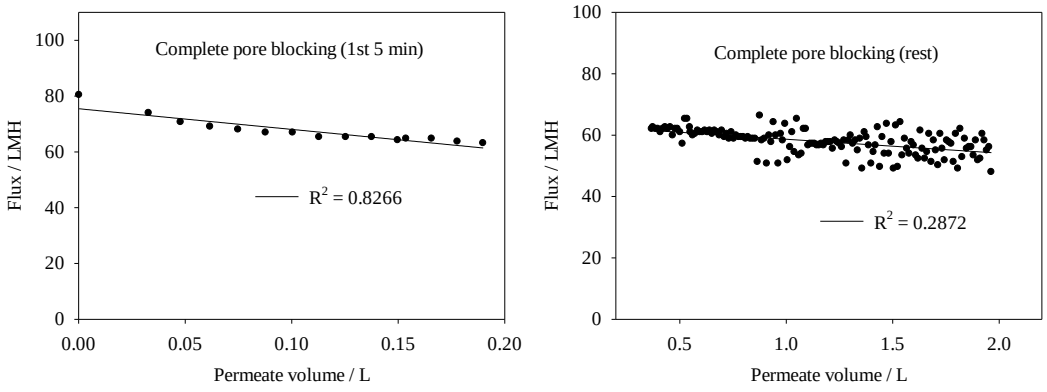

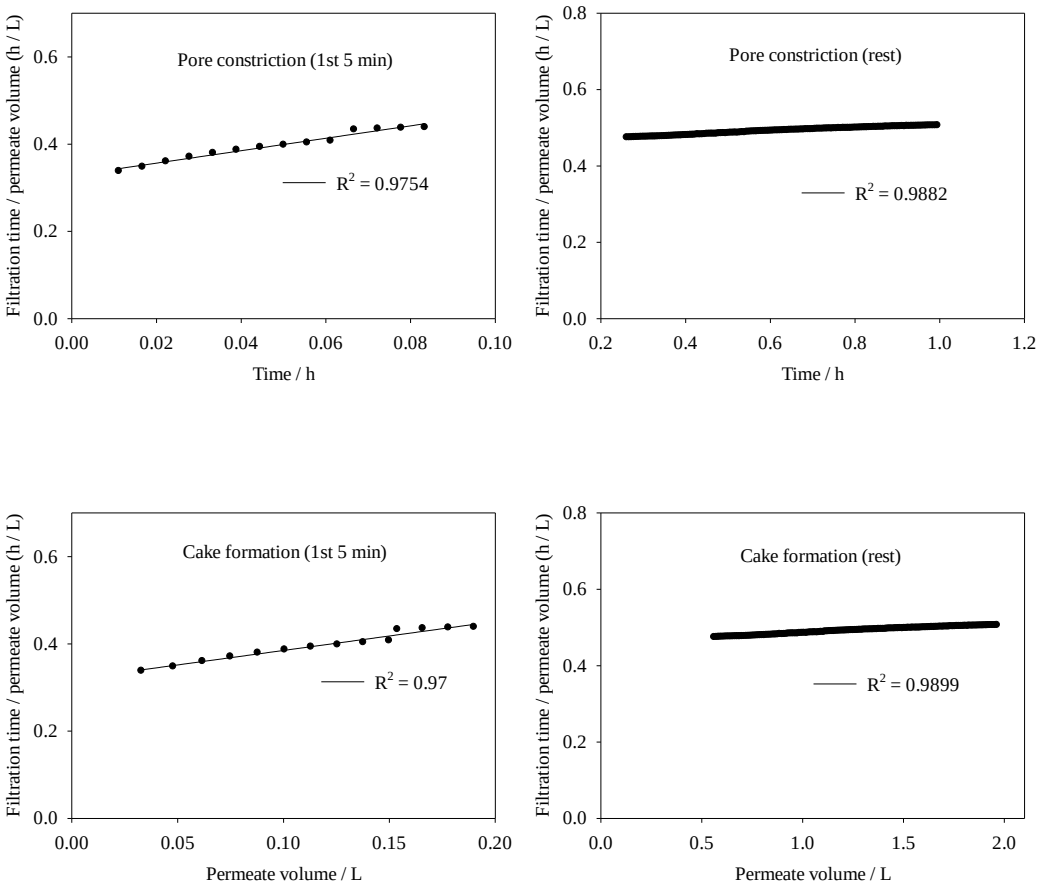

Figure C.3: Linearised Hermia modelling plots for the filtration of 2 wt% gum arabic using 0.8 µm PS membranes

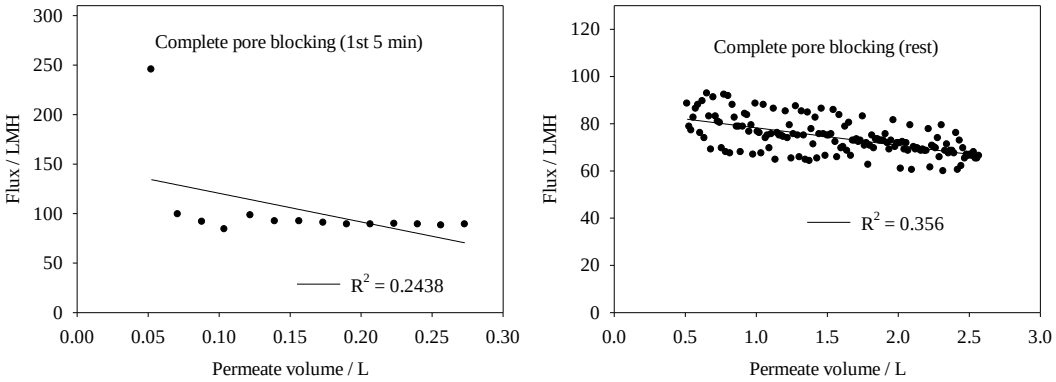

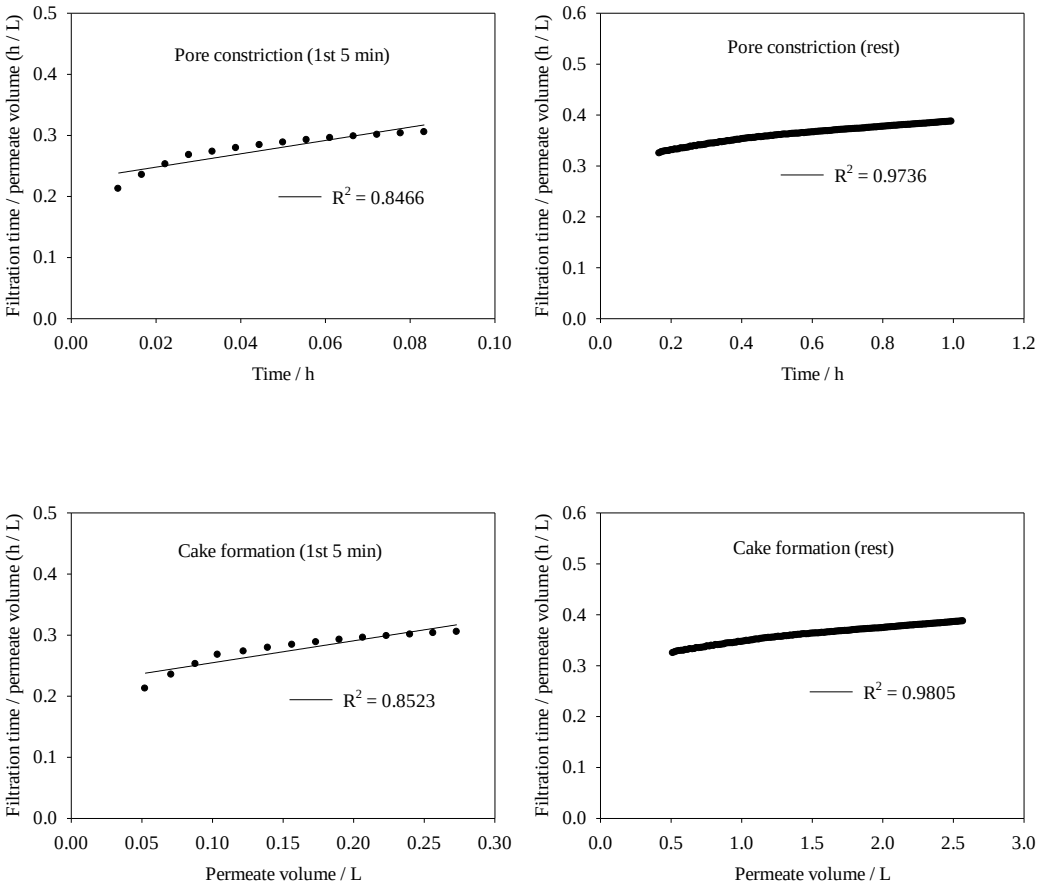

Figure C.4: Linearised Hermia modelling plots for the filtration of 2 wt% gum arabic using 0.5 µm FP membranes

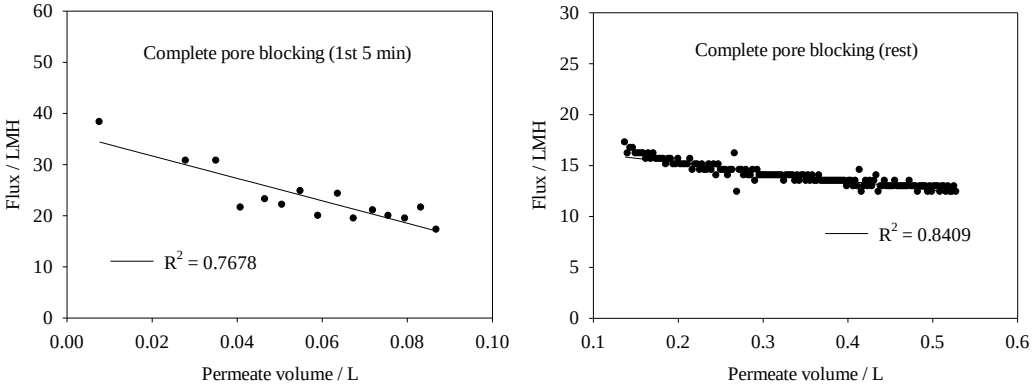

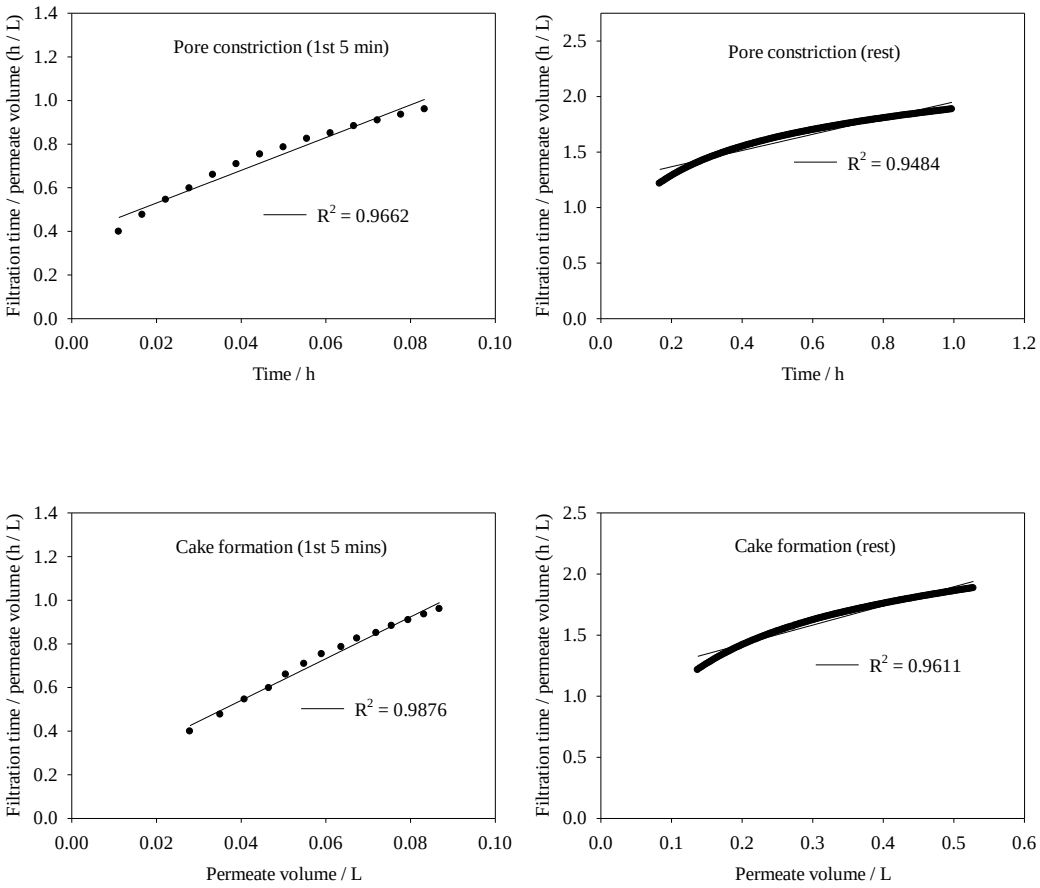

Figure C.5: Linearised Hermia modelling plots for the filtration of 2 wt% gum arabic using 0.45 µm CA membranes